Thermal Casimir Effect at Fluid Interfaces:
Fluctuation–Induced Forces between Anisotropic Colloids

Dissertation

zur Erlangung des Grades

"Doktor der Naturwissenschaften"

am Fachbereich Physik, Mathematik und Informatik

der Johannes-Gutenberg-Universität Mainz

vorgelegt von

Ehsan Noruzifar

geboren in Teheran (Iran)

Mainz, im Dezember 2009

JOHANNES
GUTENBERG
UNIVERSITÄT
MAINZ

1. Berichterstatter:

2. Berichterstatter:

Tag der mündl. Prüfung: 1. Dezember 2009

Ehsan Noruzifar

Thermischer Casimir-Effekt an fluiden Grenzflächen:

Fluktuationsinduzierte Kräfte zwischen anisotropen Kolloidteilchen

Wir untersuchen für zwei ellipsodalen Teilchen an der Grenzfläche zweier fluider Phasen die effektive Wechselwirkung, welche durch thermische Fluktuationen der Grenzfläche übertragen wird. Innerhalb eines Vergröberungsbildes werden die Eigenschaften von fluiden Grenzflächen sehr gut durch einen effektiven Kapillarwellen-Hamiltonian beschrieben, welcher sowohl die Konfiguration der Gleichgewichtsgrenzfläche als auch die thermischen Fluktuationen (Kapillarwellen) um diese Gleichgewichtsposition beschreibt. Wie vom Goldstone-Theorem vorausgesagt, sind die Kapillarwellen langreichweitig korrelliert. Die Grenzfläche bricht die kontinuierliche Translationssymmetrie des Systems und muss im Grenzfall verschwindender externer Felder - wie z.B. der Gravitation - begleitet werden von leicht anregbaren langwelligen (Goldstone)-Moden - dies sind die Kapillarwellen. Auf der Grenzfläche führt die Einschränkung der langreichweitigen Kapillarwellen durch die Anwesenheit der Kolloidteilchen zu fluktuationsinduzierten Kräften. Diese sind äquivalent zu Wechselwirkungen vom Casimir-Typ und sind anisotrop in der Ebene der Grenzfläche. Da die Position und die Orientierung der Kolloide in Bezug auf die Oberflächensenkrechte ebenfalls fluktuieren können, ist dieses System ein Beispiel für den Casimireffekt mit fluktuierenden Randbedingungen. In dem hier gewählten Zugang wird die Casimirwechselwirkung umformuliert in eine Wechselwirkung zwischen fluktuierenden Multipolmomenten einer elektrostatischen Ladungsdichte, welche auf den von den Dreiphasen-Kontaktlinien eingeschlossenen Flächen als Hilfsfeld eingeführt wird. Diese Fluktuationen sind aufgrund der möglichen Positions- und Orientierungsfluktuationen der Kolloide an Fluktuationen der Kontaktlinienposition gekoppelt. Wir erhalten explizite Ausdrücke für das Verhalten der Casimir-Wechselwirkung bei großen Entfernungen für beliebige Achsenverhältnisse der Ellipsoide. Werden Kolloidfluktuationen unterdrückt, dann sind die Casimirwechselwirkungen bei großen Entfernungen isotrop, attraktiv und langreichweitig (doppelt logarithmisch im Abstand zwischen den beiden Kolloiden). Werden dagegen Kolloidfluktuationen zugelassen, ändert sich die Casimirwechselwirkung bei großen Entfernungen in ein Potenzgesetz im inversen Abstand und wird anisotrop. Die führende Potenz ist 4, wenn nur vertikale Fluktuationen des Kolloidschwerpunktes erlaubt werden und wird 8, wenn auch Fluktuationen in der Orientierung der Symmetrieachsen der Kolloide berücksichtigt werden [1, 2].

Ehsan Noruzifar

Thermal Casimir Effect at Fluid Interfaces:

Fluctuation–Induced Forces between Anisotropic Colloids

We study the effective interaction between two ellipsoidal particles at the interface of two fluid phases which are mediated by thermal fluctuations of the interface. Within a coarse–grained picture, the properties of fluid interfaces are very well described by an effective capillary wave Hamiltonian which governs both the equilibrium interface configuration and the thermal fluctuations (capillary waves) around this equilibrium (or mean-field) position. As postulated by the Goldstone theorem the capillary waves are long-range correlated. The interface breaks the continuous translational symmetry of the system, and in the limit of vanishing external fields – like gravity – it has to be accompanied by easily excitable long wavelength (Goldstone) modes – precisely the capillary waves. In this system the restriction of the long–ranged interface fluctuations by particles gives rise to fluctuation–induced forces which are equivalent to interactions of Casimir type and which are anisotropic in the interface plane. Since the position and the orientation of the colloids with respect to the interface normal may also fluctuate, this system is an example for the Casimir effect with fluctuating boundary conditions. In the approach taken here, the Casimir interaction is rewritten as the interaction between fluctuating multipole moments of an auxiliary charge density–like field defined on the area enclosed by the contact lines. These fluctuations are coupled to fluctuations of multipole moments of the contact line position (due to the possible position and orientational fluctuations of the colloids). We obtain explicit expressions for the behavior of the Casimir interaction at large distances for arbitrary ellipsoid aspect ratios. If colloid fluctuations are suppressed, the Casimir interaction at large distances is isotropic, attractive and long ranged (double–logarithmic in the distance). If, however, colloid fluctuations are included, the Casimir interaction at large distances changes to a power law in the inverse distance and becomes anisotropic. The leading power is 4 if only vertical fluctuations of the colloid center are allowed, and it becomes 8 if also orientational fluctuations are included [1, 2].

Dedicated to

my parents,

for all their love, support and encouragement ...

Contents

Contents 11

List of Figures

14

Chapter 1

Introduction

Colloids (colloid stems from a Greek word "κολλα" which means glue) are solid particles, droplets or bubles that are dispersed in one or more dispersing phases. They can have different shapes such as spheres, cubes, plates, rods, ellipsoids, etc. The size of these objects lies between 1 nm and 1000 μm. Due to this characteristic size, a colloid has a large interfacial area, giving rise to various interfacial phenomena [3]. Colloids can be classified into five groups, namely *simple colloids*, *network colloids*, *multiple colloids*, *macromolecular colloids* and *association colloids* [4].

Simple colloids, also known as colloidal dispersions, are a heterogenous system composed of two distinguishable phases, a continuous phase and a discontinuous phase which are called dispersion medium and dispersed phase, respectively.

In our every day life, we have a lot of contact with this type of colloids. Milk (fat droplets in a liquid phase), fog (droplets dispersed in a gas), smoke (solid particles dispersed in a gas) are some familiar examples of simple colloids.

There are many instances of colloidal structures in biological system, e.g. blood (corpuscles dispersion in serum) and bone (calcium phosphate dispersion in collagen).

For network colloids, the distinction between two phases is not as easy as for colloidal dispersions as the networks consist of interpenetrating continuous channels,

like in the case of porous solids where the gas and solid networks interpenetrate such that they can not be simply distinguished.

Multiple Colloids are a kind of solution with three or more coexisting phases in which two or more of them are finely divided from others. As an example we mention an oil bearing porous rock, since the oil and water coexist in solid pores.

Macromolecules in a solution can be viewed as tiny colloids of size 1 nm (or even larger). These particles are known as macromolecular colloids. Jellies (macromolecules dispersed in liquid) are an example of this kind of colloids.

Association colloids or self-assembled structures form when molecules of surface active agents (surfactant) are associated together to form small aggregates in water, known as micelles.

Colloids can be subdivided into two categories with respect to their surface specifications. Colloids attarcted by the dispersion medium molecules are called lyophilic which means "solvent loving" and colloids with the exactly opposite characteristics are named lyophobic which means "solvent hating". In the case that the dispersion medium is water one use the terms "hydrophilic" and "hydrophobic", meaning "water loving" and "water hating", respectively.

In this thesis we are dealing with colloidal dispersions which are quite popular in science and technology due to their simple nature and wide applications [5].

In simple colloids stabilty of the dispersion is a very important topic, as for instance particles which are less dense than the dispersion medium have the tendency to rise to the surface of the dispersion. On the contrary if particles are more dense than the dispersion medium they will sediment at the bottom of the dispersion. These two effects are attributed to gravity. If the size of dispersed colloids becomes smaller than $1\mu m$, the gravitational force on the colloids become small compared to random thermal forces and they perform a random Brownian motion, resulting in collisions between colloids that increases the likelihood of aggregation. In order to avoid this phenomenon and formation of bigger clusters of particles , colloidal

dispersions have to be stabilized; e.g. by employing electrostatic interactions in the charge stabilization method or attaching polymers on the surface of the colloids in the steric stabilization method [6].

Since this thesis is mainly concentrated on the colloidal particles that are trapped at a fluid interface , i.e. the interface between two fluid phases, in the following section (Sec. 1.1) we shortly introduce the definition of these interfaces as well as the situation of colloidal particles located on them.

Having introduced colloids at interfaces, in Sec. 1.2 we investigate the interaction between micro- and nanocolloidal particles in brief.
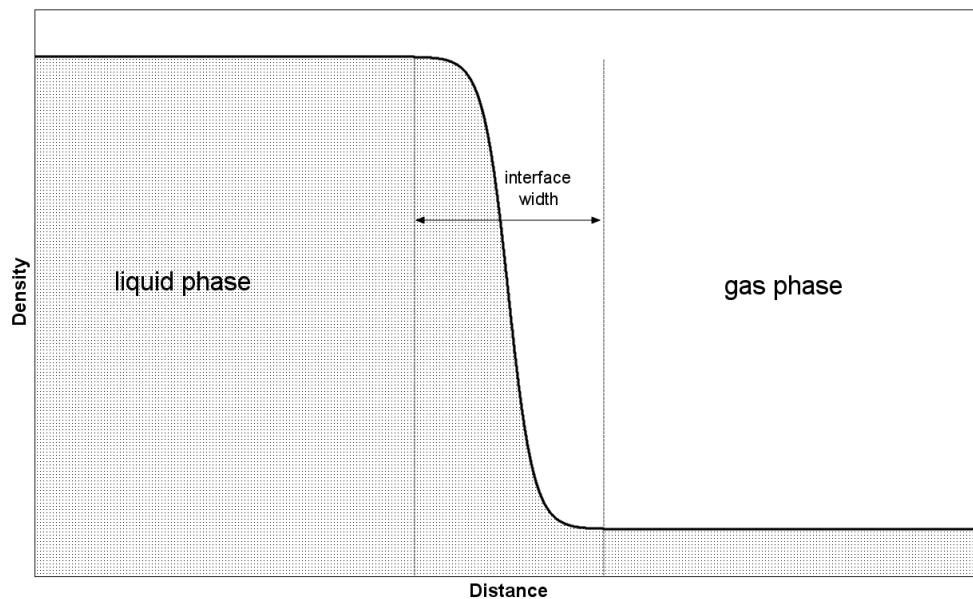
Figure 1.1: Schematic plot of the density profile of a liquid–gas interface area. The distance is measured with respect to the axis perpendicular to the equilibrium interface mean position.

1.1 Colloids at fluid interfaces

An interface is the boundary region between two dissimilar phases, such as liquid–gas, liquid–solid, solid–gas. However, an interface may also form between two liquids and solids if the two phases are immiscible, (e.g. oil–water interface). Obviously, one can not speak of gas–gas interfaces as it is not possible to keep two gases unmixed without a third, intervening non–gaseous phase [8].

A fluid interface (i.e. liquid–gas or liquid–liquid) is usually associated with the Gibbs concept of "a surface with zero thickness" between two fluid phases. However, as it is illustrated in the schematic liquid–gas interface density profile curve in Fig. (1.1), the density of the liquid phase does not fall sharply to the density of the gaseous phase upon changing from the bulk liquid to the bulk gas phase, but con-

tinuously decreases in the vicinity of interface. This implies that one can attribute an effective interface width to the interface separating two fluid phases.

It is also possible to observe a finite interfacial thickness in terms of orientations of molecules. In the case of air–water interface the water molecules are oriented such that their negative tips direct towards the gas phase. This orientational order gradually randomizes as the distance from the interface increases [8].

The free energy associated with a fluid interface can be interpreted on the molecular scale. Since a molecule in a bulk fluid is surrounded by more molecules than a molecule at a fluid interface, it has a lower potential energy and consequently energy is required for moving a molecule from bulk to the interface. Therefore to increase the interface area, energy has to be transfered to the molecules in the bulk to bring them to the interface. This energy dE is proportional to the change of the interface area dA

$$dE = \gamma dA \ , \tag{1.1}$$

where γ is a positive coefficient known as the "surface tension" or "surface free energy".

Solid particles with homogeneous composition and chemical properties on their surface can be trapped at a fluid interface [9]. This phenomenon was found in the beginning of the last century by Ramsden and Pickering [10–12].

There is a class of synthetic particles known as Janus particles, comprised of two different surface regions carrying distinctive chemical and wetting properties. These particles are both surface active and amphiphilic (compounds with both hydrophilic and hydrophobic characteristics) at the same time, similar to surfactant molecules (compounds with hydrophobic tails and hydrophilic heads, soluble in both water and organic solutions; lowering the surface tension of a fluid) [13, 14]. Because of the specific features of such particles, if such a Janus particle is trapped at a fluid interface, the three phase contact line is pinned to the particle surface at the position where the two different surface regions meet.
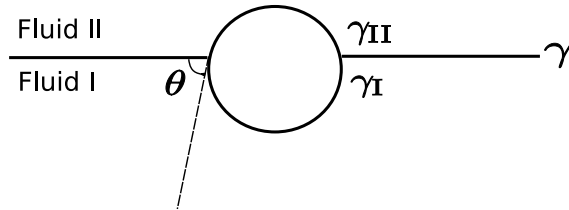
Figure 1.2: Three phase system; a colloidal particle trapped at a fluid interface.

One of the most important quantities for a colloid at a fluid interface is the three phase contact angle θ which is the angle between the tangents to the colloid surface and the fluid interface at the point where the colloid surface and the interface are in contact. Denoting the surface tensions between the colloidal particle and fluid phase I by γ_I, and between the colloidal particle and fluid phase II by γ_{II}, as well as the surface tension of the fluid interface by γ, the contact angle θ can be determined by the Young's equation [15]

$$\cos\theta = \frac{\gamma_{II} - \gamma_I}{\gamma} \; .\tag{1.2}$$

For spherical colloids, this relation follows after equilibrating the forces on particle at the interface (see Fig. 1.2). For anisotropic particles, Young's equation can not be fulfilled for every point at the three–phase contact line if one assumes a flat interfaces. Thus, the interface must neccessarily be deformed (see Subsec. 1.2.3).

1.2 Interaction between colloidal particles

Interactions between colloids in a solution may result in novel structures or new phases. In this thesis we are interested in a particular type of interactions between colloids at fluid interfaces , therefore we will discuss some general aspects of colloidal interaction at fluid interfaces in the present section.

In Subsec. 1.2.1, the well–known van der Waals interaction is investigated for colloidal particles. The origin of van der Waals forces is shortly derived for the case of a Hydrogen molecule. Then the van der Waals potential is discussed for colloids in the bulk and at interfaces.

In Subsec. 1.2.2 we explain the electrostatic interaction between colloidal particles in bulk and at a fluid interface.

Subsec. 1.2.3 is focused on static interface–mediated interactions for colloidal particles that are trapped at the interface of two fluid phases (capillary interaction).

In Subsec. 1.2.4 we introduce fluctuation–induced forces for colloidal particles. The relevant fluctuations in our system of interest are thermally excited height fluctuations of the interface (capillary waves).

Finally in Subsec. 1.2.5 we investigate different possibilities of strengthening fluctuation–induced interactions in order to discriminate it from other contributions in the effective interaction of colloidal particles.

1.2.1 Van der Waals interactions

Van der Waals forces are the consequence of quantum mechanical interactions between ”instantaneous“ electric dipoles of molecules and atoms. To be more clear, for non–polar atoms, the quantum mechanical average of its dipole moment is zero, but the quatum mechanical average of dipole interaction with another atom is not zero. This may be interpreted as the effect of ”instantaneous“ dipoles [16].

This type of force was discovered by Fritz London by considering the Coulomb
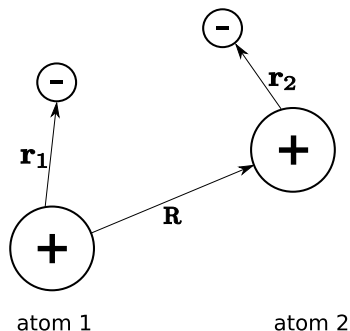
Figure 1.3: Illustrative sketch of two atoms separated by distance $\mathbf{R}$, circles with "plus label" and "minus label" represent nuclei and electrons, respectively.

interactions between the electrons and nuclei of two identical neutral atoms in second order perturbation theory [17, 18]. In order to give a quantitative picture of what London did to derive this force, we consider two hydrogen atoms separated by a distance R shown by the vector $\mathbf{R} = \mathbf{e}_R R$, where $\mathbf{e}_R$ is the unit vector along the line connecting the atoms, and their electrons are positioned at $\mathbf{r}_1$ and $\mathbf{r}_2$ from their nuclei. The Hamiltonian of this system reads

$$\hat{H} = \hat{H}_0 + \hat{V} \ , \tag{1.3}$$

where $\hat{V}$ contains the Coloumb interactions across the two atoms and $\hat{H}_0$ is the unperturbed Hamiltonian $(R \to \infty)$

$$\hat{H}_0 = \hat{H}_1 + \hat{H}_2 \ , \tag{1.4}$$

with the eigenstates $|0n\rangle = |n_1\rangle|n_2\rangle$ corresponding to eigenenergies $E_{0n} = E_{n_1} + E_{n_2}$. The interaction potential V in terms of all Coulomb energies between the electrons and atoms of the Hydrogen atom is given by

$$\hat{V} = \frac{e^2}{R} + \frac{e^2}{|\mathbf{R} + \mathbf{r}_2 - \mathbf{r}_1|} - \frac{e^2}{|\mathbf{R} + \mathbf{r}_1|} - \frac{e^2}{|\mathbf{R} + \mathbf{r}_2|} \ . \tag{1.5}$$

After Taylor expanding of the above potential in terms of $1/R$, we obtain

$$\hat{V} = -\frac{e^2}{R^3}(3(\mathbf{r}_1.\mathbf{u}_R)(\mathbf{r}_2.\mathbf{u}_R) - \mathbf{r}_1.\mathbf{r}_2) + O(R^{-5}) \tag{1.6}$$

where the first term of the expansion that we have included in the above expansion corresponds to the dipole-dipole interaction, and higher order terms give interactions which are associated with dipole-quadrupole, quadrupole-quadrupole, ... interactions. We treat this Hamiltonian as a perturbation potential and use the quantum perturbation theory up to second order for non-degenerate states

$$E_n = E_{0n} + \langle 0n|\hat{V}|0n\rangle + \sum_{j \neq n} \frac{|\langle 0n|\hat{V}|0j\rangle|^2}{E_{0n} - E_{0j}} + ... \tag{1.7}$$

The first order terms contain the expectation values of the type

$$\langle n_1|\hat{x}_{i,1}|n_1\rangle\langle n_2|\hat{x}_{i,2}|n_2\rangle = 0 , \tag{1.8}$$

which vanish, since each atom has a vanishing electric dipole in its ground state. Therefore

$$E_n(R) = E_{n_1} + E_{n_2} - \frac{e^2}{a_0}\frac{A_n}{(R/a_0)^6} , \tag{1.9}$$

where the Bohr radius a_0 has been introduced to define the dimensionless amplitude

$$A_n = \frac{e^2}{a_0^5} \sum_{(j_1,j_2) \neq (n_1,n_2)} \frac{|\langle n_1|\langle n_2|(\hat{x}_1\hat{x}_2 + \hat{y}_1\hat{y}_2 - 2\hat{z}_1\hat{z}_2)|j_1\rangle|j_2\rangle|^2}{E_{j_1} + E_{j_2} - E_{n_1} - E_{n_2}} . \tag{1.10}$$

If $|0n\rangle$ is the ground state, then $E_n - E_{n0} > 0$, thus the van der Waals force is attractive.

When two atoms are separated by a considerable distance, it takes time before the electric field of one atom "reaches" the second one. Therefore the interaction force decays faster than for the case in which the atoms are close. This effect which is related to the finite speed of light is known as the retardation effect. Including the retardation effect to the calculation of the van der Waals interaction results in an interaction potential which decays $\propto -1/r^7$ [19]. This effect was found by Casimir and Polder. If two molecules are in the vaccum the retardation effect becomes inportant when the molecules are more than 5 nm apart from each other. On the other hand if the atoms or molecules are in a medium where the light speed is slower, retardation effects play a role at smaller separations [16].

To calculate van der Waals forces between two rigid bodies, one can sum over the van der Waals interaction between all pairs of atoms in the bodies. This calculation is based on two simplifying assumptions: that the van der Waals interaction is pairwise additive and they are non-retarded. Such a summation amounts to a double volume integral [20]

$$U_{\text{vdW}} = -\frac{A_{12}}{\pi^2} \int_{V_1} \int_{V_2} \frac{dV_1 \, dV_2}{|\mathbf{r}_1 - \mathbf{r}_2|^6} \,, \tag{1.11}$$

where $|\mathbf{r}_1 - \mathbf{r}_2|$ is the distance between two volume elements dV_1 of body 1 and dV_2 of body 2, and A_{12} is the Hamaker constant [21] which has the dimension of the energy and determines the effective strength of the van der Waals potential between two bodies. The Hamaker constant for most condensed phases is in the range $(0.4-4) \times 10^{-19}$J, and it depends on the material constituting the bodies [22].

In the discussion above, van der Waals forces were obtained by neglecting the retardation effects and multi-body intermolecular forces, Lifshitz developed an alternative quantum electrodynamical approach to calculate this type of interaction between two macroscopic bodies. In the Lifshitz theory [23–26] the particles are considered as continuum dielectric objects in a dielectric medium. In this theory instead of the polarizability of atoms, the frequency dependent dielectric permittivities of the bulk media are employed. However, in the resulting interaction force the dependence on distance is the same as what one obtains in the pairwise summation method, but it should be noted that in this case the Hamaker constant is given as a function of frequency-dependent dielectric functions.

If the intervening medium in which the objects are placed is dielectrically anisotropic, the van der Waals interaction will also depend upon the mutual orientation of the objects [27].

The form of the van der Waals interaction between the colloidal particles at a fluid interface is more intricate compared to such interactions in the bulk [28]. In a method proposed by Wiliams and Berg the effective Hamaker constant is estimated by using the fractional volume of the particle in the liquid . For the case of a

liquid–vapor interface the following equation was proposed [29]

$$A_{\text{int}} = A_{\text{vac}} + f^2(3 - 2f)(A_{\text{liquid}} - A_{\text{vac}}) \, . \tag{1.12}$$

Here, f is a linear fractional immersion, A_{vac} and A_{liquid} are the Hamaker constants of the particles in vacuum and in the liquid. This expression implies that the van der Waals interaction at liquid–vapor interface should be stronger than in the bulk liquid. However, in this approach the interface thickness, and the large variations in the density around it are ignored, thus it is inaccurate for nanoparticle systems [28].

More considerations about the van der Waals interactions between nanoparticles can be found in the review by Bresme and Oettel [28].

1.2.2 Electrostatic interactions

Electrostatic interactions are usually stronger in charged colloidal systems, and consequently play an important role for their stability and phase behavior.

In polar dispersions with charged colloidal particles and mobile ions, the electrostatic field of the fixed ions at the colloids surfaces interact with the mobile ions. The charges on a colloid surface are partly neutralized by a layer of counterions absorbed from the solution. Hereby, the charge density on the colloid surface is usually several $\mu C/cm^2$ which corresponds to the range $0.1 - 1$ e/nm^2, where e is the electron's charge [30].

The layer which is tightly bound to the charged colloid surface is known as Stern layer [31]. Away from the Stern layer, solution ions form a a diffuse concentration profile.

To find the ions concentration profile, we need to obtain the electrostatic potential $\phi(\mathbf{r})$ which is connected to the ion number density $n(\mathbf{r})$ through the Boltzmann equation

$$n(\mathbf{r}) = n_0 \left[\exp \left(\frac{-ze\phi(\mathbf{r})}{k_{\mathrm{B}}T} \right) + \exp \left(\frac{+ze\phi(\mathbf{r})}{k_{\mathrm{B}}T} \right) \right] , \qquad (1.13)$$

where n_0 is the ionic concentration in the bulk solution, ze is the charge of the ions, k_{B} is the Boltzmann constant, and T is the temperature. The first and second terms in r.h.s. of Eq. (1.13) represent the number density of positive and negative ions, respectively.

On the other hand, using the Poisson equation, the electrostatic potential ϕ can be found via

$$\rho(\mathbf{r}) = -\epsilon \nabla^2 \phi(\mathbf{r}) . \qquad (1.14)$$

where ϵ is the permitivity of the solution. The net charge density $\rho(\mathbf{r})$ is given by

$$\rho(\mathbf{r}) = ze\, n(\mathbf{r}) . \qquad (1.15)$$

After identifying Eq. (1.13) and Eq. (1.15), Eq. (1.14) is rewritten as

$$\nabla^2 \phi(\mathbf{r}) = \frac{2zen_0}{\epsilon} \sinh \left(\frac{ze\phi(\mathbf{r})}{k_{\mathrm{B}}T} \right) . \qquad (1.16)$$

The above equation known as Poisson–Boltzmann equation has to be solved self–consistently by using the appropriate boundary conditions for a given system.

In the Debye–Hückel approximation [32], $\phi(\mathbf{r}) \ll 1$, we have $\sinh(ze\phi(\mathbf{r})/k_{\mathrm{B}}T) \approx (ze\phi(\mathbf{r})/k_{\mathrm{B}}T)$; thus Eq. (1.16) reduces to the Debye–Hückel equation for the electrostatic potential ϕ

$$\nabla^2\phi - \kappa^2\phi = 0 \;, \tag{1.17}$$

with the solution in spherical symmetry around the (point) charge q

$$\phi(r) = q\frac{\exp(-\kappa r)}{4\pi\epsilon r} \;, \tag{1.18}$$

where κ^{-1} is the Debye screening length

$$\kappa = \left(\frac{2e^2 n_0 z^2}{\epsilon k_{\mathrm{B}}T}\right)^{1/2} \;, \tag{1.19}$$

which gives the radius of the effective screening cloud around a charged colloid. If the distance from the charged colloid is much greater than the Debye screening length, the direct electrostatic interaction quickly falls to zero [6]. In this approximation the interaction potential between charged colloids is simply given by $U = q\phi(r) = q^2\exp(-\kappa r)/(4\pi\epsilon r)$, where q is the total charge on each of the colloids and r is their distance.

The electrostatic interaction between charged colloidal particles trapped at a fluid interface is altered significantly compared to such interactions in the bulk [28]. For colloids that are trapped at the air–water interface, the surface charge density of the colloid part which is in the water remains high compared to the case that charged colloids are in the bulk. For the part of the colloid which is in the air, for equilibrium reasons, the surface charges are reneutralized by distributing them on the water side of the colloid.

Stillinger and Hurd in a simple model considered charged colloids at a water interface as point charges and investigated the ions distribution in water phase by the Debye–Hückel approximation. This model results in a dipole–dipole interaction besides

the screened Coulomb potential. The screened Coulombic and dipole contributions to the interaction energy of two point charges $q = Ze = \sigma_{\mathrm{c}} A$, where A is the colloid surface area exposed to water and σ_{c} the surface charge density, by using the linearized Poisson–Boltzmann equation are given by [33]

$$U_{\mathrm{dipole}} \propto 2 \left(\frac{Ze}{\epsilon \kappa} \right)^2 \frac{1}{d^3} \propto \frac{1}{\epsilon} \frac{\sigma_{\mathrm{c}}^2 \kappa^{-2}}{d^3} \qquad (kd > 10)$$

$$U_{\mathrm{Coulomb}} \propto 2 \left(\frac{Z^2 e^2}{\epsilon d} \right) \frac{\epsilon^2}{\epsilon^2 - 1} \exp(-\kappa d) \qquad (kd < 10) \qquad (1.20)$$

where ϵ is the ratio of dielectric constants of water and the nonpolar medium, and d is the intercolloidal distance.

This approximation is expected to be accurate when the intercolloidal distances are long, since the potential is smaller than $k_{\mathrm{B}} T$ and consequently the linearization becomes a good approximation [28].

However, the dependence on the electrolyte concentration through the Debye screening length κ^{-1} is subject to strong charge renormalization of the charge densities on colloid–water surfaces [34].

If the surface charge density of the water side of a charged colloidal particle is high the Debye–Hückel approximation is not valid any more and nonlinear screening effects have to be considered through the Poisson–Boltzmann equation (See Eq. (1.16)). Although Eq. (1.16) neglects the correlations between ions in water, it should give precise results for microcolloids and water with only monovalent ions [30]. For spherical colloids of radius R it has been shown [34] that the squared dependence on the charge density and the screening length of the strength of U_{dipole} is changed to a logarithmic one upon including the nonlinearities in the Poisson–Boltzmann equation

$$U_{\mathrm{dipole}} \sim g \frac{\epsilon_{\mathrm{np}} \epsilon_0}{\beta^2 e^2} \frac{R^4}{d^3} \ln^2 \left(\frac{\sigma_{\mathrm{c}} \kappa^{-1} \beta e}{\epsilon_{\mathrm{w}} \epsilon_0} \right) , \qquad (1.21)$$

where ϵ_{np} and ϵ_{w} are the dielectric constant of the nonploar phase and water phase respectively, ϵ_0 is the dielectric constant of the vacuum and $\beta = 1/(k_{\mathrm{B}} T)$ is the

inverse temperature. Moreover, $g = 0(1)$ is a geometry factor depending on the contact angle which determines the position of the colloid interface. It should be noted that g is independent of σ_c and weakly depends on κ^{-1}. If κ^{-1} is smaller than the colloid size, the renormalized form of the dipole interaction in Eq. (1.21) is expected to be valid for colloids of arbitrary shape.

For oil–water interfaces, if the oil has a low–dielectric constant like decalin with $\epsilon \approx 2$, it is still an open question wether charges stay on the oil side of the colloid after equilibration or not [30]. If the oil has a higher permittivity ($\epsilon \approx 5$), charges can be stable on the colloids surface with a lower charge density [35]. Charge renormalization effects on the water side of the colloids reduce the electrostatic interaction to a great extent, and therefore even a low charge density on the oil side may nevertheless change the effective intercolloidal interactions considerably.

1.2.3   Capillary forces

The presence of an interface gives rise to interactions mediated by deformations of that interface, thus these are absent in bulk solutions of colloids. As it is discussed in the previous subsection, if the interface deformations are caused by thermal fluctuations, one can speak of fluctuation–induced interactions between the colloidal particles which are trapped at the interface. If these deformations are static, one speaks of capillary interactions [36]. For spherical colloids at free interfaces, the formation of self–organized structures is mainly governed by the "direct" interactions (such as van der Waals or electrostatic forces, present also in the bulk) whereas for particles of nonspherical shape capillary interactions appear to be dominant [28].

Static interface deformations arise if the colloids experience forces in the direction parallel to the interface normal (e.g. if they are pushed into the lower phase) and/or stress distributions act on the interface [30]. For microcolloids of sizes less than 10 μm, the omnipresent gravitational force on the colloids can be neglected. However, meniscus deformations also arise in conjunction with direct interactions (like electrostatic forces) which lead to forces and stresses on colloids and interface, respectively. If the system "colloids + interface" is mechanically isolated (usually this applies for colloid experiments in a Langmuir trough or on large droplets), then the force on the colloids directed vertical to the interface is balanced by the total force on the interface (obtained by integrating the stress distribution over the interface area) [37–39]. The ensuing capillary interactions decay with a power–law in the intercolloidal distance d, e.g., in the case of charged colloidal spheres at air–water or oil–water interfaces they are attractive, $\propto d^{-3}$, but for large d they are usually weaker than the direct electrostatic repulsion which is also $\propto d^{-3}$ [40–42]. – On the other hand, in the absence of forces on the colloids and stresses on the interface, static interface deformations can also be induced by an anisotropic colloid shape; more precisely if the colloid is not symmetric with respect to rotations around any axis through the colloid which is parallel to the normal on the undisturbed interface.

Young's equation requires that at the three–phase contact line the angle between the local interface normal and the local normal on the colloid surface is given by the contact angle θ. Thus for an anisotropic colloid this condition cannot be met if the interface remains flat; the contact line will not be located in the plane of the undisturbed interface. The associated interface deformations around one such colloid can be calculated in terms of a two–dimensional multipolar expansion [1,43]. For asymptotically large distances from the colloid, the leading nonvanishing multipole is in general the quadrupole, since monopole and dipole are absent through the conditions of force and torque balance. The interaction energy between two quadrupoles depends on the colloid orientation in the interface plane and decays according to a power law, $\propto d^{-4}$. For the ellipsoids, experimental results on the effective pair potential for intermediate distances d [46] indicate a strong orientation dependence not captured by the aforementioned leading quadrupole interaction. Ellipsometric measurements of the interface deformation around one particle are consistent with a quadrupolar pattern [48] which, however, appears to be deformed considerably for stretched ellipsoids.

1.2.4 Fluctuation–induced forces or Casimir interaction

Existence of long-ranged fluctuations in a colloidal dispersion may cause a new type of intercolloidal interaction if the fluctuations are restricted by the presence of the colloidal particles. This type of interactions are named after Casimir, the scientist who discovered them for the case of two parallel conductive walls in the zero–point fluctuations of vacuum [49]. As these interactions are induced by fluctuations in a medium, they are also called fluctuation–induced interactions.

Originally Casimir forces were associated with the zero–point fluctuations of the vacuum. However, they can exist in all media with long–ranged fluctuations restricted by the presence of some boundaries [50]. It should be noted that the resulting sign and behavior of the Casimir interaction is determined by the shape of boundaries and the way that they restrict the fluctuations. However, in all instances of the Casimir effect the resulting Casimir force is long-ranged, i.e. power–like in the inverse distance between the boundaries.

Returning to the system of our interest, we deal with thermal fluctuations of the interface, with the fluctuations being restricted by colloidal particles. These interface fluctuations, which are deviations of the interface from its equilibrium mean position are termed capillary waves. Due to the gravity these capillary waves are damped only on a sub–mm length scale. More precisely, colloids that are trapped on a fluid interface can be regarded as objects which restrict the possible fluctuations of the capillary waves via the boundary conditions imposed on the three–phase contact line and therefore give rise to Casimir–like interaction.

General aspects of the Casimir interaction associated with thermal Gaussian fluctuations (which capillary waves belong to) are discussed in Ref. [51]. It should be noted that the amplitude of the corresponding Casimir energy is fixed by $k_{\mathrm{B}}T$, therefore these forces become more dominating for nanocolloidal particles than microcolloids.

In a system of two spherical colloids trapped at a fluid interface, the fluctuation–induced interaction is determined by two contributions [52, 53]:

1. The effects of interface fluctuations with the three phase contact line held to be fixed at its equilibrium position, corresponding to the "standard Casimir problem".

2. The effects of the three–phase contact line fluctuations, as in general the colloids also may fluctuate freely within the interface. This contribution can be varied by the specific constraints imposed on the colloidal particles.

For the instance of spherical colloids of radius R and contact angle, $(\theta = 90°)$ at large colloidal separations $(d \gg R)$, the resulting interaction potential is double logarithmic in distance for fixed colloids (e.g. by laser tweezers), and it is a weak power law for freely fluctuating colloids [52, 53],

$$U_{\text{Cas}} \sim \begin{cases} k_{\text{B}} T \ln \ln \left(\frac{d}{R} \right) & \text{(fixed colloid)} \\[2em] -k_{\text{B}} T \left(\frac{R}{d} \right)^8 & \text{(free colloid).} \end{cases} \tag{1.22}$$

This potential is independent on the constraints on the colloids as they are close and it is divergent when the surface–to–surface distance $h = d - 2R$ goes to zero

$$U_{\text{Cas}} = -k_{\text{B}} T \frac{\pi^2}{24} \sqrt{\frac{R}{h}} \qquad (h \to 0). \tag{1.23}$$

Consequently the thermal Casimir interaction has a comparatively small prefactor $(k_{\text{B}} T)$ but it is diverging for $h \to 0$, similar to the van der Waals interaction for which the prefactor $A_{12} \sim k_{\text{B}} T$ and it is also diverging, albeit $\propto 1/h$ (for spherical particles). This means that when the effective Hamaker constant of an interface is small and thus van der Waals forces are weaker than the fluctuation–induced forces, the colloid coagulation will be triggered by the thermal Casimir interaction.

Fluctuation–induced forces for anisotropic colloids leads to anisotropies in the resulting Casimir interaction. This will be the main focus of this thesis. It will be shown that for fixed particles at the interafce the leading term of the fluctuation interaction is again $\propto \ln \ln d$ and of isotropic nature and it is stronger than the

anisotropic subleading terms.

The anisotropy in the thermal Casimir potential starts to play its role as soon as one includes the fluctuations of colloidal particles themselves. As an example the Casimir potential between two freely–fluctuating thin rods of length L is given by [54]

$$U_{\text{Cas}} = -\frac{k_{\text{B}}T}{128}\left(\frac{L}{d}\right)^4 \cos^2(\phi_1 + \phi_2) \,, \tag{1.24}$$

where ϕ_i is the orientation of rod $i = 1, 2$ in the interface plane.

In this thesis we will investigate the thermal fluctuation–induced interactions between ellipsoidal colloids trapped at the interface of two fluid phases. The specific geometry of the colloidal particles gives us this opportunity to study the effect of the anisotropy of the ellipsoidal colloid on the resulting Casimir force with special attention to the fact that the "obstacles" may also fluctuate.

1.2.5   Fluctuation–induced interactions versus other types of interactions

As it is mentioed before, in this thesis we will investigate the thermal Casimir in-
teraction between nano-scale uncharged colloidal particles which are trapped at a
fluid interface. Since the colloids are not charged there is not any sort of electro-
static interaction between them. The dominating interactions between such colloidal
particles at a fluid interface are van der Waals, capillary and fluctuation–induced
interactions. To discriminate fluctuation–induced forces from other aforementioned
interactions, some methods should be employed to strengthen the contribution of
fluctuation–induced interactions such that other interactions become comparatively
unimportant.

To reduce the effect of capillary interaction, one can use nano–colloidal particles,
as the capillary interaction between them is negligible compared to the fluctuation–
induced forces but we note that synthesizing nano–particles is not very easy with
the current experimental equipment and techniques. An alternative option to extin-
guish the capillary interaction is to use spherical particles [28, 30].

In order to reduce the strength of the van der Waals interaction , one can choose
one of the following scenarios [52]:

- Lowering the Hamaker constant by means of index matching.

- Using thin disks, since the fluctuation–induced forces between them due to
  their specific geometry is much greater than the van der Waals interaction .

- Coating colloids with light polymers decreases the distance between the poly-
  mer shell of colloids. This surface-to-surface distance is relevant for calculating
  the Casimir interaction. However, only the distance between the cores is rele-
  vant for the van der Waals force. Therefore the resulting Casimir interaction
  can be rendered larger than the van der Waals interaction.

Chapter 2

Casimir Interaction: experimental proofs and theoretical methods

When a fluctuating medium with long-ranged, power-law correlations is confined between a set of boundaries, forces with likewise long-ranged character are induced between the boundaries. This type of interaction was theoretically discovered by the Dutch theoretical physicist Hendrik Casimir in 1948 for the case of two parallel, conductive and uncharged plates in vacuum which he attributed to zero point fluctuations of the electromagnetic field [49]. This phenomenon which has been coined the Casimir effect thereafter can be attractive or repulsive depending on the fluctuations and the physical properties of the boundaries.

The discovery of the Casimir effect is historically connected to research performed on intermolecular and inter-particle interactions [55]. In 1873 the Dutch physicist van der Waals postulated an intermolecular force resulting in the semi–empirical equation of state for a non-ideal gas named after him [56]. At that time the physical nature of the intermolecular interactions had not yet been completely realized.

In 1930 the German-American physicist Fritz London explained this force using

quantum mechanics on the basis of second–order perturbation theory. [17]. In London's calculations the perturbation potential is the Coulomb interaction between the electrons and nuclei of one molecule with the electrons and nuclei of another molecule at a distance R. Using the multipole expansion of the perturbation potential for calculating the energy shift to second order gives rise to an interaction potential which is always attractive between like molecules and proportional to R^{-6}.

Later on the Dutch experimental physicists Theo Overbeek and Evert Verwey at Philips Research Laboratories observed that there was a discrepancy between their inter-colloidal interaction measurements and the predictions of London's theory . Therefore they asked their colleague Hendrik Casimir to investigate this problem. Hence Casimir together with Dirk Polder discovered that the interaction potential at large distances due to the finite speed of light – known as the retardation effect – is governed by R^{-7} [19]. Shortly afterwards, Bohr proposed to Casimir that the intermolecular interaction could be due to the zero-point vacuum energy [57]. Following Bohr's suggestion, Casimir calculated the interaction between two parallel conductive, uncharged plates and predicted that there would be an attractive force between the plates.

In 1956 Lifshitz extended Casimir's work to dielectric materials by considering the electrodynamic mode boundary problem [24]. This work was in association with the experimental project of Boris Derjaguin and Irina Abrikosova on short-range attractive interactions between dielectric materials. Lifshitz's work is based on two premises [55]:

(a) The polarizability of an atom or a molecule is altered in the presence of other atoms and molecules. This effect has to be taken into account for bulk materials.

(b) The van der Waals forces are not pairwise additive [58] because the interaction between a pair would be changed by the presence of third atom.

However Casimir phenomena are not only restricted to the quantum world, there is

also a classical equivalent of the Casimir force observable between objects immersed in a fluid in the vicinity of its critical point which was predicted by Fisher and de Gennes 30 years later [59]. In this classical instance, the fluctuations of the order parameter field near the critical point are long-ranged, and thus they give rise to a Casimir-like, fluctuation induced force. This effect has recently been observed in an experiment probing the force on colloidal particles immersed in a near-critical binary mixture in the vicinity of a wall [60].

Another classical variant of the Casimir interaction is found between particles (colloids) that are trapped at membranes [54, 61] or at the interface of two fluid phases [50]. In this two dimensional latter instance, thermally excited height fluctuations of the interface which have a long-ranged nature are disturbed by the presence of colloids and consequently there would result a long-range force between the colloidal particles.

In this chapter we are going to review some methods of evaluating and measuring the Casimir interaction. This chapter is structured as follows:

In Sec. 2.1 we briefly review the most prominent experiments which give evidence for the presence of the Casimir interaction in various fluctuating systems.

Besides these experimental studies many theoretical studies have also been conducted to calculate the Casimir forces. Thus, in Sec. 2.2, we review these theoretical methods which have been used to evaluate the Casimir energy.

2.1 Casimir effect: experimental attestation

The first attempt to measure the quantum Casimir effect between parallel conductive plates was made by Sparnaay at Philips laboratories in 1958 [62]. Although the result of this measurement was not in conflict with Casimir's prediction, it could not be treated as a conclusive result because of a large uncertainty of 100% in their measurements.

Maintaining two conductive plates parallel with respect to each other is very difficult and leads to inaccuracies in the measurements, therefore successive experimental verifications have been focused on the Casimir effect between a conductive sphere and a conductive plate in which the closest distance between the sphere and the plate is utilized instead of the distance between parallel plates [63, 64].

In 1997 Lamoureaux measured the Casimir force between a conductive sphere and a conductive plate by means of an electromechanical system based on a torsion pendulum [63]. The statistical precision of that measurement was $\pm 5\%$ [63, 64]. The inaccuracies in the measurements might be a consequence of large experimental systematic error due to the fact that the electrostatic force between surfaces was 5 times the Casimir force.

Mohideen and Roy in 1998 made precision measurements of the Casimir force between a metalized sphere and a flat plate using an atomic force microscope [64–67]. Their experimental result is in agreement with the theoretical calculations including the finite conductivity, roughness, and finite temperature corrections [64].

In 2002 the occurrence of a lateral Casimir force was demonstrated by Chen and Mohideen [68, 69], in a system consisting of a sinusoidally corrugated gold coated plate and large sphere, using an atomic force microscope. The measured force shows the periodicity corresponding to the corrugations. Their result was also in good agreement with theoretical calculations.

In addition to the experiments done to verify the quantum Casimir effect, there have also been attempts to measure the critical Casimir forces [?, 70–73]. However

most of the research in this field was focused on measuring the critical Casimir force indirectly. For instance, reversible flocculation of silica colloids observed in a water–2,6-lutidine mixture close to its critical point [74] was considered to be an evidence for critical Casimir forces. But such reversible flocculation was also observed far away from the critical point, therefore it does not provide clear evidence for the existence of these forces [75, 76].

Recently a group in Stuttgart succeeded to directly measure the critical Casimir interaction between a single colloidal sphere and a planar surface immersed in a binary liquid mixture near its critical point [60]. In their experiment, by choosing different combinations of colloidal particles with the wall, they investigated repulsive and attractive Casimir forces which depended strongly on the adsorption properties of the confining surfaces.

This group also measured the critical Casimir forces for the case of spherical colloids immersed in a binary liquid mixture using a chemically patterned substrate. Near the critical point of the binary liquid mixture, they observed critical Casimir forces with components normal and parallel to the surface. As a consequence one may utilize the critical Casimir interaction to form highly ordered monolayers [73].

2.2 Theoretical methods

Casimir forces occur in fluctuating media restricted by the presence of some boundaries. As mentioned above, this type of interaction was calculated for the first time by the Dutch physicist Hendrik Casimir [49]. Later it was found that such phenomena can in principle exist in different systems as long as long-ranged fluctuations are present in them. Additionally, due to the strong desire of contemporary technology to make devices smaller, the importance of Casimir forces that are significant at short ranges has become more apparent.

To evaluate such forces, various methods based on the field theoretical means have been developed so far. Although different types of fluctuations require their particular field theories, the general approach to evaluate the Casimir interaction in all methods does not vary significantly. As the main purpose of this thesis is to calculate the Casimir energy in a soft condensed matter system, it is worthwhile to survey the theoretical methods which are broadly used for evaluating it. We will review the most important methods of calculating the Casimir energy to provide a deeper insight for the following chapter in which we are going to find the Casimir force for the case of two ellipsoidal colloids trapped at the interface of two fluid phases. The thermal height fluctuations of this interface are treated by a classical scalar field, and the whole system is investigated by statistical field theory techniques. Hence in order not to wander off the main route, in this section all the methods are recapitulated using scalar fields.

On the other hand most of these methods have been originally derived for quantum field theory, more specifically the quantized radiation field. Since this section only covers a selective review of other researchers works, we will use the Minkowski metric in most cases. However, one should keep in mind that the connection between the statistical and quantum mechanical field theories is easily given by a Wick rotation. This is equivalent to solving a problem in Minkowski space and by replacing real Minkowski time with imaginary time the problem would be transformed into

the real Euclidean space. As a consequence, imaginary time is equivalent to another space dimension and the action of the Minkowski space field theory corresponds to the Hamiltonian of the statistical field theory.

This section is structured as follows:

In Subsec. 2.2.1 for historical reasons we investigate the "*mode summation method*", the first approach of calculating the Casimir energy. In this method the Casimir energy is worked out as the difference between the zero–point energy with and without constraints. The term "mode summation" is given to this method since for calculating the zero point energy, one simply sums over all field modes. Since this simple method is not always practical for more complicated systems and geometries, we also recapitulate other methods that are used to find the Casimir energy.

In Subsec. 2.2.2 we discuss a widely used field theoretical method known as "*Green's function method*" , a common approach to work out the Casimir energy. This method employs the energy-momentum tensor to evaluate the Casimir interaction. Then in Subsec. 2.2.3 we discuss a variant of this approach in which the constraints in the system are entered into the calculations as δ-function potentials.

In Subsec. 2.2.4 a more recent method of calculating the Casimir interaction based on functional integral formalism is investigated. In this subsection the Casimir energy is understood with regard to the interaction between quantum fluctuations of charge and current in metals or dielectrics. This concept is implemented in the functional integral formalism, and the Casimir energy is found in terms of scattering matrices. In Subsec. 2.2.5, we use the functional integral formalism to calculate the Casimir force in a classical soft condensed matter system. This subsection introduces the necessary tools needed in the next chapter for calculating the Casimir interaction in our considered system.

The methods of Subsecs. 2.2.1-2.2.4 are discussed using the example of free (Gaussian) field theories. In Subsec. 2.2.5 we briefly comment on the important case of the Casimir effect in an interacting field theory which corresponds to the

critical Casimir effect.

Using the example of two spherical colloids that are immersed in a binary liquid mixture near its critical point, we discuss a mean–field approach to this problem.

2.2.1 Mode summation method

The Casimir interaction occurs when a set of boundaries are placed in zero–point vacuum fluctuations, therefore the Casimir energy can be defined as the difference in the zero–point energy of vacuum represented by $E_0[0]$ and the zero–point energy in the presence of boundaries denoted by $E_0[\partial S]$ [77]

$$E_{\text{cas}} = E_0[\partial S] - E_0[0] \,. \tag{2.1}$$

To calculate the Casimir energy based on Eq. (2.1), a scalar field which is constrained by two parallel "conductive" 2–dimensional plates (imposing a zero–field [Dirichlet] boundary condition on the field) separated by a distance a is considered. The ground state energy of this system is found by introducing a large finite quantization volume bounded by a surface Σ.

Because of the geometry, the quantization volume in this problem is chosen to be a big rectangular box of size $L \times L \times a$, therefore all possible vibrations in the box are confined by

$$0 \leq x \leq L, \ 0 \leq y \leq L, \ 0 \leq z \leq a \,. \tag{2.2}$$

Having assumed the periodic boundary conditions for the purpose of field quantization, the zero–point energy associated with a constrained and an unconstrained system can be estimated by summing over all eigenenergies of the field's normal modes. The wave numbers of the quantized field reads

$$k_x = \frac{\pi}{L} n_x, \ k_y = \frac{\pi}{L} n_y, \ k_z = \frac{\pi}{a} n_z \,, \tag{2.3}$$

where n_x, n_y, n_z are positive integers;

$$k = \sqrt{k_x^2 + k_y^2 + k_z^2} = \sqrt{r^2 + k_z^2} \,. \tag{2.4}$$

The zero–point energy of the system constrained by two parallel plates ∂S is

$$
\begin{aligned}
E_0[\Sigma, \partial S] &= \frac{1}{2} \sum_k \hbar \omega_k[\Sigma, 0] \\
&\stackrel{L \to \infty}{=} \hbar c \frac{L^2}{\pi^2} \int_0^\infty \int_0^\infty dk_x \, dk_y \left[\frac{1}{2} \sqrt{k_x^2 + k_y^2} + \sum_{n=1}^\infty \sqrt{\frac{n^2 \pi^2}{a^2} + k_x^2 + k_y^2} \right]
\end{aligned}
\tag{2.5}
$$

where ω_k is the eigenmode frequency.

After introducing polar coordinates in the $k_x - k_y$–plane, the above equation can be rewritten as

$$
E_0[\Sigma, \partial S] = \hbar c \frac{L^2}{\pi^2} \frac{\pi}{2} \sum_{n=0(1)}^\infty \int_0^\infty r \, dr \sqrt{\frac{n^2 \pi^2}{a^2} + r^2} \, ,
\tag{2.6}
$$

where $(0)1$ means that the leading term with $n = 0$ must be multiplied by $\frac{1}{2}$. In a similar fashion, the zero–point energy for a system without any external constraints is

$$
\begin{aligned}
E_0[\Sigma, 0] &= \frac{1}{2} \sum_k \hbar \omega_k[\Sigma, 0] \\
&\stackrel{L \to \infty}{=} \hbar c \, a \frac{L^2}{2\pi^2} \int_{-\infty}^\infty dk_x dk_y dk_z \sqrt{k_x^2 + k_y^2 + k_z^2} \, ,
\end{aligned}
\tag{2.7}
$$

thus, according to Eq. (2.1) the Casimir energy is given by

$$
\begin{aligned}
E_{\text{cas}} &= \frac{1}{2} \sum_k \hbar (\omega_k[\Sigma, \partial S] - \omega_k[\Sigma, 0]) \\
&= \hbar c \frac{L^2}{\pi^2} \frac{\pi}{2} \left[\sum_{n=(0)1}^\infty \int_0^\infty r \, dr \sqrt{r^2 + \frac{n^2 \pi^2}{a^2}} - \int_0^\infty \int_0^\infty r \, dr \left(\frac{a}{\pi} dk_z \right) \sqrt{r^2 + k_z^2} \right] .
\end{aligned}
\tag{2.8}
$$

Eq. (2.8) is infinite and has to be regularized. Therefore we need a regularization scheme close to the physics of the problem.

In our system the "conductivity" of the plates decreases at high frequencies. This means that the "conductive" plates behave like a pair of transparent plates if they are exposed to waves with a very short wavelength. Consequently the defined cutoff

function of the system should mathematically impose that high frequency modes do not play any role in the resulting regularized Casimir interaction. Based on this physical argument one can define a high frequency cutoff $f(k/k_c)$

$$f(k/k_c) = \begin{cases} 1 & k \ll k_c \\ 0 & k \gg k_c \end{cases} , \qquad (2.9)$$

where the cutoff wave number k_c is determined by the properties of the material. This cutoff function also smoothens our chosen Dirichlet boundary conditions (mimicking "perfect conductor" boundary conditions) such that the field can penetrate into the plates as it does in real materials.

Introducing $u = a^2 r^2 / \pi^2$, the regularized Casimir energy reads

$$
\begin{aligned}
E_{\text{cas}}^{\text{reg}}[\Sigma, \partial S, f] &= \frac{\hbar}{2} \sum_k f(k/k_c) \left(\omega_k[\Sigma, \partial S] - \omega_k[\Sigma, 0] \right) \\
&= L^2 \hbar c \frac{\pi^2}{4a^3} \left[\sum_{(0)1}^{\infty} \int_0^{\infty} du \, \sqrt{n^2 + u} \, f\left(\frac{\pi \sqrt{n^2 + u}}{ak_c} \right) \right. \\
&\quad \left. - \int_0^{\infty} \int_0^{\infty} du \, dn \sqrt{n^2 + u} f\left(\frac{\pi \sqrt{n^2 + u}}{ak_c} \right) \right] \quad (2.10)
\end{aligned}
$$

Defining $w = u + n^2$ and

$$F(n) = \int_{n^2}^{\infty} dw \, w^{1/2} \, f\left(\frac{\pi w}{ak_c} \right) , \qquad (2.11)$$

where

$$
\begin{aligned}
F'(n) &= -2n^2 f\left(\frac{\pi n^2}{ak_m} \right) \\
F'(0) &= 0 \\
F'''(0) &= -4.
\end{aligned}
\qquad (2.12)
$$

Using the above definition in Eq. (2.10) we have

$$E_{\text{cas}}^{\text{reg}} = L^2 \hbar c \frac{\pi^2}{4a^3} \sum_{(0)1}^{\infty} F(n) - \int_0^{\infty} F(n) dn = -\frac{1}{12} F'(0) + \frac{1}{24 \times 30} F'''(0) + ... , \quad (2.13)$$

where to obtain the right hand side of Eq. (2.13) the Euler–Maclaurin formula [78] has been used. Thus we find the Casimir energy per unit area

$$\frac{E_{\text{cas}}}{L^2} = -\hbar c \frac{\pi^2}{720} \frac{1}{a^3} \ , \tag{2.14}$$

and the force per unit area is

$$\frac{F_{\text{cas}}}{L^2} = -\hbar c \frac{\pi^2}{240} \frac{1}{a^4} \ , \tag{2.15}$$

Eq. (2.14) states that there is an attractive force between two conductive plates that is independent of the material of the two plates. Due to the inverse power law of the Casimir force, it becomes larger when the plates are close to each other.

This method, which was employed in Casimir's original work [49] for a rectangular box, also applies for the case of conductive spherical shells in vacuum [79,80]. In both rectangular and spherical boundary conditions, it turns out that the resulting Casimir interaction is cutoff–independent.

However this simple method encounters serious difficulties if the geometry of the constraints becomes more complicated. The cumbersomeness of the boundary conditions also makes it almost impossible to find an analytical expression for the eigenmode energies ω_k. For this reason it is obvious that one needs to acquire more efficient methods for non-trivial geometries. In the following subsection we introduce a more efficient method of calculating the Casimir effect which is based on Green's function methods.

2.2.2   Green's function method

In the previous subsection it was mentioned that finding the zero-point energy sum for complicated geometries is not a mathematically simple task. In this section we review a method that partly circumvents the possible difficulties due to the specific geometry of the objects that are immersed in a fluctuating medium.

To calculate the vacuum energy needed for evaluating the Casimir force, this method utilizes the energy-momentum tensor $T^{\mu\nu}$ of the field attributed to fluctuations. The physical properties of vacuum can be deduced by using the components of this tensor, for instance, T^{00} is the energy density of vacuum, $T^{0\nu}$ and $T^{\mu 0}$ are associated with energy flow and the momentum density, respectively. Therefore to calculate the sum of the zero-point energy of the modes, one can simply use the 00 component of the energy-momentum tensor

$$\frac{1}{2} \sum_n \hbar \omega_n = \int d\mathbf{x} \, \langle T^{00}(\mathbf{x}) \rangle \, . \tag{2.16}$$

As was mentioned in the previous subsection, in vacuum, the sum in Eq. (2.16) is divergent. Nonetheless this can not cause any trouble in our later calculations since by applying appropriate boundary conditions the divergence will be removed [81].

We use this formalism to calculate the Casimir interaction between two parallel d–dimensional plates separated by a distance a and immersed in a massless scalar field ϕ which is produced by a source K with the equation of motion

$$-\Box \phi = K \, , \tag{2.17}$$

where $\Box = \frac{\partial^2}{\partial t^2} - \nabla^2$ is the d'Alembert operator. We also note that the natural units $c = \hbar = 1$ are used to simplify the calculations.

It is supposed that the field ϕ fulfills the Dirichlet boundary conditions on the plates

$$\phi(0) = \phi(a) = 0 \, . \tag{2.18}$$

On the other hand the canonical energy-momentum tensor for a massless scalar field

is

$$T^{\mu\nu} = \partial^\mu\phi\partial^\nu\phi - \frac{1}{2}g^{\mu\nu}\partial^\lambda\phi\partial_\lambda\phi \,, \tag{2.19}$$

where $g^{\mu\nu}$ is the Minkowski metric.

The "00" component of the energy-momentum tensor which is needed for our calculations reads

$$T_{00} = \frac{1}{2}\sum_{\lambda=0}^{3} \partial_\lambda\phi\,\partial_\lambda\phi \,. \tag{2.20}$$

To find $\partial_\lambda\phi\,\partial_\lambda\phi$ we can use the Green's function of this scalar field which is the expectation value of the time ordered product of the fields

$$G(\mathbf{x},t;\mathbf{x}',t') = i\langle\mathbf{T}\phi(\mathbf{x},t)\phi(\mathbf{x}',t')\rangle \,. \tag{2.21}$$

This Green's function can be found from the equation of motion of the field ϕ in Eq. (2.17)

$$\left(-\nabla^2 + \frac{\partial^2}{\partial t^2}\right)G(\mathbf{x},t;\mathbf{x}',t') = \delta(\mathbf{x}-\mathbf{x}')\delta(t-t') \,. \tag{2.22}$$

The reduced Green's function $g(z,z';k,\omega)$ based on the Fourier transforms is defined as

$$G(\mathbf{x},t;\mathbf{x}',t') = \int\frac{d^d k}{(2\pi)^d}e^{i\mathbf{k}.(\mathbf{x}_\parallel-\mathbf{x}_\parallel')}\int\frac{d\omega}{2\pi}e^{-i\omega(t-t')}g(z,z';k,\omega) \,, \tag{2.23}$$

where $x_\parallel$, $x_\parallel'$ are coordinates in the plane of the plates and z is chosen to be the coordinate perpendicular to the plates. The reduced Green's function satisfies the differential equation

$$\left(-\frac{\partial^2}{\partial z^2} - \lambda^2\right)g(z,z') = \delta(z-z') \,, \tag{2.24}$$

where $\lambda^2 = \omega^2 - k^2$ and $g(z,z') \equiv g(z,z';k,\omega)$.

Applying the Dirichlet boundary conditions (2.18) on Eq. (2.24) gives rise to

$$g(0,z') = g(a,z') = 0 \,, \tag{2.25}$$

thus the solution of Eq. (2.24) is

$$g(z,z') = \begin{cases} A\sin\lambda z & (0 < z < z' < a) \,, \\ B\sin\lambda(z-a) & (a > z > z' > 0) \,, \end{cases} \tag{2.26}$$

According to Eq. (2.24) $g(z, z')$ is continuous at $z = z'$ and its derivative has a unit step discontinuity at $z = z'$

$$A \sin \lambda z' - B \sin \lambda(z' - a) = 0 \ ,$$

$$A\lambda \cos \lambda z' - B\lambda \cos \lambda(z' - a) = 1 \ , \tag{2.27}$$

using the relations in (2.27), one can obtain A and B

$$A = -\frac{1}{\lambda} \frac{\sin \lambda(z' - a)}{\sin \lambda a} \ , \qquad B = -\frac{1}{\lambda} \frac{\sin \lambda z'}{\sin \lambda a} \ , \tag{2.28}$$

and finally the reduced Green's function reads

$$g(z, z') = -\frac{1}{\lambda \sin \lambda a} \sin \lambda z_< \sin \lambda(z_> - a) \tag{2.29}$$

where $z_>(z_<)$ is the greater (lesser) of z and z'.

As discussed above the vacuum expectation value of T_{00} is obtained from Eqs. (2.20), (2.21) and (2.29)

$$
\begin{aligned}
\langle T_{00} \rangle &= -i \lim_{\substack{\mathbf{x} \to \mathbf{x}' \\ t \to t'}} \partial_\lambda \partial_{\lambda'} G(\mathbf{x}, t; \mathbf{x}', t') \\
&= -\frac{1}{2i\lambda \sin \lambda a}[(\omega^2 + k^2) \sin \lambda z \sin \lambda(z - a) + \lambda^2 \cos \lambda z \cos \lambda(z - a)] \\
&= -\frac{1}{2i\lambda \sin \lambda a}[\omega^2 \cos \lambda a - k^2 \cos \lambda(2z - a)] \ , \tag{2.30}
\end{aligned}
$$

Integrating the above equation over z gives the energy per d-dimensional area between the plates. Integration of the second term produces a constant independent of a, therefore it does not have any effect in the Casimir interaction. Thus from the first term we have

$$\int_0^a dz \ \langle T_{00} \rangle = -\frac{\omega^2 a}{2i\lambda} \cot \lambda a \ . \tag{2.31}$$

Now we must integrate over the transverse momentum and frequency to obtain the energy density. This integration can be done by using a complex frequency rotation

$$\omega \to i\zeta, \quad \lambda \to i\sqrt{k^2 + \zeta^2} \equiv i\rho \ , \tag{2.32}$$

using these rotations we have

$$E_{\text{cas}} = -\frac{a}{2} \int \frac{d^d k}{(2\pi)^d} \int \frac{d\zeta}{2\pi} \frac{\zeta^2}{\rho} \coth \rho a \ , \tag{2.33}$$

putting back a correct dimensional factor $\hbar c$, multiplying the result of the above equation into $\hbar c$ to change back from the normal units, finally we find the Casimir energy density between the plates

$$E_{\text{cas}} = -\frac{\hbar c}{2^{d+2} \pi^{d/2+1}} \frac{1}{a^{d+1}} \Gamma\left(1 + \frac{d}{2}\right) \zeta(d+2) \ , \tag{2.34}$$

where $\Gamma(m)$ is the Gamma function and $\zeta(m)$ is the Riemann zeta function. Eq. (2.34) states that the Casimir interaction between two parallel d–dimensional plates is attractive and long–ranged.

Setting $d = 2$ into Eq. (2.34), the original Casimir result for a pair of two dimensional plates in Eq. (2.14) is recovered.

This result can also be used for a classical thermal field. This is possible after a Wick rotation

$$E_{\text{cas}}^{\text{cl}} = -\frac{k_{\text{B}} T}{2^{d+2} \pi^{d/2+1}} \frac{1}{a^{d+1}} \Gamma\left(1 + \frac{d}{2}\right) \zeta(d+2) \ . \tag{2.35}$$

The dimensions of Eq. (2.35) is $\text{Kg}/(\text{m}^{d-1}\text{s}^2)$ which differs by a factor of $1/\text{m}$ from the dimensions of the quantum Casimir energy density in Eq. (2.34). This is because of the dimensional difference between the quantum mechanical energy factor $\hbar c$ and the classical energy factor $k_{\text{B}} T$ originating from the extra time dimension in the quantum field theory. Thus $E_{\text{cas}}^{\text{cl}}$ corresponds to the energy density between $(d+1)$-dimensional plates in a $(d+2)$-dimensional fluctuating medium.

Using Eq. (2.35) for two parallel lines that are immersed in a two dimensional classical field and separated by the distance a, one obtains

$$E_{\text{cas}}^{\text{cl}} = -\frac{\pi\, k_{\text{B}} T}{24\, a} \ , \tag{2.36}$$

recalling that $\zeta(2) = \pi^2/6$.

In Subsec. 2.2.5, using a completely different approach, we recapitulate this result by

considering classical fields from the beginning of the calculations. The energy density in Eq. (2.36) will be recovered in the next subsection for a quantum mechanical field but with a new perspective on the boundaries in the system.

2.2.3 δ-potential approach

In the last subsection we reviewed a field theoretical method of calculating the Casimir effect based on the Green's function of the system's field. In this subsection we will go over a similar method which implements the Dirichlet boundary conditions differently through an interaction Lagrange density involving Dirac delta functions which represent the boundaries in the fluctuating medium [82]. Furthermore, it makes use of the spatial components of $T^{\mu\nu}$ instead of the temporal components used in the previous subsection. This approach was used for the first time by Bordag and coworkers [83, 84].

To demonstrate more clearly how this approach is employed to calculate the Casimir interaction, we consider two parallel lines $(1 + 1$ dimensions) in a massless scalar field ϕ and derive the Casimir interaction between them [85]. The boundaries in the system are implemented as an interaction of the field ϕ with two δ-potentials located at $z = 0$ and $z = a$. This can be described in terms of an interaction Lagrange density

$$\mathcal{L}_{\text{int}} = -\frac{\lambda}{a}\,\delta(z)\phi^2(z) - \frac{\lambda'}{2a}\delta(z-a)\phi^2(z) \tag{2.37}$$

where coupling constants λ and λ' are dimensionless. If the coupling constants tend to infinity $(\lambda \to \infty)$, these potentials enforce Dirichlet boundary conditions at the location of the two lines

$$\lambda, \; \lambda' \to \infty : \quad \phi(0), \; \phi(a) \to \; 0. \tag{2.38}$$

The Casimir interaction is evaluated by using the Green's function G which is the expectation value of the time ordered product of the fields, see Eq. (2.21), this Green's function satisfies

$$\left[\Box^2 + \frac{\lambda}{a}\delta(z) + \frac{\lambda'}{a}\delta(z-a)\right] G(z,t;z',t') = \delta(z-z')\delta(t-t') \,, \tag{2.39}$$

where $\Box^2 \equiv -\frac{\partial^2}{\partial z^2} + \frac{\partial^2}{\partial t^2}$ is the d'Alembert operator in $(1+1)$-dimensions. Similar to Eq. (2.23), the time Fourier transform $g(z, z'; \omega)$ of the Green's function

G is given by

$$G(z, t; z', t') = \int \frac{d\omega}{2\pi} \, \exp(-i\omega(t - t')) \, g(z, z'; \omega) \,, \qquad (2.40)$$

where the frequency contour of integration in Eq. (2.40) must pass below the singularities in ω on the negative real axis, and above those on the positive real axis [86,87]. The reduced Green's function of G satisfies

$$\left[-\frac{\partial^2}{\partial z^2} + \omega^2 + \frac{\lambda}{a}\delta(z) + \frac{\lambda'}{a}\delta(z - a) \right] g(z, z') = \delta(z - z') \,. \qquad (2.41)$$

Having found the solution to Eq. (2.41), we can find the Casimir *force* (instead of the energy) on one of the δ-function points by calculating the discontinuity of the energy–momentum tensor

$$\langle T^{\mu\nu} \rangle = \left(\partial^\mu \partial^{\nu\prime} - \frac{1}{2}g^{\mu\nu}\partial^\lambda \partial'^\lambda \right) \frac{1}{i}G(z, z')|_{z=z'} \,, \qquad (2.42)$$

To use $g(z, z')$ we define the reduced energy–momentum tensor

$$\langle T^{\mu\nu} \rangle = \int \frac{d\omega}{2\pi} t^{\mu\nu} \,. \qquad (2.43)$$

The energy–momentum tensor to the left of the point $z = a$ is

$$t_{zz}|_{z=a^-} = -\frac{\omega}{2}\left\{1 + 2\left[\left(\frac{2i\omega a}{\lambda} + 1\right)\left(\frac{2i\omega a}{\lambda'} + 1\right) e^{2i\omega a} - 1\right]^{-1}\right\} \qquad (2.44)$$

and the reduced energy–momentum tensor to the right of the point $z = a$ is

$$t_{zz}|_{z=a^+} = -\frac{\omega}{2} \qquad (2.45)$$

therefore the Casimir force on the point $z = a$ due to the quantum fluctuations in the massless scalar field reads

$$F_{\text{cas}} = \langle T_{zz} \rangle|_{z=a^-} - \langle T_{zz} \rangle|_{z=a^+} = -\frac{1}{4\pi a^2} \int_0^\infty dy\, y \frac{1}{(y/\lambda + 1)(y/\lambda' + 1)e^y - 1} \,. \qquad (2.46)$$

In the limit of $\lambda, \lambda' \to \infty$, the well-known result for two parallel lines [88, 89] is reproduced

$$\lim_{\lambda=\lambda'\to\infty} F_{\text{cas}} = -\frac{\pi\hbar c}{24a^2} \,. \qquad (2.47)$$

We mention that the above result has been multiplied by $\hbar c$ to recover the dimensions of the Casimir force.

This result is in agreement with the result obtained for two parallel lines using Eq. (2.36) in the previous subsection.

2.2.4   Path integral formalism: scattering matrix method

Up to this point in the section, we have investigated mode summation and Green's function methods. Although the mode summation method gives an idea how the evaluation of Casimir phenomenon was produced historically, it can not serve as an appropriate approach for more complicated geometries. Therefore we introduced the Green's function method that provides a field theoretical tool for calculating the Casimir interaction. However, obtaining an explicit solution for the Green's function in other geometries may also be difficult.

If the number of objects in a fluctuating medium increases or their shapes become more complex, employing more efficient methods is inevitable. On the other hand, the Casimir interaction is not analytically calculable for non-trivial shapes and consequently it has to be evaluated numerically in such cases. Thus the fast convergence of the method in terms of some expansion parameters is another determining issue.

In this subsection we review one of the most recent methods of calculating the Casimir interaction in a system composed of compact objects. This method provides the necessary tools for finding the Casimir force between a number of objects with a reliable convergence speed.

In this approach the Casimir force is treated as an interaction between fluctuations of source distributions defined on the surfaces of the compact objects. These source distributions are expanded in terms of multipoles and finally the resulting Casimir interaction can be obtained by a functional integral over the effective action of these multipoles [90, 91]. All the information about the shape of the objects and their boundary conditions in the system are introduced into the effective action via the scattering matrices of the objects. This concept is inspired by Schwinger's earlier work [92] that the Casimir interaction in a system consisting of metal and dielectric objects can be realized with regard to the electromagnetic interactions between fluctuations of charge and current in these objects.

To calculate the fluctuation-induced forces utilizing this concept, the partition function is written as a logarithm of a functional integral over all field fluctuations constrained by a set of boundary conditions.

According to Ref. [90], we consider a scalar quantum field , $\phi(\mathbf{x}, t)$ which is constrained by boundary conditions denoted by $\mathcal{C}$ on a set of fixed surfaces Σ_α, for $\alpha = 1, 2, ..., N,$. The surfaces are supposed to be closed and compact. The partition function of this system reads in path integral language

$$\mathcal{Z}[\mathcal{C}] = \int [\mathcal{D}\phi]_\mathcal{C}\, e^{(i/\hbar)S[\phi]} \,, \tag{2.48}$$

where the subscript $\mathcal{C}$ is representing the constraints imposed by the boundary conditions. The action for a free complex field is given by

$$S[\phi] = \int_0^T dt \int d\mathbf{x} \left(\frac{1}{c^2}|\partial_t \phi|^2 - |\nabla\phi|^2 \right) \,. \tag{2.49}$$

The Casimir energy of the system is obtained by subtracting the ground state energy when the objects are infinitely separated

$$\mathcal{E}[\mathcal{C}] = -\lim_{\Lambda \to \infty} \frac{\hbar c}{\lambda} \ln(\mathcal{Z}[\mathcal{C}]/\mathcal{Z}_\infty) \,, \tag{2.50}$$

where $\Lambda = icT$ and by taking the limit $\Lambda \to \infty$ the ground state energy is projected out in the trace in Eq. (2.48).

For Dirichlet boundary conditions, the corresponding constraint can be entered into the integral by introducing the sources ϱ_α

$$\int [\mathcal{D}\phi(\mathbf{x})]_\mathcal{C} = \int [\mathcal{D}\phi(\mathbf{x})] \prod_{\alpha=1}^{N} \int [\mathcal{D}\varrho_\alpha(\mathbf{x})] \exp\left[i\frac{T}{\hbar} \int_{\Sigma_\alpha} d\mathbf{x}(\varrho_\alpha^*(\mathbf{x})\phi(\mathbf{x}) + \text{c.c.}) \,. \right] \tag{2.51}$$

In Eq. (2.50) the integrals over the field $\phi(\mathbf{x}, t)$ can be written as an infinite product of integrals over the Fourier components, and the logarithm of $\mathcal{Z}$ turns into a sum. In the limit of $T \to \infty$, it is possible to replace the sum with an integral over $k = 2\pi n/(cT)$ and find the partition function in Fourier space at fixed k

$$3_\mathcal{C}(k) \equiv \prod_{\alpha=1}^{N} \int [\mathcal{D}\varrho_\alpha(\mathbf{x})] \int [\mathcal{D}\phi(\mathbf{x})] \exp\left(i\frac{T}{\hbar}\tilde{S}[\phi, \varrho] \right) \,, \tag{2.52}$$

where the new action $\tilde{S}$ includes both the fields and sources and is given by

$$\tilde{S}[\phi, \varrho] = \int d\mathbf{x} \, (k^2 |\phi(\mathbf{x})|^2 - |\nabla \phi(\mathbf{x})|^2) + \sum_\alpha \int_{\Sigma_\alpha} (\varrho_\alpha^*(\mathbf{x}) \phi(\mathbf{x}) + \text{c.c.}) \, . \tag{2.53}$$

To solve Eq. (2.52), the field $\phi(\mathbf{x})$ is separated into a classical and a fluctuation part

$$\phi(\mathbf{x}) = \phi_{\text{cl}}(\mathbf{x}) + \delta\phi(\mathbf{x}) \, , \tag{2.54}$$

where $\delta\phi(\mathbf{x})$ is the fluctuation part and $\phi_{\text{cl}}(\mathbf{x})$ is the solution to $\delta\tilde{S}[\phi, \varrho]/\delta\phi(\mathbf{x}) = 0$, which describes a complex scalar field coupled to a set of sources on the surfaces. ϕ_{cl} should satisfy the Helmholtz equation which for $r \to \infty$ is given by

$$\Phi(\mathbf{k}, \mathbf{x}) \sim e^{i\mathbf{k}.\mathbf{x}} + \frac{e^{ikr}}{r} f(\mathbf{k}, \mathbf{k}') \, , \tag{2.55}$$

where $f(\mathbf{k}, \mathbf{k}')$ is the scattering amplitude

$$f(\mathbf{k}, \mathbf{k}') = \frac{4\pi}{ik} \sum_{l'm'lm} i^{l-l'} \mathcal{T}_{l'm'lm}(k) Y_{l'm'}(\hat{\mathbf{k}}') Y_{lm}^*(\hat{\mathbf{k}}) \, , \tag{2.56}$$

where $\mathcal{T}_{l'm'lm}(k) \equiv \langle l'm'|\mathbb{T}(k)|lm\rangle$ and Y_{lm} are spherical harmonics. $\mathbb{T}$ is the transition matrix and its relation to the scattering matrix $\mathbb{S}$ is given by

$$\mathbb{T}(k) = \frac{1}{2}(\mathbb{S}(k) - \mathbb{1}) \, . \tag{2.57}$$

We recall that $\mathbb{S}$ connects the initial and final multipole states. It is possible to write the classical field in terms of the expansion of the free outgoing Helmholtz Green's function which is given by

$$\begin{aligned} \mathcal{G}_0(\mathbf{x}, \mathbf{x}', k) &\equiv \frac{e^{ik|\mathbf{x}-\mathbf{x}'|}}{4\pi|\mathbf{x}-\mathbf{x}'|} \\ &= ik \sum_{lm} j_l(kr_<) h_l^{(1)}(kr_>) \, Y_{lm}(\mathbf{x}) Y_{lm}^*(\mathbf{x}') \, . \end{aligned} \tag{2.58}$$

Here j_l and h_l are the spherical Bessel and Hankel functions, respectively. After performing the integral over ϕ in Eq. (2.52) one obtains

$$\mathfrak{Z}_\mathcal{C}(k) = \prod_{\alpha=1}^N \int [\mathcal{D}\varrho_\alpha(\mathbf{x})] \exp \left[\frac{i}{2} \frac{T}{\hbar} \sum_{\alpha,\beta} \int_{\Sigma_\alpha} \int_{\Sigma_\beta} d\mathbf{x} \, d\mathbf{x}' \varrho_\alpha^*(\mathbf{x}) \mathcal{G}_0(\mathbf{x}, \mathbf{x}', k) \varrho_\beta(\mathbf{x}') \right] \, , \tag{2.59}$$

where $\mathcal{G}_0$ is the Green's function introduced in Eq. (2.58).

To evaluate the above integral, first we calculate the integral in the exponential function argument in Eq. (2.59)

$$3_\mathcal{C}(k) = \prod_{\alpha=1}^{N} \int [\mathcal{D}Q_\alpha \, \mathcal{D}Q_\alpha^*] \exp[\frac{iT}{2\hbar} \begin{pmatrix} \mathbf{Q_1} \\ \mathbf{Q_2} \\ \vdots \end{pmatrix}^{\mathrm{T}} \begin{pmatrix} (\mathbb{T}^1)^{-1} & \mathbb{U}^{12} & \cdots \\ \mathbb{U}^{21} & (\mathbb{T}^2)^{-1} & \cdots \\ \vdots & \vdots & \vdots \end{pmatrix} \begin{pmatrix} \mathbf{Q_1} \\ \mathbf{Q_2} \\ \vdots \end{pmatrix}] \,,$$

$$(2.60)$$

where $\mathbb{U}^{\alpha\beta}$ is the translation matrix which translates the multipole indices of the same quantity from the coordinate system fixed to object α to the one fixed to object β, and $\mathbf{Q}_i$ is the multipole matrix consisting of multipole moments $Q_{\lambda,lm}$ of the source ϱ_λ

$$Q_{\lambda,lm} \equiv \int_{\Sigma_\lambda} d\mathbf{x}_\lambda \, j_l(kr_\lambda) Y_{lm}^*(\hat{\mathbf{x}}_\lambda) \varrho_\lambda(\hat{\mathbf{x}}_\lambda) \,. \tag{2.61}$$

Performing the last integral over the sources in Eq. (2.60) gives the Casimir interaction in the system.

For the case of two objects this interaction is

$$\mathcal{E}_2[\mathcal{C}] = \frac{\hbar c}{\pi} \int_0^\infty d\kappa \, \ln \det(1 - \mathbb{T}^2 \mathbb{U}^{21} \mathbb{T}^1 \mathbb{U}^{12}) \,, \tag{2.62}$$

where $\mathbb{T}^\alpha$ is the transition matrix and $\mathbb{U}^{\alpha\beta}$ is the translation matrix for the two objects.

For three objects the Casimir interaction takes the form

$$\begin{aligned} \mathcal{E}_3[\mathcal{C}] = \frac{\hbar c}{\pi} \int_0^\infty d\kappa \Big\{ & \ln \det(1 - \mathbb{T}^2 \mathbb{U}^{21} \mathbb{T}^1 \mathbb{U}^{12}) + \ln \det(1 - \mathbb{T}^3 \mathbb{U}^{31} \mathbb{T}^1 \mathbb{U}^{13}) \\ & + \ln \det[1 - (1 - \mathbb{T}^3 \mathbb{U}^{31} \mathbb{T}^1 \mathbb{U}^{13})^{-1} \\ & \times (\mathbb{T}^3 \mathbb{U}^{32} + \mathbb{T}^3 \mathbb{U}^{31} \mathbb{T}^1 \mathbb{U}^{12})(1 - \mathbb{T}^2 \mathbb{U}^{21} \mathbb{T}^{-1} \mathbb{U}^{12})^{-1} \\ & \times (\mathbb{T}^2 \mathbb{U}^{23} + \mathbb{T}^2 \mathbb{U}^{21} \mathbb{T}^1 \mathbb{U}^{13})] \Big\} \,, \end{aligned} \tag{2.63}$$

The first two terms in Eq. (2.63), similar to Eq. (2.62), produce the mutual scattering between objects 1 and 2 and objects 1 and 3, therefore they can be interpreted as the

separate two-body Casimir energies of two pairs of objects. The cumbersomeness of the third term is due to the fact that the Casimir forces are not pairwise additive. In other words, the interaction of objects 2 and 3 involves not only direct scattering between these two objects but also contains multiple scatterings off object 1.

This procedure can also be applied for more particles with a similar interpretation for the resulting Casimir effect. As mentioned in the beginning of this subsection, one of the advantages of this method is its optimal quick convergence.

In the following subsections we are going to discuss the Casimir phenomena for some classical systems. In the next subsection we represent the path integral formalism for a classical soft matter system. We will apply this approach for a pair of parallel lines and at the end we compare its result with what we obtained in the previous subsections by quantum fields.

2.2.5 Path integral formalism: application to a classical system

In the previous subsection we used the path integral formalism to derive the Casimir energy for a quantum scalar field. The partition function of the system was written in terms of the effective action of the sources distributed on the surface of the objects which were immersed in a fluctuating field. The specific characteristics of this approach is to enter the objects details through their scattering matrix.

In this subsection we intend to use the path integral formalism to find the Casimir interaction for colloidal particles immersed in a fluctuating medium. Although the method that we introduce in this subsection is similar to the approach of the previous subsection, the scattering matrix is not employed directly in the calculations. Here the partition function of the system is defined as the functional integral over the Boltzmann factor of the Hamiltonian describing a given fluctuating system [93]. This approach constitutes the basis of our calculations in the next chapter in which we will calculate the Casimir interaction between ellipsoidal colloids trapped at the interface of two fluid phases. In order to investigate this method more closely, we consider a general example of two manifolds immersed in a fluctuating medium, characterized by coordinates $\mathbf{r}_\alpha(x_\alpha)$. Here, x_α is a D_α dimensional internal coordinate for the αth manifold, and $\mathbf{r}_\alpha$ gives the position of the manifold in the d-dimensional fluid. The manifolds are separated by distance H and furthermore the fluid fluctuations are represented by a scalar field u which is governed by a Gaussian Hamiltonian

$$\mathcal{H}_0[u] = \frac{\beta\gamma}{2} \int d^d r \, u(\mathbf{r})(-\Delta + \lambda_c^{-2})u(\mathbf{r}) \,. \qquad (2.64)$$

The Casimir interaction between the manifolds are calculated by integrating over all possible fluid fluctuations, thus the partition function of this system reads

$$\mathcal{Z} = \mathcal{Z}_0^{-1} \int \mathcal{D}u(\mathbf{r}_\alpha(x_\alpha))|_{\mathbf{r}\in\Omega} \, \exp(-\beta\mathcal{H}_0)|_{u(\partial l)=0} \,. \qquad (2.65)$$

The trick to treat the Dirichlet boundary condition in Eq. (2.65), is to use a Dirac-delta function by defining auxiliary fields $\psi_\alpha(x_\alpha)$ on the manifolds (see also

Eq. (2.48))

$$\delta(u(\mathbf{r}_\alpha)) = \int \mathcal{D}\psi_\alpha(x_\alpha) \exp\left[i \int dx_\alpha \, \psi_\alpha(x_\alpha) \, u_\alpha(\mathbf{r}_\alpha(x_\alpha))\right] , \qquad (2.66)$$

inserting Eq. (2.66) into Eq. (2.65), we obtain

$$\mathcal{Z} = \mathcal{Z}_0^{-1} \int \mathcal{D}u \prod_{\alpha=1}^{2} \mathcal{D}\psi_\alpha(x_\alpha) \exp\left[i \int dx_\alpha \, \psi_\alpha(x_\alpha) \, u_\alpha(\mathbf{r}_\alpha(x_\alpha))\right] e^{-\beta \mathcal{H}_0} , \qquad (2.67)$$

where $\mathcal{Z}_0$ is the partition function for the undisturbed fluid and is multiplied into the partition function for regularization purposes. We put Eq. (2.64) into Eq. (2.67), thus

$$\mathcal{Z} = \mathcal{Z}_0^{-1} \int \prod_{\alpha=1}^{2} \mathcal{D}\psi_\alpha(x_\alpha) \int \mathcal{D}u \exp\left[-\frac{1}{2}\int d^d r \, u(-\Delta + \lambda_c^{-2})u + i \int dx_\alpha \psi_\alpha u\right] , \qquad (2.68)$$

where $\Delta \equiv \nabla^2$. The Gaussian integral over the field u in the above equation can be performed easily by recalling the general result of a Gaussian integral over a bilinear form

$$\int \mathcal{D}\mathbf{x} \exp(-\frac{1}{2}\mathbf{x}\mathbf{A}\mathbf{x} + \mathbf{b}\mathbf{x}) = (2\pi)^2(\det \mathbf{A})^{-1/2} \exp(\frac{1}{2}\mathbf{b}\mathbf{A}^{-1}\mathbf{b}) , \qquad (2.69)$$

thus

$$\mathcal{Z} = \int \prod_{\alpha=1}^{2} \mathcal{D}\psi_\alpha(x_\alpha) \exp\left[-\sum_{\alpha,\beta=1}^{2} \int dx_\alpha dx_\beta \, \psi_\alpha(x_\alpha) \, G^d(\mathbf{r}_\alpha - \mathbf{r}_\beta) \, \psi_\beta(x_\beta)\right] , \qquad (2.70)$$

where $G^d(\mathbf{r}_\alpha - \mathbf{r}_\beta)$ is the Green's function of the operator $\Delta' = \Delta - \lambda_c^{-2}$. Introducing $\mathcal{H}_1[\boldsymbol{\Psi}]$ as

$$\mathcal{H}_1[\boldsymbol{\Psi}] = \boldsymbol{\Psi}\mathbf{M}\boldsymbol{\Psi}^{\mathrm{T}} = -\sum_{\alpha,\beta=1}^{2} \int dx_\alpha \, dx_\beta \, \psi_\alpha(x_\alpha) \, G^d(\mathbf{r}_\alpha(\mathbf{x}_\alpha) - \mathbf{r}_\beta(\mathbf{x}_\beta)) \, \psi_\beta(x_\beta) , \qquad (2.71)$$

using $\mathcal{H}_1[\boldsymbol{\Psi}]$ in Eq. (2.70), the partition function may be rewritten as

$$\mathcal{Z} = \int \prod_{\alpha=1}^{2} \mathcal{D}\psi_\alpha(x_\alpha) \exp(-\mathcal{H}_1[\psi_\alpha(x_\alpha)]) . \qquad (2.72)$$

Computing the above integral gives

$$\mathcal{Z} = \sqrt{\det(\mathbf{M}[\mathbf{r}_\alpha(x_\alpha)])} \ . \tag{2.73}$$

At this point we can use the partition function in Eq. (2.73) and calculate the Casimir force between two manifolds that are separated by a distance H. In order to determine the Casimir force between the manifolds one needs to find the free energy of the system. The Casimir energy due to the insertion of the manifolds is given by the free energy of the constrained system (up to a constant)

$$\mathcal{F} = -k_{\mathrm{B}}T \ln \mathcal{Z} = \frac{k_{\mathrm{B}}T}{2} \ln \det(\mathbf{M}[\mathbf{r}_\alpha(x_\alpha)]) \ , \tag{2.74}$$

using $\ln \det(\mathbf{M}) = \mathrm{Tr} \ln(\mathbf{M})$, we can rewrite this as

$$\mathcal{F} = -\frac{k_{\mathrm{B}}T}{2} \mathrm{Tr} \ln(\mathbf{M}[\mathbf{r}_\alpha(x_\alpha)]) \ . \tag{2.75}$$

Similar to Eq. (2.62) or (2.63), this is a rather general result for the Casimir energy.

We will illustrate the actual computation of the Casimir energy again for the case of the manifolds being two D-dimensional parallel walls. This will also explain the technique used later on in the next chapter.

Supposing that $\mathbf{r}_1 = (\mathbf{x}, 0)$, $\mathbf{r}_1' = (\mathbf{y}, 0)$ are two points located on manifold 1 and $\mathbf{r}_2 = (\mathbf{x}, H)$, $\mathbf{r}_2' = (\mathbf{y}, H)$ are the points on manifold 2, then the matrix M in Eq. (2.75) reads

$$M(\mathbf{x}, \mathbf{y}) = \begin{pmatrix} G^d(\mathbf{x} - \mathbf{y}, 0) & G^d(\mathbf{x} - \mathbf{y}, H) \\ G^d(\mathbf{x} - \mathbf{y}, H) & G^d(\mathbf{x} - \mathbf{y}, 0) \end{pmatrix} \ , \tag{2.76}$$

Since the matrix M only depends on the difference $(\mathbf{x} - \mathbf{y})$ we can diagonalize it by transforming to Fourier space with the Fourier-transformed Green's functions

$$\tilde{G}^d(\mathbf{p}, \mathbf{q}; 0) = \int d^D x \, d^D y \, \exp(i\mathbf{p}.\mathbf{x} + i\mathbf{q}.\mathbf{y}) \, G^d(\mathbf{x} - \mathbf{y}, 0)$$

$$\tilde{G}^d(\mathbf{p}, \mathbf{q}; H) = \int d^D x \, d^D y \, \exp(i\mathbf{p}.\mathbf{x} + i\mathbf{q}.\mathbf{y}) \, G^d(\mathbf{x} - \mathbf{y}, H) \ . \tag{2.77}$$

Changing the variables in Eq. (2.77) with $\mathbf{x} - \mathbf{y} = \mathbf{r}$, $d^D x = d^D r$, we have

$$\tilde{G}^d(\mathbf{p}, \mathbf{q}; 0) = \int d^D r \, \exp[i\mathbf{p}.\mathbf{r}] \, G^d(\mathbf{r}, 0) \int d^D y \, \exp[i(\mathbf{p} + \mathbf{q}).\mathbf{y}] \tag{2.78}$$

which leads to

$$\tilde{G}^d(\mathbf{p}, \mathbf{q}; 0) = \tilde{G}^d(\mathbf{p}; 0) \, (2\pi)^D \, \delta^D(\mathbf{p} + \mathbf{q}) \, . \tag{2.79}$$

Inserting the above Fourier-transformed Green's function into Eq. (2.76) we obtain

$$\tilde{M}(\mathbf{p}, \mathbf{q}) = \begin{pmatrix} \tilde{G}^d(\mathbf{p}) & \tilde{G}^d(\mathbf{p}, H) \\ \tilde{G}^d(\mathbf{p}, H) & \tilde{G}^d(\mathbf{p}) \end{pmatrix} (2\pi)^D \, \delta^d(\mathbf{p} + \mathbf{q}) \, , \tag{2.80}$$

or equivalently

$$\tilde{M}(\mathbf{p}, \mathbf{q}) = \underbrace{\tilde{G}^d(\mathbf{p})}_{\mathbf{B}} \underbrace{\begin{pmatrix} \mathbb{1} & \frac{\tilde{G}^d(\mathbf{p}, H)}{\tilde{G}^d(\mathbf{p})} \\ \frac{\tilde{G}^d(\mathbf{p}, H)}{\tilde{G}^d(\mathbf{p})} & \mathbb{1} \end{pmatrix}}_{\mathbf{A}} (2\pi)^D \, \delta^d(\mathbf{p} + \mathbf{q}) \, , \tag{2.81}$$

thus the logarithm of $\tilde{M}$ separates into two parts

$$\ln[\tilde{M}] = \ln[\mathbf{A}] + \ln[\mathbf{B}] \, . \tag{2.82}$$

$\ln[A]$ can be calculated by using the Taylor expansion of a logarithm

$$\ln[\mathbf{A}] = \sum_{n=0}^{\infty} \frac{(-\mathbb{1})^n}{n+1} (\mathbf{A} - \mathbb{1})^{n+1} \, , \tag{2.83}$$

where

$$\mathbf{A} - \mathbb{1} = \frac{\tilde{G}^d(\mathbf{p}, H)}{\tilde{G}^d(\mathbf{p})} \begin{pmatrix} 0 & \mathbb{1} \\ \mathbb{1} & 0 \end{pmatrix} \, . \tag{2.84}$$

Eq. (2.83) is evaluated by noting

$$\mathbf{A}'^n = \begin{pmatrix} 0 & \mathbb{1} \\ \mathbb{1} & 0 \end{pmatrix}^n = \begin{cases} \mathbf{A}' & \text{if } n \text{ is odd} \\ \mathbf{I} & \text{if } n \text{ is even} \end{cases} \, , \tag{2.85}$$

here $\mathbf{I}$ is the unit matrix. Thus we have

$$\ln[\mathbf{A}] = \begin{pmatrix} -\sum_{n=1}^{\infty} \frac{1}{2n} \left(\frac{\tilde{G}^d(\mathbf{p}, H)}{\tilde{G}^d(\mathbf{p})} \right)^{2n} & \sum_{n=1}^{\infty} \frac{1}{2n+1} \left(\frac{\tilde{G}^d(\mathbf{p}, H)}{\tilde{G}^d(\mathbf{p})} \right)^{2n+1} \\ \sum_{n=1}^{\infty} \frac{1}{2n+1} \left(\frac{\tilde{G}^d(\mathbf{p}, H)}{\tilde{G}^d(\mathbf{p})} \right)^{2n+1} & -\sum_{n=1}^{\infty} \frac{1}{2n} \left(\frac{\tilde{G}^d(\mathbf{p}, H)}{\tilde{G}^d(\mathbf{p})} \right)^{2n} \end{pmatrix} \tag{2.86}$$

According to Eq. (2.75), to calculate the free energy, one has to determine the trace of $\ln M$, which can be found by using Eqs. (2.82) and (2.86).

$$\text{Tr}(\ln \tilde{M}) = 2\text{Tr}(\ln[\tilde{G}^d(\mathbf{p})]) + \text{Tr}\left(-\sum_{n=1}^{\infty} \frac{1}{n}\left(\frac{\tilde{G}^d(\mathbf{p}, H)}{\tilde{G}^d(\mathbf{p})}\right)^{2n}\right), \qquad (2.87)$$

using again the Taylor series of a logarithm, see Eq. (2.83), Eq. (2.87) can be contracted into

$$\text{Tr}(\ln[\tilde{M}]) = \text{Tr}\left(2\ln[\tilde{G}^d(\mathbf{p})] + \ln\left[1 - \left(\frac{\tilde{G}^d(\mathbf{p}, H)}{\tilde{G}^d(\mathbf{p})}\right)^2\right]\right) \qquad (2.88)$$

Using Eq. (2.88) and $\text{Tr} = \sum_m a_{mm} = \int dm$, where $dm = (S/(2\pi)^D)d^Dp$ and S is a D-dimensional area, we may rewrite the partition function in Eq. (2.75) as

$$-\frac{\ln \mathcal{Z}}{S} = \int \frac{d^Dp}{(2\pi)^D} \ln[\tilde{G}^d(\mathbf{p})] + \frac{1}{2}\int \frac{d^Dp}{(2\pi)^D} \ln\left[1 - \left(\frac{\tilde{G}^d(\mathbf{p}, H)}{\tilde{G}^d(\mathbf{p})}\right)^2\right]. \qquad (2.89)$$

Therefore, the Helmholtz free energy reads as

$$\begin{aligned}\mathcal{F} &= -k_B T \ln \mathcal{Z} \\ &= k_B T S \int \frac{d^Dp}{(2\pi)^D}\left(\ln[\tilde{G}^d(\mathbf{p})] + \frac{1}{2}\ln\left[1 - \left(\frac{\tilde{G}^d(\mathbf{p}, H)}{\tilde{G}^d(\mathbf{p})}\right)^2\right]\right). \qquad (2.90)\end{aligned}$$

Taking the derivative of $\mathcal{F}$ gives the Casimir force between two D-dimensional manifolds immersed in a d-dimensional fluid.

Let us look at a specific example. We consider two parallel lines ($D = 1$) trapped at a fluctuating interface between two fluid phases ($d = 2$), in this case the free energy in Eq. (2.90) takes the form

$$\mathcal{F} = k_B T l \int \frac{dp}{2\pi}\left(\ln[\tilde{G}^2(\mathbf{p})] + \frac{1}{2}\ln\left[1 - \left(\frac{\tilde{G}^2(\mathbf{p}, H)}{\tilde{G}^2(\mathbf{p})}\right)^2\right]\right), \qquad (2.91)$$

where l is the length of the lines.

In Eq. (2.91), $\tilde{G}^2$ is the Fourier transformed-Green's function of the Hamiltonian given in Eq. (2.64), thus $G^2(x - y)$ must satisfy

$$(-\Delta + \lambda_c^{-2})G^2(x - y) = \delta^2(x - y), \qquad (2.92)$$

wherefore the Fourier transform of G^2 is

$$\tilde{G}^2(\mathbf{p}) = \frac{1}{(p^2 + \lambda_c^{-2})} \; . \tag{2.93}$$

We find $\tilde{G}^2(\mathbf{p}, H)$ by using the definition of the Fourier transforms in Eq. (2.77)

$$
\begin{aligned}
\tilde{G}^2(\mathbf{p}, H) &= \int dx \, \exp(-\mathrm{i}px) \int \frac{d^2p'}{(2\pi)^2} \frac{\exp(\mathrm{i}p'x + \mathrm{i}p'_z H)}{(p'^2 + p'^2_z + \lambda_c^{-2})} \\
&= \int \frac{dp'_z}{2\pi} \frac{\exp(\mathrm{i}p'_z H)}{p^2 + p'^2_z + \lambda_c^{-2}} \; ,
\end{aligned}
\tag{2.94}
$$

or

$$\tilde{G}^2(\mathbf{p}, H) = \int \frac{dp'_z}{2\pi} \frac{\exp(\mathrm{i}p'_z H)}{(p'_z + \mathrm{i}\sqrt{p^2 + \lambda_c^{-2}})(p'_z - \mathrm{i}\sqrt{p^2 + \lambda_c^{-2}})} \; , \tag{2.95}$$

taking advantage of Cauchy's residue theorem we obtain

$$\tilde{G}^2(\mathbf{p}, H) = \frac{\exp(-H\sqrt{p^2 + \lambda_c^{-2}})}{2\sqrt{p^2 + \lambda_c^{-2}}} \; . \tag{2.96}$$

Putting Eqs. (2.93) and (2.96) into Eq. (2.91), the free energy of the system of two lines at the interface reads

$$\mathcal{F} = k_\mathrm{B} T l \int \frac{dp}{2\pi} \left(-\ln(2\sqrt{p^2 + \lambda_c^{-2}}) + \frac{1}{2}\ln(1 - \exp(-2H\sqrt{p^2 + \lambda_c^{-2}})) \right) \; . \tag{2.97}$$

We perform the latter integral over p in the limit $\lambda_c \to \infty$, thus

$$
\begin{aligned}
\mathcal{F} &= \frac{k_\mathrm{B} T l}{4\pi} \int_0^\infty dp \, \ln(1 - \exp(-2pH)) \\
&= -\frac{k_\mathrm{B} T l \pi}{24H} \; ,
\end{aligned}
\tag{2.98}
$$

taking the derivative of the above equation gives the Casimir force density between two parallel lines

$$\frac{F}{l} = -\frac{\partial \mathcal{F}}{\partial H} = -\frac{\pi k_\mathrm{B} T}{24H^2} \; . \tag{2.99}$$

As it is observed the Casimir force in this classical system is in accordance with the previous results for quantum systems, see Eqs. (2.34) and (2.47). This illustrates the equivalance of the classical Casimir interaction with the standard quantum Casimir effect.

As mentioned in the beginning, in the next chapter we use this approach to evaluate the Casimir interaction between two ellipsoidal colloids trapped at the interface of two fluid phases. There we investigate the Casimir interaction by paying special attention to the anisotropy of the colloidal particles and the interesting fact that the colloids (boundaries) are also fluctuating.

2.2.6 Critical Casimir interactions

In this concluding subsection we are going to investigate the critical Casimir forces that are associated with classical soft matter systems. Such interactions occur between the colloidal particles immersed in, e.g., a binary liquid mixture which is near its critical point. The fluctuations in these systems are provided by the fluctuations of the order parameter of a binary liquid mixture, and the geometrical restriction is imposed by the presence of some colloidal particles in the liquid mixture. This type of Casimir force causes the dissolved colloidal particles to flocculate.

In this section, based on Ref. [75], we review a mean-field method of calculating this kind of Casimir interaction between spherical colloids immersed in a binary liquid mixture.

The behavior of a binary liquid mixture near its critical point is governed by fluctuations of the order parameter Φ on a large length scale such that the resulting properties are independent of microscopic details. The continuum description of such a system can be found by a coarse-graining procedure in terms of the Ginzburg-Landau Hamiltonian [94] of an order parameter Φ in volume V

$$
\begin{aligned}
\mathcal{H}[\Phi] \;\; = \;\; & \int_V d^d r \left(\frac{1}{2}[\nabla\Phi(\mathbf{r})]^2 + \frac{\tau}{2}\Phi^2(\mathbf{r}) + \frac{u}{24}\Phi^4(\mathbf{r}) - h\Phi(\mathbf{r}) \right) \\
& + \int_S dS \left(\frac{c}{2}\Phi^2(\mathbf{r}_s) - h_1\Phi(\mathbf{r}_s) \right) \;,
\end{aligned}
\tag{2.100}
$$

the second integral runs over the surface $S = \partial V$ which bounds the critical liquid. In Eq. (2.100), $\tau = (T - T_c)/T_c$ is the reduced temperature, h is the external bulk field, c is related to the strength of the coupling of critical degrees of freedom near the surface, u is the coupling constant, h_1 is the surface analogue of the bulk field, and in the considered liquid system Φ is a scalar field.

As it is observed in Eq. (2.100), the theoretical basis of the Critical Casimir interaction is rather different from the previous approaches as it has to be dealt with by using the interacting ϕ^4 field theory.

The partition function of the system reads

$$\mathcal{Z} = \int \mathcal{D}\Phi \exp\left(-\mathcal{H}[\Phi(\mathbf{r})]\right) \tag{2.101}$$

and the corresponding free energy is given by

$$\mathcal{F} = -k_B T \ln \mathcal{Z} . \tag{2.102}$$

The Euler-Lagrange equation of the order parameter Φ is obtained by minimizing the free energy functional with respect to $\Phi(\mathbf{r})$. This minimization corresponds to the mean-field realization of the system

$$\left.\frac{\delta\mathcal{H}[\Phi(\mathbf{r})]}{\delta\Phi(\mathbf{r})}\right|_{\Phi=\langle\Phi\rangle} = 0 , \tag{2.103}$$

where $\langle\Phi\rangle$ is the mean-value of the fluctuating order parameter Φ. Minimization of Eq. (2.103) results in

$$-\Delta m + \tau m + m^3 - H = 0 , \tag{2.104}$$

where the coupling constant u has been observed in the new order parameter m and in the new bulk magnetic field H

$$m = \sqrt{\frac{u}{6}}\langle\Phi\rangle, \qquad H = \sqrt{\frac{u}{6}}h. \tag{2.105}$$

The order parameter profile, $m(\mathbf{r})$, can be found at the critical point analytically in terms of elliptic functions [95] and in the off criticality, it is worked out in terms of a short distance expansion [75]. Calculating the full profile is only possible numerically by discretization of the order parameter profile in the two sphere geometry [75]. Having found the order parameter profile, the necessary tools to calculate the critical Casimir interaction are at hand. The usual way of determining the Casimir interaction from free energy Eq. (2.102) and then calculating the derivative with respect to the inter-particle distance is not useful here, as one has to deal numerically with differences between large numbers that bring about large errors [75]. Consequently, one may calculate the force directly from the stress tensor $T_{\mu\nu}$

$$\delta\mathcal{H} = \int_V d^d r \frac{\partial b_\mu}{\partial x_\nu} T_{\mu\nu}(\mathbf{r}) \tag{2.106}$$

where $\mathbf{b}$ is a non-conformal coordinate transformation, μ and ν index the spatial coordinates, and $\delta\mathcal{H}$ is the energy shift.

In order to go beyond the mean-field approach, one may calculate universal scaling functions for microscopic Hamiltonians belonging to the same universality class as ϕ^4-field theory. In practice this is achieved via Monte-Carlo simulations of Ising model systems with appropriate obstacles inserted [96, 97]. We do not go deeper into these matters since the treatment of the Casimir effect in interacting systems is outside the scope of this thesis.

Chapter 3

Casimir Interaction between Ellipsoidal Colloids at a Fluid Interface

In this chapter we calculate the Casimir effect in a particular soft condensed matter system composed of two ellipsoidal particles that are trapped at the interface of two fluid phases. Since the interface height fluctuations are restricted by the presence of the particles there will be a fluctuation–induced force (or equivalently Casimir force) between the ellipsoids. This interaction is calculated here by employing the path integral method. This chapter is organized as follows. In Sec. 3.1 the physical system and the Hamiltonians that are used to describe our colloidal system are explained. Then we explain the method used to calculate the fluctuation–induced interaction between the particles for different boundary conditions. In Sec. 3.2 the Casimir interaction is derived as an expansion of the free energy for large distances between the particles that are fixed at the interface. In Sec. 3.3 along with the interface fluctuations, we allow particle fluctuation across the interface. In practical terms, this is the case when the colloids are not trapped by external forces like laser tweezers. In this section, the resulting Casimir interaction is found again as a series

for large interparticle distances. Finally we compare the Casimir force between fixed and fluctuating boundaries.

3.1 Model

The investigated system consists of two nano- or microscopic, uncharged spheroidal colloids with principal axes a, b, b ($a > b$), which are trapped at the interface of two fluid phases I and II. The effective interaction between the colloids is mediated by thermal height fluctuations of the (sharp) interface. Without fluctuations, the equilibrium interface is flat and is set to be at $z = 0$. Deviations from this planar reference meniscus are considered to be small, without overhangs and bubbles, therefore the Monge representation $(x, y, z = u(x, y)) = (\mathbf{x}, z = u(\mathbf{x}))$ is employed to describe the interface position. To have closer look on the physics of the thermal height fluctuations of the interface u, in the following subsection we recapitulate some properties of the capillary wave model of a fluid interface at finite temperatures [98]. These will be useful for discussing the properties of the Casimir-like forces in this chapter.

3.1.1 Capillary wave model of a free interface

We consider a free interface between two fluid phases and we set the flat equilibrium interface to be at $z = 0$, the xy-plane. This interface is deformed by thermally excited height fluctuations of the interface. To calculate the energy costs of the interface deformations we need to determine the free energy of the deformed interface, thus

$$\mathcal{F} = \gamma \int dA \tag{3.1}$$

where dA is the element of the interface, and γ is the surface tension for the flat equilibrium interface. An interface which is perturbed from its equilibrium position without overhanges and bubbles can be described by a field $u(x, y)$ of the coordinates

(x, y). The interface element dA is given by the vector product of the vectors tangent to the interface $\mathbf{a_x}$ and $\mathbf{a_y}$, therefore

$$dA = |\mathbf{a_x} \times \mathbf{a_y}| \, d\mathbf{r} \tag{3.2}$$

where $\mathbf{a_x} = (1, 0, \frac{\partial u}{\partial x})$, $\mathbf{a_y} = (0, 1, \frac{\partial u}{\partial y})$,

$$
\begin{aligned}
dA &= d\mathbf{r} \sqrt{1 + \left(\frac{\partial u}{\partial x}\right)^2 + \left(\frac{\partial u}{\partial y}\right)^2} \\
&\cong d\mathbf{r} \left(1 + \frac{(\nabla u)^2}{2}\right) .
\end{aligned} \tag{3.3}
$$

The second line of Eq.(3.3) is obtained after a small gradient expansion for a weakly undulated interface, $\frac{\partial u}{\partial x} \ll 1$ and $\frac{\partial u}{\partial y} \ll 1$. The first line of Eq. (3.3) constitutes the drumhead model which is well-known in the renormalization group analysis of interface problems, but is also used for the description of elastic surfaces (c.f. Ref. [99]).

After inserting Eq.(3.3) in Eq.(3.1) the free energy reads:

$$\mathcal{F} = \gamma \int d\mathbf{r} \; + \; \frac{\gamma}{2} \int d\mathbf{r} (\nabla u)^2 . \tag{3.4}$$

The capillary wave model basically assumes that excitations from the flat interface are thermally weighted by the capillary wave Hamiltonian

$$\mathcal{H}_{\text{cw}}[u] = \mathcal{F} - \gamma \int d\mathbf{r} = \frac{\gamma}{2} \int d\mathbf{r} \, (\nabla u)^2 , \tag{3.5}$$

which is the Taylor–expanded free energy difference between the total interface free energy and the free energy of the flat interface. .

Partition function

The partition function of the capillary wave model is the Boltzmann factor of the capillary wave Hamiltonian $\exp(-H_{\text{cw}}/k_{\text{B}}T)$ which is summed over all possible interface configurations

$$\mathcal{Z} \sim \int \mathcal{D}u \exp(-\beta \mathcal{H}_{\text{cw}}[u]) , \tag{3.6}$$

where $u \equiv u(\mathbf{r})$ is the interface position field. The integrals in Eq.(3.6) are performable in a more straightforward manner within Fourier space, thus as the first step the capillary wave Hamiltonian in Eq.(3.5) is treated in Fourier space by introducing the following Fourier representation for a system of size $L \times L$

$$u(\mathbf{r}) = \frac{1}{L^2} \sum_{\mathbf{k}} \tilde{u}(\mathbf{k}) \exp(-i\mathbf{k}.\mathbf{r}) ,$$

$$\tilde{u}(\mathbf{k}) = \int d\mathbf{r} \, u(\mathbf{r}) \exp(i\mathbf{k}.\mathbf{r}) , \qquad (3.7)$$

thus

$$\mathcal{H}_{\mathrm{cw}} = \frac{\gamma}{2L^2} \sum_{\mathbf{k}} \mathbf{k}^2 \, |\tilde{u}(\mathbf{k})|^2 . \qquad (3.8)$$

Therefore the partition function of the capillary wave Hamiltonian in Fourier space is a simple Gaussian integral

$$\mathcal{Z} \sim \int \mathcal{D}\tilde{u}(\mathbf{k}) \exp\left[-\frac{\beta\gamma}{2L^2} \sum_{\mathbf{k}} \mathbf{k}^2 |\tilde{u}(\mathbf{k})|^2 \right] . \qquad (3.9)$$

Average interface width

Using the partition function eq.(3.9) we can calculate the average interface width

$$\langle |\tilde{u}(\mathbf{k})|^2 \rangle = \mathcal{Z}^{-1} \int \mathcal{D}\tilde{u} \, |\tilde{u}(\mathbf{k})|^2 \exp\left[-\frac{\beta\gamma}{2L^2} \sum_{\mathbf{k}} \mathbf{k}^2 |\tilde{u}(\mathbf{k})|^2 \right] , \qquad (3.10)$$

separating the k-mode from other modes the average width may be rewritten as

$$\langle |\tilde{u}(\mathbf{k})|^2 \rangle = \frac{\int d\tilde{u}(\mathbf{k}) \, |\tilde{u}(\mathbf{k})|^2 \exp\left[-\frac{\beta\gamma}{2L^2} \mathbf{k}^2 |\tilde{u}(\mathbf{k})|^2 \right] \int \prod_{\mathbf{k}' \neq \mathbf{k}} d\tilde{u}(\mathbf{k}') \exp\left[-\frac{\beta\gamma}{2L^2} \sum_{\mathbf{k}' \neq \mathbf{k}} \mathbf{k}'^2 |\tilde{u}(\mathbf{k}')|^2 \right]}{\int d\tilde{u}(\mathbf{k}) \exp\left[-\frac{\beta\gamma}{2L^2} \mathbf{k}^2 |\tilde{u}(\mathbf{k})|^2 \right] \int \prod_{\mathbf{k}' \neq \mathbf{k}} d\tilde{u}(\mathbf{k}') \exp\left[-\frac{\beta\gamma}{2L^2} \sum_{\mathbf{k}' \neq \mathbf{k}} \mathbf{k}'^2 |\tilde{u}(\mathbf{k}')|^2 \right]} ,$$

which reduces to

$$\langle |\tilde{u}(\mathbf{k})|^2 \rangle = \frac{\int d\tilde{u}(\mathbf{k}) \, |\tilde{u}(\mathbf{k})|^2 \exp\left[-\frac{\beta\gamma}{2L^2} \mathbf{k}^2 |\tilde{u}(\mathbf{k})|^2 \right]}{\int d\tilde{u}(\mathbf{k}) \exp\left[-\frac{\beta\gamma}{2L^2} \mathbf{k}^2 |\tilde{u}(\mathbf{k})|^2 \right]} . \qquad (3.11)$$

Taking advantage of one dimensional Gaussian integrals we obtain the average interface width in Fourier space

$$\langle |\tilde{u}(\mathbf{k})|^2 \rangle = \frac{L^2}{\beta\gamma\mathbf{k}^2} \ . \tag{3.12}$$

In order to interpret the average width physically, we should transform eq.(3.12) back to real space. Using the Fourier transform of the field u introduced in Eq. (3.7), the Fourier transform of the average width reads

$$\langle u(\mathbf{r})^2 \rangle = \frac{1}{L^4} \sum_{\mathbf{k},\mathbf{k}'} \langle \tilde{u}(\mathbf{k})\tilde{u}(\mathbf{k}') \rangle \, e^{-i\mathbf{k}.\mathbf{r}} e^{+i\mathbf{k}'.\mathbf{r}} \ , \tag{3.13}$$

noting that $\langle u(\mathbf{k})u(-\mathbf{k}') \rangle = \delta_{\mathbf{k}\mathbf{k}'}\langle |\tilde{u}(\mathbf{k})|^2 \rangle$, the above equation simplifies to

$$
\begin{aligned}
\langle u(\mathbf{r})^2 \rangle &= \frac{1}{L^4} \sum_{\mathbf{k}} \langle |\tilde{u}(\mathbf{k})|^2 \rangle \\
&= \frac{1}{L^2\beta\gamma} \sum_{\mathbf{k}} \frac{1}{k^2} \ .
\end{aligned}
\tag{3.14}
$$

In large systems the sum over all Fourier modes can be replaced by an integral

$$\frac{1}{L^2} \sum_{\mathbf{k}} = \frac{1}{(2\pi)^2} \int d\mathbf{k} \ .$$

Using this, the average interface width becomes

$$\langle u(\mathbf{r})^2 \rangle = \frac{1}{4\pi^2\beta\gamma} \int_{k_{\mathrm{min}}}^{k_{\mathrm{max}}} \frac{d\mathbf{k}}{k^2} \ . \tag{3.15}$$

The upper and lower integration bounds in eq.(3.15) can be determined by the physical characteristic lengths in the system. The lower bound $k_{\mathrm{min}} = 2\pi/L$ is determined by the system size and the upper bound $k_{\mathrm{max}} = 2\pi/\sigma$ is determined by the molecular length scale. After changing the integration bounds, the integral in eq.(3.15) can be calculated easily. Lastly the average interface width in real space is

$$\langle u(\mathbf{r})^2 \rangle = \frac{1}{2\pi\beta\gamma} \ln\left(\frac{L}{\sigma}\right) \ . \tag{3.16}$$

Eq.(3.16) shows that the interface width is divergent as it increases logarithmically with the system size. Nevertheless, in practice this is not an important issue because the logarithmic divergence is quite weak.

Corrected capillary wave Hamiltonian

In the earth's gravitational field, we suppose that the undisturbed interface is located at $u(r) = 0$ which can be taken as the reference point of the potential. After elevation of the interface, the potential of phase I increases to

$$\int_0^u du\, \rho_{\mathrm{I}}\, g\, u(\mathbf{r}) = \frac{1}{2}\rho_{\mathrm{I}}\, g\, u(\mathbf{r})^2$$

per unit horizontal area, on the other hand the potential energy of the phase II decreases to $-\frac{1}{2}\rho_{\mathrm{II}} g u(\mathbf{r})^2$ per unit horizontal area. Consequently the potential energy correction to the capillary Hamiltonian is

$$\frac{1}{2}\int d\mathbf{r}(\rho_{\mathrm{I}} - \rho_{\mathrm{II}})g u^2(\mathbf{r}) = \frac{\gamma}{2}\int d\mathbf{r}\frac{u^2}{\lambda_{\mathrm{c}}^2}\;. \tag{3.17}$$

Adding the above result to the capillary wave Hamiltonian, we obtain

$$\mathcal{H}'_{\mathrm{cw}} = \frac{\gamma}{2}\int d\mathbf{r}\left[(\nabla u)^2 + \frac{u^2}{\lambda_{\mathrm{c}}^2}\right]\;. \tag{3.18}$$

As demonstrated above, the Hamiltonian $\mathcal{H}_{\mathrm{cw}}$ in its original form (Eq. (3.5)) is plagued with both a short-wavelength and a long-wavelength divergence which, however, we treated by physical cutoffs. As discussed before, the short-wavelength cutoff is set by the molecular length-scale σ of the fluid at which the capillary wave model ceases to remain valid. The long wavelength divergence is reminiscent of the fact that the capillary waves are Goldstone modes. Of course, in real systems, instead of the system size L, the gravitational field provides a natural damping for capillary waves which is given by the second term in Eq. (3.18). Usually, in simple liquids, λ_{c} is in the range of millimeters and, therefore, is by far the longest length scale in the system. In fact, here it plays the role of a long wavelength cutoff of the capillary wave Hamiltonian $\mathcal{H}_{\mathrm{cw}}$, and we will discuss our results in the limit $\lambda_c \gg R$ and $\lambda_c \gg d$.

Eq. (3.18) in Fourier space reads

$$\mathcal{H}'_{\mathrm{cw}} = \frac{\gamma}{2L^2}\sum_{\mathbf{k}}(\mathbf{k}^2 + \lambda_{\mathrm{c}}^{-2})u^2(\mathbf{k})\;. \tag{3.19}$$

Corrected average interface width

At this point we can calculate the average interface width using the corrected capillary Hamiltonian

$$\langle |\tilde{u}(\mathbf{k})|^2 \rangle = \mathcal{Z}^{-1} \int \mathcal{D}\tilde{u}(\mathbf{k}) \, |\tilde{u}(\mathbf{k})|^2 \exp\left[-\frac{\beta\gamma}{2L^2} \sum_{\mathbf{k}} (\mathbf{k}^2 + \lambda_c^{-2}) \, |\tilde{u}(\mathbf{k})|^2 \right] . \qquad (3.20)$$

Similar to the derivation of Eq. (3.12) we obtain

$$\langle |\tilde{u}(\mathbf{k})|^2 \rangle = \frac{L^2}{\beta\gamma(\mathbf{k}^2 + \lambda_c^{-2})} , \qquad (3.21)$$

and the average interface width in real space is

$$\langle u(\mathbf{r})^2 \rangle = \frac{1}{4\pi^2 \beta\gamma} \int_0^{2\pi/\sigma} \frac{d\mathbf{k}}{k^2 + \lambda_c^{-2}} . \qquad (3.22)$$

Analogously to Eq. (3.16) we have

$$\langle u(\mathbf{r})^2 \rangle = \frac{1}{4\pi\beta\gamma} \ln\left(\frac{(\frac{2\pi}{\sigma})^2 + \lambda_c^{-2}}{\lambda_c^{-2}} \right) , \qquad (3.23)$$

since $\sigma \ll \lambda_c$, Eq. (3.23) reduces to

$$\langle u(\mathbf{r})^2 \rangle \sim \frac{1}{2\pi\beta\gamma} \ln\left(\frac{\lambda_c}{\sigma} \right) . \qquad (3.24)$$

Comparing the interface width in Eqs. (3.16) and (3.24), we see that the precise way of incorporating the long-wavelength cut-off is unimportant for the effects on the colloidal length scale, see the discussion in Ref. [100] . Nonetheless, in both approaches ($k_{\min} = 2\pi/L$ and $2\pi/\lambda_c$) the width of the interface related to the capillary wave is logarithmically divergent, $\langle u(0)^2 \rangle \sim \ln \lambda_c[L]/\sigma$.

Capillary wave Hamiltonian correlation length

The height–height correlation function of the capillary Hamiltonian $G_0(\mathbf{r}) = \langle u(\mathbf{r})u(0) \rangle$ in Fourier space is

$$G_0(\mathbf{r}) = \frac{1}{L^4} \sum_{\mathbf{k},\mathbf{k}'} \langle \tilde{u}(\mathbf{k})\tilde{u}(-\mathbf{k}') \rangle \, e^{-i\mathbf{k}.\mathbf{r}} . \qquad (3.25)$$

after suming over $\mathbf{k}'$ and using $\langle \tilde{u}(\mathbf{k})\tilde{u}(-\mathbf{k}')\rangle = \delta_{\mathbf{kk}'}\langle|\tilde{u}(\mathbf{k})|^2\rangle$ we find

$$
\begin{aligned}
G_0(\mathbf{r}) &= \frac{1}{L^2}\sum_{\mathbf{k}}\langle|\tilde{u}(\mathbf{k})|^2\rangle\, e^{-i\mathbf{k}.\mathbf{r}} \\
&= \frac{1}{4\pi^2}\int\frac{d\mathbf{k}}{\beta\gamma(k^2+\lambda_{\mathrm{c}}^{-2})}\,e^{-i\mathbf{k}.\mathbf{r}}\ ,
\end{aligned}
\tag{3.26}
$$

which leads to

$$
G_0(\mathbf{r}) = \frac{1}{4\pi^2\beta\gamma}\int dk\,d\theta\,\frac{k\,e^{-ikr\cos\theta}}{k^2+\lambda_{\mathrm{c}}^{-2}}\ .
\tag{3.27}
$$

The integral over θ may be straightforwardly evaluated by noting that

$$
\int_0^{2\pi} d\theta\,e^{-ikr\cos\theta} = 2\pi J_0(kr)\ ,
$$

therefore

$$
G_0(\mathbf{r}) = \frac{1}{2\pi\beta\gamma}\int dk\,\frac{k\,J_0(kr)}{k^2+\lambda_{\mathrm{c}}^{-2}}\ .
\tag{3.28}
$$

The integral in Eq. (3.28) can be calculated by using Hankel-Nicholson type integrals
[78]

$$
\int_0^{\infty}\frac{t^{\nu+1}\,J_\nu(at)\,dt}{(t^2+z^2)^{\mu+1}} = \frac{a^\mu z^{\nu-\mu}}{2^\mu\,\Gamma(\mu+1)}K_{\nu-\mu}(az)\ .
\tag{3.29}
$$

In order to evaluate Eq. (3.28), one has to use the above integral with $\nu = \mu = 0$,
that gives

$$
G_0(\mathbf{r}) = \frac{1}{2\pi\beta\gamma}K_0\left(\frac{r}{\lambda_{\mathrm{c}}}\right)\ .
\tag{3.30}
$$

For small x and $0 < x \le 1$, we have $K_0(x) \approx -\ln(\frac{\gamma_{\mathrm{e}} x}{2})$, where γ_{e} is the Euler-
Mascheroni constant exponentiated. Thus for $r \ll \lambda_{\mathrm{c}}$

$$
G_0(\mathbf{r}) \sim -\frac{1}{2\pi\beta\gamma}\ln\left(\frac{\gamma_{\mathrm{e}} r}{\lambda_{\mathrm{c}}}\right)\ .
\tag{3.31}
$$

The correlation function in Eq. (3.31) corresponds to the Green's function of the
capillary wave Hamiltonian. To show this, we apply the capillary wave operator
$\beta\gamma(-\Delta+\lambda_{\mathrm{c}}^{-2})$ in Eq. (3.18) to Eq. (3.26) and obtain

$$
\begin{aligned}
\beta\gamma(-\Delta+\lambda_{\mathrm{c}}^{-2})G_0(\mathbf{r}) &= \beta\gamma\frac{-\Delta+\lambda_{\mathrm{c}}^{-2}}{4\pi^2}\int\frac{d\mathbf{k}}{\beta\gamma(k^2+\lambda_{\mathrm{c}}^{-2})}\,e^{-i\mathbf{k}.\mathbf{r}} \\
&= \delta(\mathbf{r})\ .
\end{aligned}
\tag{3.32}
$$

It is also possible to recover the capillary wave model by analyzing the correlation between density fluctuations at the interface. An extensive analysis of such correlations was done by Wertheim in terms of the two dimensional Fourier transform of the direct and total correlation functions of the liquid–vapor interface of a simple fluid [101]

$$\frac{1}{L^2} \sum e^{i\mathbf{k.r}} \langle \delta\rho(\mathbf{r}, z)\delta\rho(0, z') \rangle \sim \frac{\rho'(z)\rho'(z')}{k^2 + \lambda_c^2} \ . \tag{3.33}$$

where $\rho(z)$ is the equilibrium intrinsic density profile across the interface and $\delta\rho(\mathbf{r}, z)$ are density fluctuations around this profile. To show the equivalence of the height–height correlation function in Eq. (3.26) and the correlation function obtained by considering the density fluctuations, we follow a work done by Stecki [102]. we suppose that the thermally excited displacement of the interface position $u(\mathbf{r})$ is connected to the density fluctuations $\delta\rho(\mathbf{r}, z)$ by

$$\delta\rho(\mathbf{r}, z) = \rho(z - u(\mathbf{r})) - \rho(z) \ . \tag{3.34}$$

Moreover, we assumed that the Gibbs interface is placed at $z = 0$. Since the displacement of the interface is considered to be small, we can use the leading term of the density fluctuation expansion

$$\delta\rho(\mathbf{r}, z) = -u(\mathbf{r}) \, \partial_z \rho(z) \, + \dots \ . \tag{3.35}$$

Therefore the total correlation function $H(\mathbf{r}_1, \mathbf{r}_2) = \langle \delta\rho(\mathbf{r}_1)\delta\rho(\mathbf{r}_2) \rangle$ leads to

$$H(\mathbf{r}_1, \mathbf{r}_2) = \langle u(\mathbf{r_1})u(\mathbf{r_2}) \rangle \, \rho'(z_1) \, \rho'(z_2) \ . \tag{3.36}$$

Identifying Eq. (3.36) and Eq. (3.33) gives

$$\frac{1}{L^2} \sum e^{i\mathbf{k.(r_1 - r_2)}} \langle u(\mathbf{r_1})u(\mathbf{r_2}) \rangle \sim \frac{1}{k^2 + \lambda_c^2} \ , \tag{3.37}$$

which is in accrod with Eq. (3.26) obtained by the capillary wave model.

3.1.2 Total Hamiltonian of ellipsoidal colloids at a fluid interface

Having familiarized ourselves with the physical properties of a free interface and introduced the capillary wave model, we return to the main system, i.e. ellipsoidal colloids trapped at the interface between two fluid phases.

As mentioned before the equilibrium position of the planar interface is set to be at $z = 0$. On the other hand the equilibrium position of the colloids is assumed to be symmetrical with respect to $z \to -z$, such that at the contact line the contact angle is $\pi/2$. The elliptic cross-section of the ellipsoids with the equilibrium interface is denoted by $S_{i,\mathrm{ref}}$ which is an ellipse with major and minor axes a, b, respectively. $S_{i,\mathrm{ref}}$ may also be expressed in confocal elliptic coordinates by the elliptic radius ξ_0, see App. A for the coordinate definitions. The equilibrium interface at $z = 0$ without the two elliptic holes $S_{i,\mathrm{ref}}$ cut out by the colloids is termed the reference meniscus $S_{\mathrm{men,ref}} = \mathbb{R}^2 \setminus \cup_i S_{i,\mathrm{ref}}$.

We note that the ellipsoidal colloids are of Janus type, thus the contact line is always pinned to their surface. The total Hamiltonian of the system which is used for calculating the free energy costs of thermal fluctuations around the flat interface is determined by the change in interfacial energy of the interface I/II between the fluid phases. In the spirit of the capillary wave model, we perform a small gradient expansion

$$
\begin{aligned}
\mathcal{H}_{\mathrm{tot}} = \gamma \Delta A_{\mathrm{men}} &= \gamma \int_{S_{\mathrm{men}}} d^2x \, \sqrt{1 + (\nabla u)^2} - \gamma \int_{S_{\mathrm{men,ref}}} d^2x \\
&\approx \frac{\gamma}{2} \int_{S_{\mathrm{men,ref}}} d^2x \, (\nabla u)^2 + \gamma \Delta A_{\mathrm{proj}} \,.
\end{aligned}
\tag{3.38}
$$

Here $\gamma \Delta A_{\mathrm{men}}$ expresses the energy needed for creating the additional meniscus area associated with the interface height fluctuations. In Eq. (3.38), S_{men} is the meniscus area projected onto the plane $z = 0$ (where the reference interface is located) and $S_{\mathrm{men,ref}}$ is the meniscus in the reference configuration mentioned above. In the second line we have applied the small gradient expansion which is valid for slopes $|\nabla u| \ll 1$
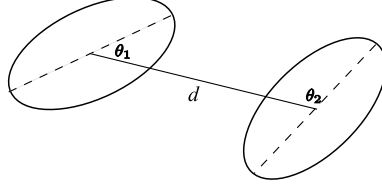
Figure 3.1: Top view of the system

and which provides the long wavelength description of the interface fluctuations we are interested in. The small gradient expansion entails that

$$\Delta A_{\text{proj}} = \int_{S_{\text{men}} \backslash S_{\text{men,ref}}} d^2x \, \sqrt{1 + (\nabla u)^2} \approx \int_{S_{\text{men}} \backslash S_{\text{men,ref}}} d^2x \qquad (3.39)$$

is approximately the change in projected meniscus area with respect to the reference configuration. We rewrite this change in projected meniscus area in terms of the interface position $f_i = u(\partial S_{i,\text{ref}})$ at the reference contact line ellipses $\partial S_{i,\text{ref}}$. f_i corresponds (in a second order approximation) to the contact line of the colloid i with fluctuating center position h_i and fluctuating orientation. The contact line which is a function of the elliptic angle η only (see App. A for the definition of elliptic coordinates) is expanded as

$$f_i = u(\partial S_{i,\text{ref}}) = \sum_{m=0} (P_{im} \, \cos(m\eta_i) + Q_{im} \, \sin(m\eta_i)) \qquad (3.40)$$

and we refer to the coefficients P_{im} and Q_{im} as boundary multipole moments below. The desired expression of ΔA_{proj} in terms of boundary multipole moments proceeds as discussed in Ref. [100] and allows us to identify it as a sum over boundary Hamiltonians $\mathcal{H}_{i,\text{b}}$ for each colloid i (see also App. C):

$$\begin{aligned} \gamma \Delta A_{\text{proj}} &\equiv \sum_i \mathcal{H}_{\text{b},i}[f_i] \\ &= \sum_i \frac{\pi\gamma}{2} \left(\tanh \xi_0 \, P_{i1}^2 + \coth \xi_0 \, Q_{i1}^2 \right) \,. \end{aligned} \qquad (3.41)$$

We note that the boundary Hamiltonians $\mathcal{H}_{\text{b,i}}$ can be viewed as the energy cost due to fluctuations of the contact line (which in turn are caused by colloid height and tilt

Figure 3.2: Side view of the system

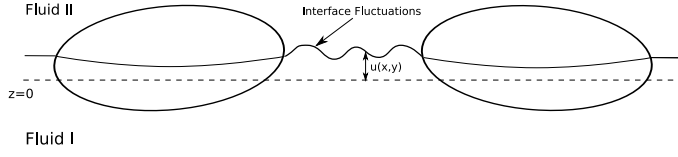fluctuations). Putting Eqs. (3.38) and (3.41) together, the total change in interfacial energy is the sum

$$\mathcal{H}_{\text{tot}} \;=\; \mathcal{H}_{\text{cw}} + \mathcal{H}_{\text{b},1} + \mathcal{H}_{\text{b},2} = \frac{\gamma}{2} \int_{S_{\text{men,ref}}} d^2x \, (\nabla u)^2 + \mathcal{H}_{\text{b},1} + \mathcal{H}_{\text{b},2} \quad (3.42)$$

where $\mathcal{H}_{\text{cw}}$ is the capillary wave Hamiltonian introduced in Eq. (3.5) and describes the energy differences associated with the additional interfacial area over the reference configuration.

3.1.3 Helmholz free energy

In order to calculate the interaction force between the colloids, one has to determine the Helmholz free energy of the system. However, via the integration domain of $\mathcal{H}_{\text{cw}}$, the total Hamiltonian of the system, Eq. (3.42), implicitly depends on the geometric configuration. This leads to a free energy $\mathcal{F}(d, \theta_1, \theta_2)$ which depends on the distance d between the colloid centers and the orientation angles θ_1 and θ_2 of their major axes with respect to the distance vector joining the colloid centers (see Fig. 3.1). The free energy is related to the partition function $\mathcal{Z}(d, \theta_1, \theta_2)$ of the system by

$$\mathcal{F}(d, \theta_1, \theta_2) = -k_{\text{B}} T \ln \mathcal{Z}(d, \theta_1, \theta_2) \quad (3.43)$$

The partition function is obtained by a functional integral over all possible interface configurations u and boundary configurations f_i; the relation between interface and boundary configurations is included by δ-function constraints,

$$\mathcal{Z} = \mathcal{Z}_0^{-1} \int \mathcal{D}u \, \exp\left\{ -\frac{\mathcal{H}_{\text{cw}}[u]}{k_{\text{B}}T} \right\} \prod_{i=1}^{2} \int \mathcal{D}f_i \prod_{\mathbf{x}_i \in \partial S_{i,\text{ref}}} \delta[u(\mathbf{x}_i) - f_i(\mathbf{x}_i)] \exp\left\{ -\frac{\mathcal{H}_{\text{b},i}[f_i]}{k_{\text{B}}T} \right\} .$$

$$(3.44)$$

Here $\mathcal{Z}_0$ is a normalization factor such that $\mathcal{Z}(d \to \infty) = 1$ and ensures a proper regularization of the functional integral. Via the δ-functions the interface field u is coupled to the contact line height f_i and therefore, the boundary Hamiltonians $\mathcal{H}_{i,\mathrm{b}}$ have a crucial influence on the resulting effective interaction between the colloids. The kind of possible contact line fluctuations f_i is solely determined by the colloid fluctuations since the contact line is pinned. These fluctuations are vertical fluctuations of the colloids on the axis normal to the equilibrium interface (height) and orientational fluctuations around that axis (tilts). In order to incorporate various boundary counditions into the solutions, we categorize them into three cases:

(A) colloids are fixed in the reference configuration, thus there are no integrations over the boundary terms.

(B) colloid heights fluctuate freely without tilting, thus the boundary monopoles must be included in the integration measure so that $\mathcal{D}f_i = dP_{i0}$.

(C) unconstrained height and tilt fluctuations. Up to second order in the tilts this corresponds to the inclusion of boundary dipoles in the integration measure, thus $\mathcal{D}f_i = dP_{i0}\, dP_{i1}\, dQ_{i1}$.

Case (A) corresponds to the "standard" Casimir effect in 2d with Dirichlet boundary conditions $f_i = u(\partial S_{i,\mathrm{ref}}) = 0$. We call this the interface fluctuation part and it will be treated in Sec. 3.2. The inclusion of the colloid height and tilt fluctuations in (B) and (C) is given in Sec. 3.3.

We summarize the model setup for our problem at hand in view of the general discussion of the Casimir effect in chapter 2. The interface fluctuations are treated with a two dimensional Gaussian scalar field theory, and the colloid appear as elliptic obstacles which are either fixed (case (A), Dirichlet boundary conditions) or fluctuate (case (B) and (C)). We recall that the Dirichlet boundary conditions in the case (A) has been also investigated in the previous chapter by applying different methods for the case of two lines immersed in a scalar field. This result (See Subsec. 2.2.5) will

be used in this chapter for calculating the Casimir interaction at close distances via the Derjaguin approximation.

On the other hand in cases (B) and (C) the colloids fluctuations are also included on top of the interface fluctuations. In these two cases the effect of the fluctuating boundaries are introduced by means of a boundary Hamiltonian. This approach is similar to the method introduced in Subsec. (2.2.3) since the interaction δ-potentials can also be viewed as a very specific form of a boundary Hamiltonian defined to treat the fluctuating boundaries.

3.2 Interface fluctuation part

The partition function $\mathcal{Z}_{\text{in}}$ for fixed contact lines $f_i = 0$ is given by

$$\mathcal{Z}_{\text{in}} = \mathcal{Z}_0^{-1} \int \mathcal{D}u \prod_{i=1}^{2} \prod_{\mathbf{x}_i \in \partial S_{i,\text{ref}}} \delta(u(\mathbf{x}_i)) \exp\left\{ -\frac{\mathcal{H}_{\text{cw}}[u]}{k_{\text{B}}T} \right\} . \qquad (3.45)$$

The disappearance of the interface fluctuations at the colloids boundaries (Dirichlet boundary condition) is included by the Dirac delta function. In this section, analytical expressions for the fluctuation induced force in the intermediate asymptotic regime $a \ll d \ll \lambda_c$ are calculated.

The course of the derivation is analogous to the derivation of the Casimir effect in the method presented in Sec. 2.2.5. Here it is performed for the case of two ellipsoidal obstacles.

We express the δ-functions in Eq. (3.45) by their integral representation via auxiliary fields $\psi_i(\mathbf{x}_i)$ defined on the reference contact lines $\partial S_{i,\text{ref}}$. This enables us to integrate out the field u leading to

$$\mathcal{Z}_{\text{in}} = \mathcal{Z}_0'^{-1} \int \prod_{i=1}^{2} \mathcal{D}\psi_i \, \exp\left\{ -\frac{k_{\text{B}}T}{2\gamma} \sum_{i,j=1}^{2} \int_{\partial S_{i,\text{ref}}} d\ell_i \int_{\partial S_{j,\text{ref}}} d\ell_j \, \psi_i(\mathbf{x}_i) \, G(|\mathbf{x}_i - \mathbf{x}_j|) \, \psi_j(\mathbf{x}_j) \right\} ,$$
$$(3.46)$$

where $d\ell_i$ is the infinitesimal line segment on the circles $\partial S_{i,\text{ref}}$. After this integration, the normalization factor is changed, $\mathcal{Z}_0 \to \mathcal{Z}_0'$, such that $\mathcal{Z}_{\text{in}}(d \to \infty) = 1$ still holds. In Eq. (3.46) we introduced the Greens function of the operator $(-\Delta + \lambda_c^{-2})$ which is given by $G(\mathbf{x}) = K_0(|\mathbf{x}|/\lambda_c)/(2\pi)$ where K_0 is the modified Bessel function of the second kind (See Eq. (3.30)). In the range $d/\lambda_c \ll 1$ and $r_0/\lambda_c \ll 1$, we can use the asymptotic form of the K_0 for small arguments, such that $2\pi \, G(|\mathbf{x}|) \approx -\ln(\gamma_{\text{e}}|\mathbf{x}|/2\lambda_c)$. Here, $\gamma_{\text{e}} \approx 1.781972$ is the Euler-Mascheroni constant exponentiated. We introduce auxiliary multipole moments as the Fourier-transforms of the

auxiliary fields ψ_i (see appendix B) on the reference contact line $\partial S_{i,\mathrm{ref}}$,

$$
\begin{aligned}
\widehat{\psi}_{im}^c &= \int_0^{2\pi} d\eta_i\, h(\eta_i)\cos(m\eta_i)\,\psi_i(\mathbf{x}_i(\eta_i))\,, \\
\widehat{\psi}_{im}^s &= \int_0^{2\pi} d\eta_i\, h(\eta_i)\sin(m\eta_i)\,\psi_i(\mathbf{x}_i(\eta_i))\,,
\end{aligned}
\tag{3.47}
$$

where η_i is the elliptic angle pertaining to a coordinate system centered around each colloid i, respectively, such that the x–axis in this colloid–specific coordinate system joins the two foci of $S_{i,\mathrm{ref}}$. Furthermore, $h(\eta_i)$ is the scale factor in elliptic coordinates (see App. A). The lengthy calculation leading to the multipole (Fourier) decomposition for the Greens function $G(|\mathbf{x}_i - \mathbf{x}_j|)$ (for general orientations θ_1 and θ_2 of the ellipsoids) is given in App. D. The final results are collected in Eq. (D.1.9) and Eqs. (D.2.40)–(D.2.42). Using this, the double integral in the exponent of Eq. (3.46) can be written as a double sum over the auxiliary multipole moments (Fourier components), consisting of a self-energy part G_{self} when x_i and x_j reside on one ellipse and G_{int} when the points x_i and x_j reside on different ellipses, respectively. The functional integral over the auxiliary fields becomes a product of integrals over their multipole moments, $\mathcal{D}\psi_i = d\widehat{\psi}_{i0}\prod_{j=1}^{\infty} d\widehat{\psi}_{ij}^c d\widehat{\psi}_{ij}^s$, and the resulting partition function then reads

$$
\mathcal{Z}_{\mathrm{in}} = \mathcal{Z}_0'^{-1}\int \prod_{i=1}^{2}\mathcal{D}\psi_i \exp\left\{ -\frac{k_{\mathrm{B}}T}{2\gamma}\begin{pmatrix} \widehat{\boldsymbol{\Psi}}_1 \\ \widehat{\boldsymbol{\Psi}}_2 \end{pmatrix}^{\mathrm{T}}\begin{pmatrix} \widehat{\mathbf{G}}_{\mathrm{self}} & \widehat{\mathbf{G}}_{\mathrm{int}} \\ \widehat{\mathbf{G}}_{\mathrm{int}} & \widehat{\mathbf{G}}_{\mathrm{self}} \end{pmatrix}\begin{pmatrix} \widehat{\boldsymbol{\Psi}}_1 \\ \widehat{\boldsymbol{\Psi}}_2 \end{pmatrix}\right\}\,,
\tag{3.48}
$$

where the vectors $\widehat{\boldsymbol{\Psi}}_i = (\widehat{\boldsymbol{\Psi}}_i^c, \widehat{\boldsymbol{\Psi}}_i^s)$ with $\widehat{\boldsymbol{\Psi}}_i^c = (\widehat{\psi}_{i0}^c, \widehat{\psi}_{i1}^c, \dots)$ and $\widehat{\boldsymbol{\Psi}}_i^s = (\widehat{\psi}_{i1}^s, \widehat{\psi}_{i2}^s, \dots)$ contain the auxiliary multipole moments of colloid i. The coupling matrix $\widehat{\mathbf{G}}$ which contains the Fourier modes of the Greens function $G(\mathbf{x}_i - \mathbf{x}_j)$ has a block structure. The self energy submatrix $\widehat{\mathbf{G}}_{\mathrm{self}}$ which describes the coupling between auxiliary moments of the same colloid are diagonal, and its form can be determined from definition (3.47) and Eq. (D.1.9).

$$
2\pi\,(\widehat{\boldsymbol{\Psi}}_i)^{\mathrm{T}}\widehat{\mathbf{G}}_{\mathrm{self}}\widehat{\boldsymbol{\Psi}}_i = -\ln\frac{\gamma_e a' e^{\xi_0}}{8\lambda_c}(\widehat{\psi}_{i0}^c)^2 + 2\sum_{n=1}\frac{e^{-n\xi_0}}{n}\left[\cosh(n\xi_0)\,(\widehat{\psi}_{in}^c)^2 + \sinh(n\xi_0)\,(\widehat{\psi}_{in}^s)^2\right]\,,
\tag{3.49}
$$

where $a'^2 = a^2 - b^2$. The off–diagonal blocks $\widehat{\mathbf{G}}_{\text{int}}$ characterise the interaction between the multipole moments residing on different colloids. It is convenient to split the matrix into a block structure describing the interaction of cosine and sine multipoles:

$$2\pi \left(\widehat{\boldsymbol{\Psi}}_1\right)^{\text{T}} \widehat{\mathbf{G}}_{\text{int}} \, \widehat{\boldsymbol{\Psi}}_2 \;\; = \;\; \begin{pmatrix} \widehat{\boldsymbol{\Psi}}_1^c \\ \widehat{\boldsymbol{\Psi}}_1^s \end{pmatrix}^{\text{T}} \begin{pmatrix} \widehat{\mathbf{G}}_{\text{int}}^{cc} & \widehat{\mathbf{G}}_{\text{int}}^{sc} \\ \widehat{\mathbf{G}}_{\text{int}}^{sc} & \widehat{\mathbf{G}}_{\text{int}}^{ss} \end{pmatrix} \begin{pmatrix} \widehat{\boldsymbol{\Psi}}_2^c \\ \widehat{\boldsymbol{\Psi}}_2^s \end{pmatrix} \tag{3.50}$$

The matrix elements of the such defined submatrices follow from Eqs. (D.2.40)–(D.2.42), and are explicitly given by:

$$\left(\widehat{\mathbf{G}}_{\text{int}}^{cc}\right)_{00} \;\; = \;\; -\ln\left(\frac{\gamma_{\text{e}} d}{2\lambda_c}\right) \tag{3.51}$$

$$\left(\widehat{\mathbf{G}}_{\text{int}}^{cc}\right)_{mn} \;\; = \;\; \sum_{l=0} \left(\frac{a'}{4d}\right)^{m+n+2l} A_{mnl}^c(\theta_1, \theta_2) \cosh(m\xi_0) \, \cosh(n\xi_0) \tag{3.52}$$

$$\left(\widehat{\mathbf{G}}_{\text{int}}^{ss}\right)_{mn} = -\sum_{l=0} \left(\frac{a'}{4d}\right)^{m+n+2l} A_{mnl}^c(\theta_1, \theta_2) \sinh(m\xi_0) \, \sinh(n\xi_0) \tag{3.53}$$

$$\left(\widehat{\mathbf{G}}_{\text{int}}^{sc}\right)_{mn} \;\; = \;\; \sum_{l=0} \left(\frac{a'}{4d}\right)^{m+n+2l} A_{mnl}^s(\theta_1, \theta_2) \sinh(m\xi_0) \, \cosh(n\xi_0) \tag{3.54}$$

From Eq. (3.48) we find that the fluctuation part of the free energy reads

$$\mathcal{F}_{\text{in}} = -k_{\text{B}}T \ln \mathcal{Z}_{\text{in}} = -\frac{k_{\text{B}}T}{2} \ln(\det \widehat{\mathbf{G}}) + \text{const.} \,, \tag{3.55}$$

where const. $= -k_{\text{B}}T \ln \mathcal{Z}_0'$. The factors $A_{mnl}^{c[s]}(\theta_1, \theta_2)$, given in Eqs. (D.2.41) and (D.2.42), contain the dependence on the orientation angles θ_1 and θ_2 of the ellipsoids (see Fig. 3.1). As can be seen from above, the interaction coefficients $\left(\widehat{\mathbf{G}}_{\text{int}}^{c[s]c[s]}\right)_{mn}$ between multipoles of order m and n take the form of a series in $1/d$, starting at $1/d^{m+n}$. (For spherical colloids, this multipole interaction coefficient only contains the order $1/d^{m+n}$ [53].) In principle, the matrix $\widehat{\mathbf{G}}$ is infinite dimensional and $\det(\widehat{\mathbf{G}})$ is divergent and its regularisation is provided by the normalization factor $\mathcal{Z}_0'$. The explicit series for the elements of $\widehat{\mathbf{G}}_{\text{int}}$ allows for a systematic expansion of the logarithm in Eq. (3.55) in powers of $1/d$,

$$\mathcal{F}_{\text{in}}(d) \;\; = \;\; k_{\text{B}}T \sum_n f_{2n}^{\text{in}} \left(\frac{1}{d}\right)^{2n} \,, \tag{3.56}$$

where the coefficients f_{2n}^{in} depend on the logarithms $-\ln(\gamma_e d/2\lambda_c))$ and $-\ln(\gamma_e a' e^{\xi_0})/8\lambda_c)$, as well as the angles θ_1 and θ_2. The number of auxiliary multipoles included in the calculation of the asymptotic form of $\mathcal{F}_{\text{fluc}}$ in Eq. (3.56) is determined by the desired order in $1/d$. Inclusion of multipoles up to order n leads to an asymptotics correct up to $1/d^{2n}$. In the limit $\lambda_c/d \to \infty$ the free energy expansion coefficients in Eq. (3.56) up to fourth order are

$$
\begin{aligned}
f_0^{\text{in}} &= \frac{1}{2}\ln\left(\ln\left(\frac{4d}{a+b}\right)\right) + \text{const.} \\
f_2^{\text{in}} &= -\frac{1}{2\ln\left(\frac{4d}{a+b}\right)}\left[\frac{(a+b)^2}{16} + \frac{3}{32}(a^2-b^2)(\cos(2\theta_1)+\cos(2\theta_2))\right] \\
f_4^{\text{in}} &= -\frac{1}{2^{11}}\left\{\frac{1}{\ln\left(\frac{4d}{a+b}\right)}\left[\;16(a-b)(a+b)^3(\cos(2\theta_1)+\cos(2\theta_2))\right.\right. \\
&\qquad +11(a^2-b^2)^2(\cos(4\theta_1)+\cos(4\theta_2)) +44(a^2-b^2)^2\cos(2\theta_1+2\theta_2) + 6(a+b)^4\;\Big] \\
&\qquad \left.+\,[8(a^2-b^2)^2\cos(2\theta_1+2\theta_2) + 8(a+b)^4]\;\right\} - \frac{1}{2}\left(f_2^{\text{in}}\right)^2
\end{aligned}
$$

$$(3.57)$$

The double–logarithmic divergence in d in the leading coefficient f_0^{in} is a reflection of the fact that the interface itself becomes ill–defined for $\lambda_c \to \infty$ due to the capillary waves, see subsection 3.1.1. For the Casimir force itself, however, we find a finite value for all d in the limit $\lambda_c \to \infty$. Anisotropies in the Casimir interaction appear here first in the subleading term f_2^{in}. Their angular dependence stems from the monopole–dipole interaction of the auxiliary field, and the attraction is maximal if both ellipses are aligned tip–to–tip.

3.2.1 Derjaguin Approximation

In the opposite limit of small surface–to–surface distance $h = d - d_{cl} \ll d_{cl}$, (where d_{cl} is the distance of the closest approach between ellipses) the fluctuation force can be calculated by using the Derjaguin (or proximity) approximation [103]. It

consists in replacing the local force density on the contact lines by the result for the fluctuation force per length $f_{2d}(\tilde{h})$ between two parallel lines with a separation distance $\tilde{h}$ and integrating over the two opposite contact lines to obtain the total effective force between the colloids (see Fig. (3.3))

$$F_{\text{in}} = \int dy \, f_{2d}(y) \, . \tag{3.58}$$

The Casimir force density between two parallel surfaces was calculated in Ref. [93] in a general approach for arbitrary dimensions (See also chapter 2). Applied to two dimensions we obtain the force line density $f_{2d}(\tilde{h}) = -k_{\text{B}}T\,\pi/(24\tilde{h}^2)$, see also Eq. (2.99)for the Casimir energy. Curvature expansion of the two opposing curves in Fig. (3.3) around the point of minimal separation, we find the relation between y and the curvature of the neighboring ellipses at the point where h is minimized

$$\begin{aligned} y^2 &= R_i^2 - (R_i - x_i)^2 \\ &= 2R_i x_i - x_i^2 \approx 2R_i x_i \, . \end{aligned} \tag{3.59}$$

From Eq. (3.59) one can determine $h(y)$

$$\begin{aligned} h(y) &= h + x_1 + x_2 \\ &\approx h + \frac{y^2}{2}\left(\frac{1}{R_1} + \frac{1}{R_2}\right) , \end{aligned} \tag{3.60}$$

then the integral in Eq. (3.58) is calculated as

$$F_{\text{in}} \approx -\frac{\pi k_{\text{B}}T}{24} \int_{-\infty}^{+\infty} dy \, \frac{1}{\left(h + \frac{y^2}{2}\left(\frac{1}{R_1} + \frac{1}{R_2}\right)\right)^2} = -k_{\text{B}}T \, \frac{\pi^2}{48h^{\frac{3}{2}}} \sqrt{\frac{2}{\frac{1}{R_1} + \frac{1}{R_2}}} + \mathcal{O}(h^{-1/2}) \, . \tag{3.61}$$

Here, R_1 and R_2 are the curvature radii of the two ellipses at the end points of the distance vector of the closest approach. It is seen that the fluctuation force diverges as $h^{-3/2}$ upon contact of the ellipsoids ($h \to 0$).
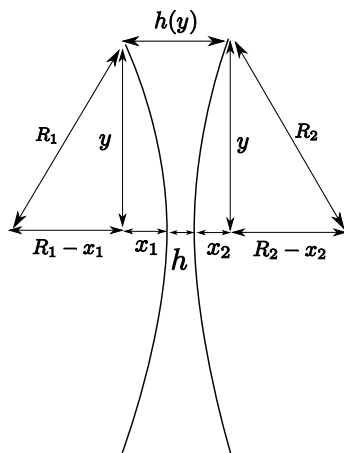
Figure 3.3: Top view of two opposing contact lines

3.2.2 Intermediate distances: Numerical calculation

For intermediate distances $d - d_{cl} \simeq a$ the fluctuation induced force has to be calculated numerically. This can be done in principle by including a number of multipoles in the numeric evaluation of the determinant in Eq. (3.55), see Ref. [90]. In order to avoid the algebraic evaluation of the multipole coefficients of $\hat{\mathbf{G}}$, it is possible to apply a method which was introduced in Ref. [104]. The starting point is Eq. (3.46) for the partition function Z_{in}. Introducing a mesh with N points η_{ij}, $j = 1 \ldots N$, on the reference contact line $\partial S_{i,\text{ref}}$ converts the double integral in the exponent to a double sum. Thus the functional integrals over the auxiliary fields $\psi_i(\eta_i)$ are replaced by ordinary Gaussian integrals over the $\psi_i(\mathbf{x}_i(\eta_{ij}))$, $\mathcal{D}\psi_i \simeq \prod_{j=0}^{N} d\psi_i(\mathbf{x}_i(\eta_{ij}))$. In the exponent, the $\psi_i(\mathbf{x}_i(\eta_{ij}))$ are coupled by a matrix $\mathbf{G}$ with elements $G_{ii'}^{jj'} = G(|\mathbf{x}_i(\eta_{ij}) - \mathbf{x}_{i'}(\eta_{i'j'})|)$. Performing the Gaussian integrals and disregarding divergent and d-independent terms immediately leads to $\mathcal{F}_{\text{in}} = (k_{\text{B}}T/2) \ln \det(\mathbf{G}_\infty^{-1} \mathbf{G}(d))$ for the fluctuation free energy. Here, $\mathbf{G}_\infty \equiv \lim_{d \to \infty} \mathbf{G}(d)$. It contains the self energy contributions and is needed for the regularization of the free energy. Deriving with respect to d, the Casimir force can

be written as

$$F_{\text{in}}(d) = -\frac{k_{\text{B}}T}{2} \, \text{tr} \left[\mathbf{G}(d)^{-1} \partial_d \mathbf{G}(d) \right] \; . \tag{3.62}$$

The advantage of the direct calculation of the force is that Eq. (3.62) does not contain any divergent parts which would require regularization, thus easing the numerical treatment considerably. The determinant is computed by using a standard LU decomposition [105]. We find good convergence of the numerical routine. The convergence can be sped up by distributing more points in the regions where the ellipses face each other. We note that computing the force by the multipole series seems to be more efficient [90]; this can partially be compensated by the point distribution on the ellipses. In Fig. 3.4 (ellipse aspect ratio 2) and 3.5 (aspect ratio 6) we compare the analytical results of Eqs. (3.56) and the Derjaguin approximation (Eq. (3.61) with the numerical results. As it is shown the analytical expressions show very good agreement with the numerical data points for both long- and short range behavior and almost cover the whole distance regime. At large distances d, the leading term of the free energy expansion in Eqs. (3.56) mainly determines the behavior of the Casimir interaction because of its long-ranged nature, hence the orientation dependence of the subleading terms can be neglected. In order to demonstrate the anisotropy of the Casimir interaction, we show results for a fixed, intermediate distance d between ellipsoid centers and varying orientation θ_2 of the second ellipsoid, see Fig. 3.6 (aspect ratio 2, $d/b = 4.1$) and 3.7 (aspect ratio 6, $d/b = 12.1$). The orientation of the first ellipse was fixed to three values, $\theta_1 = 0$, $\theta_1 = \pi/4$ and $\theta_1 = \pi/2$. As can be seen, the fluctuation–induced interaction is maximally attractive for $\theta_1 = \theta_2 = 0$ (tip–to–tip configuration). When θ_2 deviates from zero then the resulting force increase. This behavior holds for both aspect ratios 2 and 6.

Effect of in–plane anisotropy

The attractiveness of the fluctuation force for all distances and orientations was analyzed. This is already suggested by the close–distance regime (where $F_{\text{fluc}} \propto -1/h_0^{3/2}$ is always attractive) and the long–distance regime (where F_{fluc} is dominated by the likewise attractive, in–plane isotropic term $-\partial f_0^{\text{in}}/\partial d = -1/[2d \ln(d/r_0)]$, see Eq. (3.57)). In order to exemplify the effect of in–plane anisotropy on the fluctuation force, the results for the force with the asymptotically leading, isotropic term subtracted ($F_{\text{sub}} = F_{\text{fluc}} + k_B T \, \partial f_0^{\text{in}}/\partial d$) are shown in Figs. 3.8– 3.10 for ellipsoids with aspect ratio $a/b = 6$ and for the three configurations (a) tip–to–tip ($\theta_1 = \theta_2 = 0^o$, Fig. 3.8), (b) side–to–tip ($\theta_1 = 90^o$, $\theta_2 = 0^o$, Fig. 3.9) and (c) side–by–side ($\theta_1 = \theta_2 = 90^o$, Fig. 3.10). In all configurations for large d, the approach to the asymptotic result given by $-\partial (f_2^{\text{in}}/d^2)/\partial d$ is fairly slow. For the configurations (a) and (b) the subtracted force F_{sub} remains attractive for all distances and there is a smooth crossover from the long–distance to the close–distance regime while for the side–by–side configuration (c) there is a sign change from the attractive close–distance regime (open circles) to the repulsive long–distance regime (full circles), in accordance with Eq. (3.57).
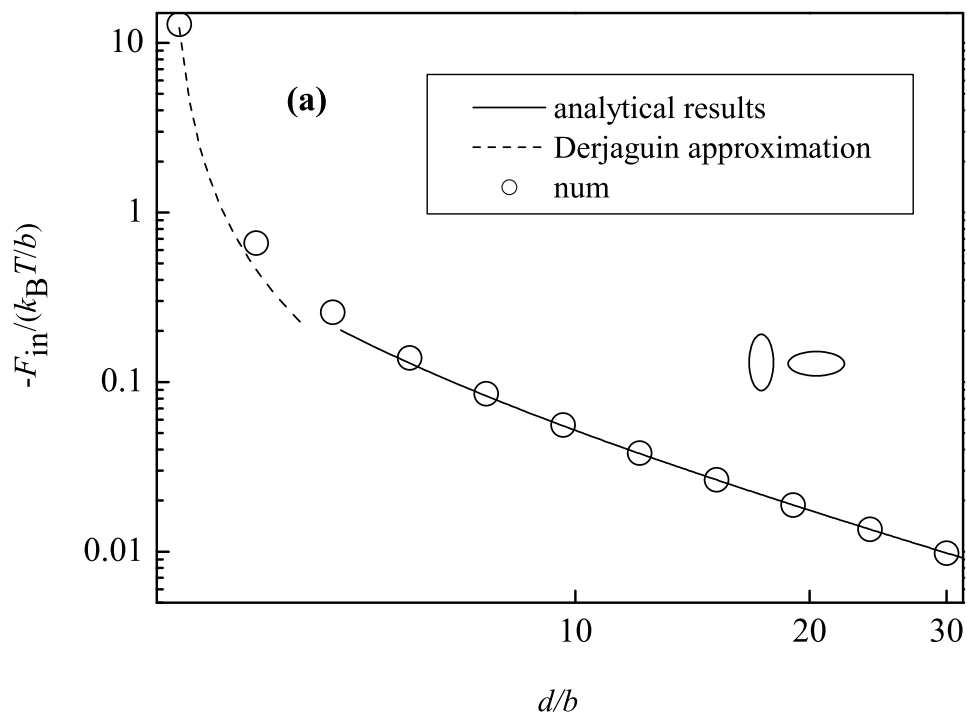
Figure 3.4: Comparison of the numerical results for the interface fluctuation Casimir force (symbols) with the analytical expressions in the asymptotic ranges of large colloid separations $d \gg a, b$ (full line) and small surface-to-surface distance $h = d - d_{cl} \ll b$ (dashed line), for ellipse aspect ratio 2.
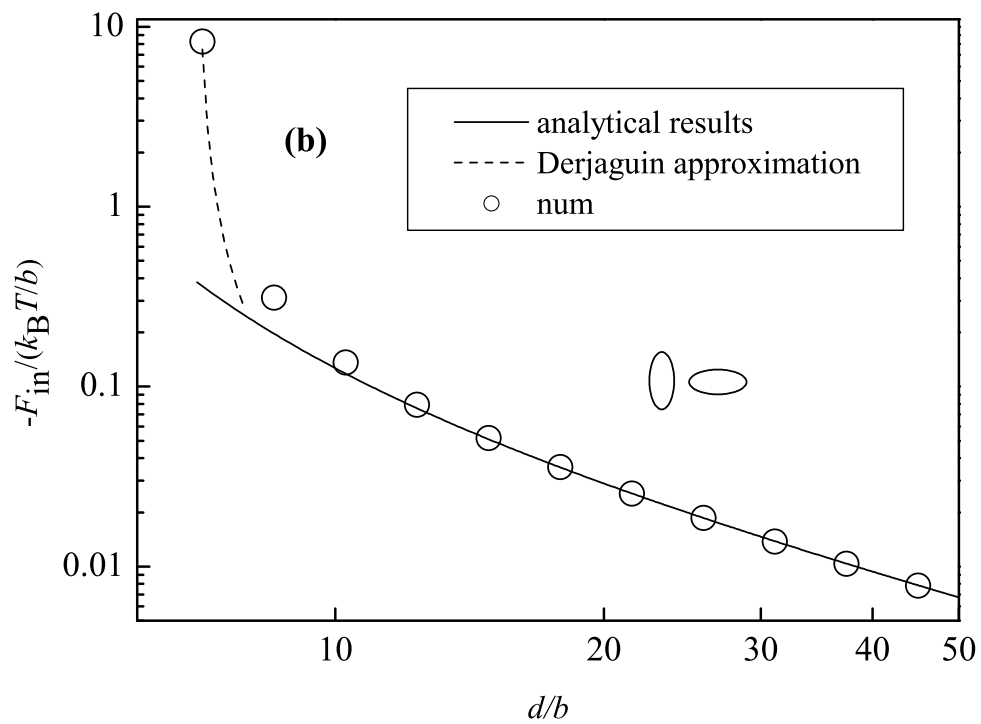
Figure 3.5: Comparison of the numerical results for the interface fluctuation Casimir force (symbols) with the analytical expressions in the asymptotic ranges of large colloid separations $d \gg a, b$ (full line) and small surface-to-surface distance $h = d - d_{cl} \ll b$ (dashed line), for ellipse aspect ratio 6.
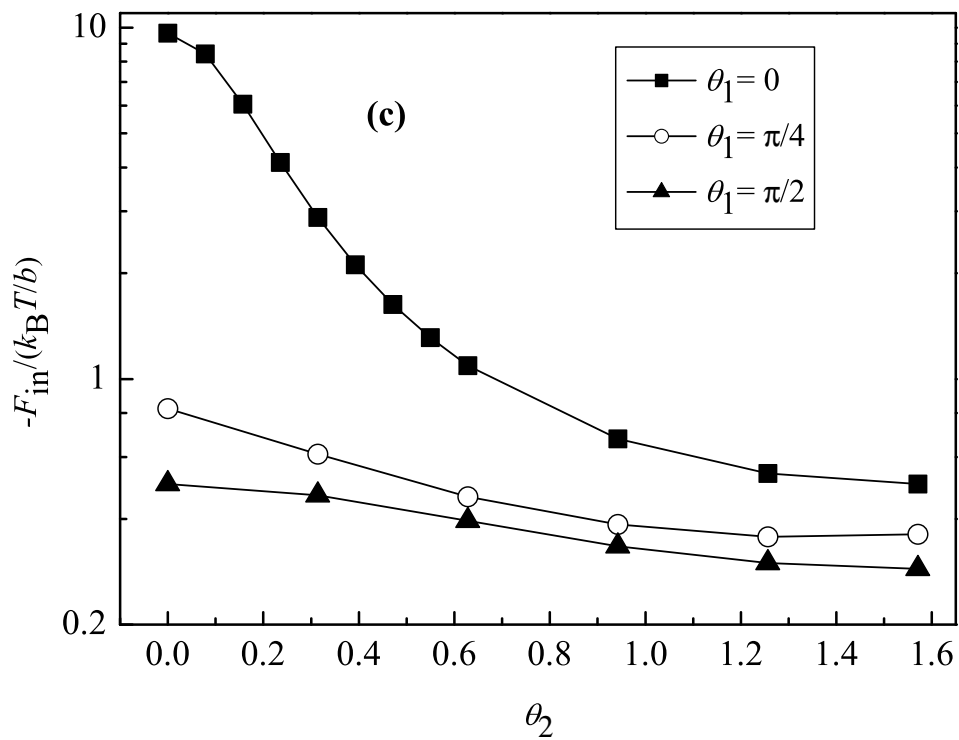
Figure 3.6: Numerical Casimir interaction between two fixed ellipsoids trapped at the interface as a function of their orientation, for $d = 4.1$ and ellipse aspect ratio 2.
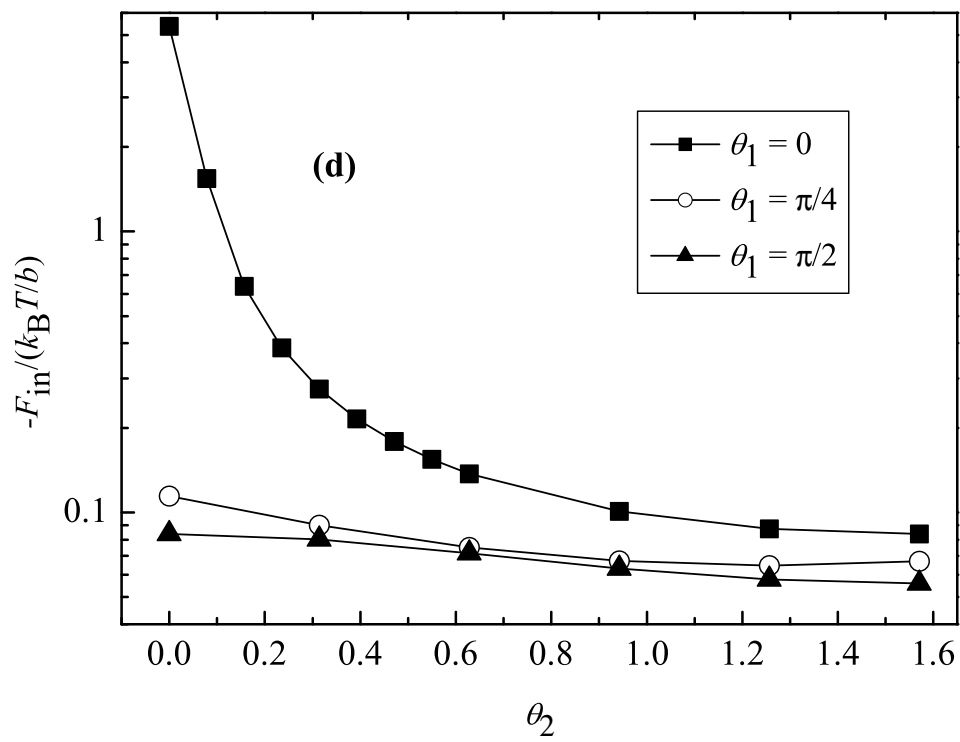
Figure 3.7: Numerical Casimir interaction between two fixed ellipsoids trapped at the interface as a function of their orientation, for $d = 12.1$ and ellipse aspect ratio 6.

Figure 3.8: Results for the fluctuation force with the leading asymptotic term subtracted, $F_{\mathrm{sub}} = F_{\mathrm{fluc}} + k_{\mathrm{B}}T\,\partial f_0/\partial d$, for ellipsoids with aspect ratio $a/b = 6$ and for the three configurations tip–to–tip ($\theta_1 = \theta_2 = 0^o$). Numerical results are shown by circles, the next–to–leading asymptotic term involving the coefficient f_2 (Eq. (3.57)) is represented by a full line, and the Derjaguin approximation is given by a dashed line, respectively. The capillary length was chosen as $\lambda_c = 10^6\,b$. Note that the sign of f_2 is positive for the filled points (repulsive) whereas it is negative for the empty points (attractive).
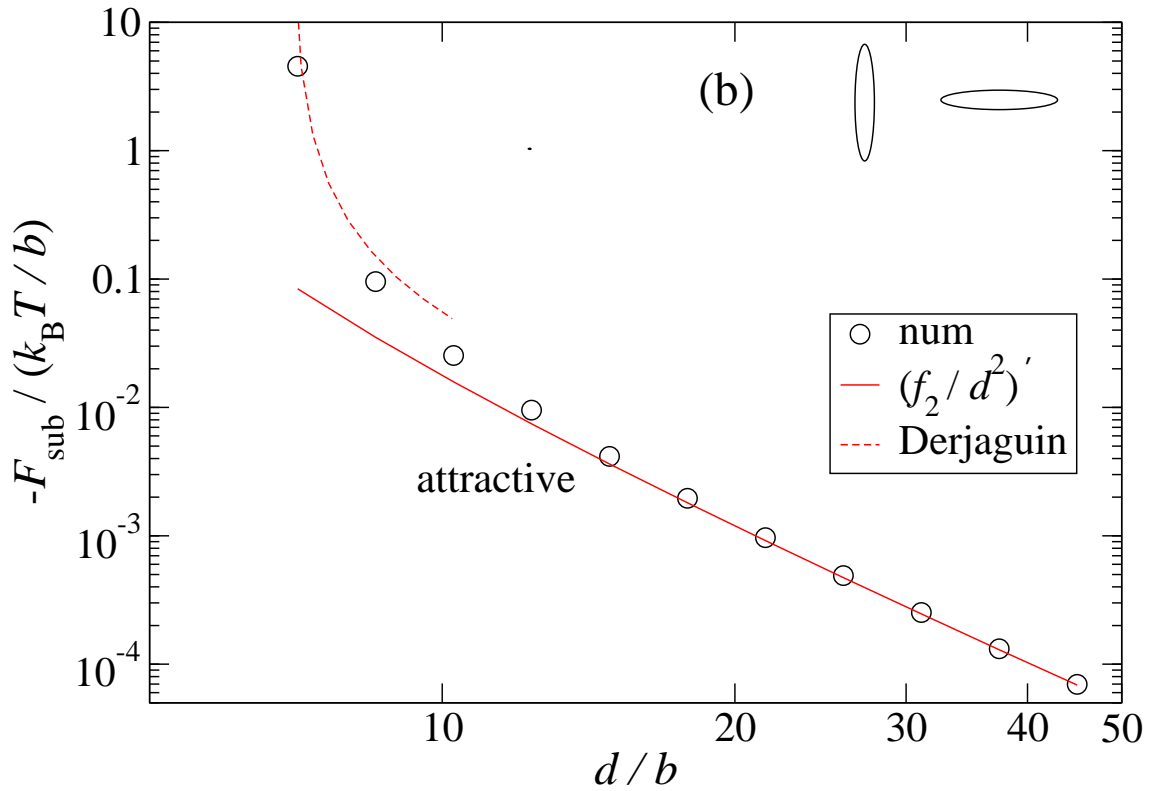
Figure 3.9: Results for the fluctuation force with the leading asymptotic term subtracted, $F_{\text{sub}} = F_{\text{fluc}} + k_{\text{B}}T\,\partial f_0/\partial d$, for ellipsoids with aspect ratio $a/b = 6$ and for the configurations side–to–tip ($\theta_1 = 90^o$, $\theta_2 = 0^o$). Numerical results are shown by circles, the next–to–leading asymptotic term involving the coefficient f_2 (Eq. (3.57)) is represented by a full line, and the Derjaguin approximation is given by a dashed line, respectively. The capillary length was chosen as $\lambda_c = 10^6\,b$. Note that the sign of f_2 is positive for the filled points (repulsive) whereas it is negative for the empty points (attractive).
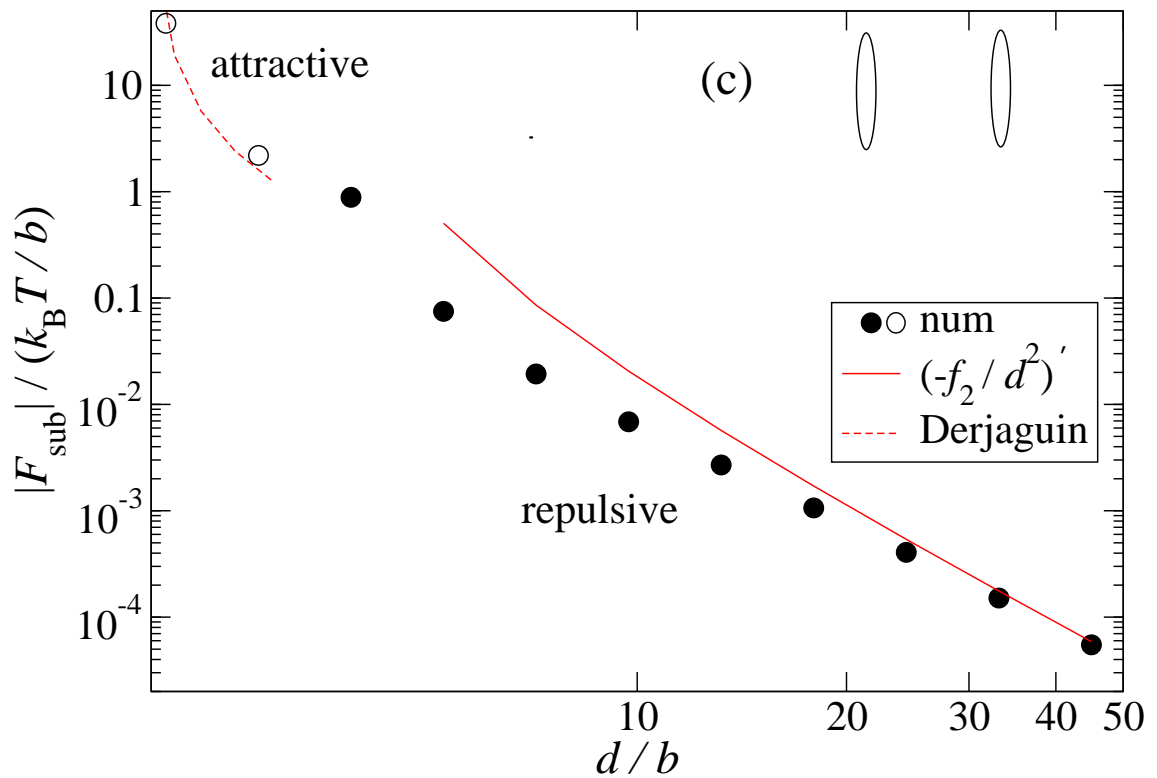
Figure 3.10: Results for the fluctuation force with the leading asymptotic term subtracted, $F_{\text{sub}} = F_{\text{fluc}} + k_{\text{B}}T\, \partial f_0/\partial d$, for ellipsoids with aspect ratio $a/b = 6$ and for the configurations side–by–side ($\theta_1 = \theta_2 = 90^o$). Numerical results are shown by circles, the next–to–leading asymp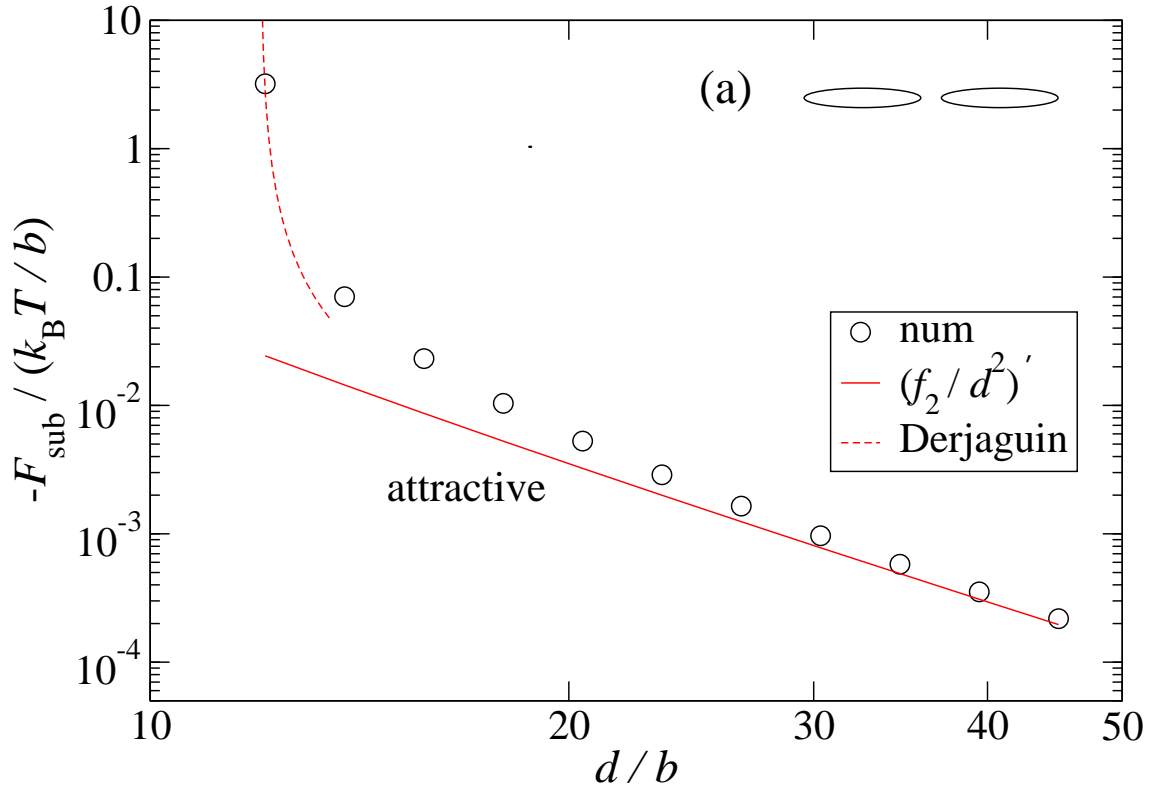totic term involving the coefficient f_2 (Eq. (3.57)) is represented by a full line, and the Derjaguin approximation is given by a dashed line, respectively. The capillary length was chosen as $\lambda_c = 10^6\, b$. Note that the sign of f_2 is positive for the filled points (repulsive) whereas it is negative for the empty points (attractive).

3.3   Inclusion of colloid fluctuations

In general, the inclusion of colloid height and tilt fluctuations into the partition function (Eq. (3.44)) can be realized by an approach used in Refs. [52, 53]. In this approach, the partition function is split into a product of a colloid fluctuation part and the interface fluctuation part. The latter contains only the contribution of the fluctuating interface, with Dirichlet boundary conditions on the colloid surface (see previous section). In the colloid fluctuation part, the fluctuations of colloid heights and tilts are weighted by a Boltzmann factor which contains the energy of the mean field solution (Euler–Lagrange equation) to the capillary problem with the boundary conditions set by the fluctuating contact line. This decomposition is possible due to the fact that capillary wave Hamiltonian is Gaussian in the field u. In principle, it is possible to use this method also for the special case of ellipsoidal colloids considered here. However, finding the mean field solution in such a geometry for arbitrary contact lines is rather cumbersome. To bypass this difficulty, we employed a trick adapted from Ref. [54] in which effective forces between rods on fluctuating membranes and films have been investigated. We extend the fluctuating interface height field $u(x, y)$ which enters the functional integral for $\mathcal{Z}$ to the interior of the ellipses $S_{i,\mathrm{ref}}$. Thus the measure of the functional integral for $\mathcal{Z}$ is extended by $\mathcal{D}u(\mathbf{x})|_{\mathbf{x} \in S_{i,\mathrm{ref}}}$ and the integration domain in the capillary wave Hamiltonian is enlarged to encompass the whole $\mathbb{R}^2$. On the colloid surfaces, the interface height field is given by the three phase contact line, $u(\partial S_{i,\mathrm{ref}}) \equiv f_i$. We extend u continuously to the interior of the circles $S_{i,\mathrm{ref}}$. Such a continuation is not unique. However, the partition function remains unchanged (up to a constant factor), if the energy cost of such a continuation is zero (as it is physically required since the interface is pinned to the ellipsoid surface). This has to be insured by appropriate counterterms [52, 53].

We choose the continuation:

$$u(S_{i,\text{ref}}) \equiv f_{i,\text{ext}}(\xi_i, \eta_i) = \sum_m \left(P_{im} \frac{\cos(hm\xi_i)}{\cosh(m\xi_0)} \cos(m\eta_i) + Q_{im} \frac{\sinh(m\xi_i)}{\sinh(m\xi_0)} \sin(m\eta_i) \right) ,$$
(3.63)

where ξ_i and η_i are the elliptic coordinates with respect to ellipse $S_{i,\text{ref}}$. The specific choice above is convenient for the further calculations since $\nabla^2 f_{i,\text{ext}} = 0$ in $S_{i,\text{ref}} \backslash \partial S_{i,\text{ref}}$. Extending the integration domain of the capillary wave Hamiltonian in Eq. (3.42), $\Omega = \mathbb{R}^2 \setminus \cup_i S_{i,\text{ref}} \to \mathbb{R}^2$ generates an additional energy contribution $-\mathcal{H}_{i,\text{corr}}$ which has to be subtracted from the extended capillary wave Hamiltonian $\mathcal{H}_{\text{cw}}[\Omega \equiv \mathbb{R}^2]$. Therefore, the total Hamiltonian reads:

$$\mathcal{H}_{\text{tot}} = \mathcal{H}_{\text{cw}} + \sum_{i=1}^2 [\mathcal{H}_{i,\text{b}} + \mathcal{H}_{i,\text{corr}}] .$$
(3.64)

The correction Hamiltonian is calculated in App. C, and we recall the boundary Hamiltonian:

$$-\mathcal{H}_{i,\text{corr}} = \frac{\gamma \pi}{2} \sum_m m \left(P_{im}^2 \tanh(m\xi_0) + Q_{im}^2 \coth(m\xi_0) \right) .$$
(3.65)

$$\mathcal{H}_{i,\text{b}} = \frac{\gamma \pi}{2} (P_{i1}^2 \tanh(\xi_0) + Q_{i1}^2 \coth(\xi_0)) .$$

In Eq. (3.65) we have already omitted the contributions from the gravitational term in $\mathcal{H}_{\text{cw}}$ which are of order $(a/\lambda)^2 \ll 1$.

As in the previous section the partition function is written as a functional integral over all possible configurations of the interface position u and the boundary lines, expressed by f_i,

$$\mathcal{Z} = \mathcal{Z}_0^{-1} \int \mathcal{D}u \prod_{i=1}^2 \int \mathcal{D}f_i \prod_{\mathbf{x}_i \in S_{i,\text{ref}}} \delta[u(\mathbf{x}_i) - f_{i,\text{ext}}(\mathbf{x}_i)] \exp \left\{ -\frac{\mathcal{H}_{\text{tot}}[f_i, u]}{k_\text{B} T} \right\} , \quad (3.66)$$

where the product over the δ-functions enforces the pinning of the interface at the positions of the colloids. In contrast to Eq. (3.44), this product extends over all $\mathbf{x} \in S_{i,\text{ref}}$ instead of $\partial S_{i,\text{ref}}$, only. The δ-functions can again be expressed by auxiliary fields ψ_i, now defined on the *two–dimensional* elliptical domains $S_{i,\text{ref}}$ as opposed to

the auxiliary fields of Sec. 3.2 which are defined on the *one–dimensional* ellipses $\partial S_{i,\mathrm{ref}}$:

$$\mathcal{Z} \;=\; \int \mathcal{D}u \int \prod_{i=1}^{2} \mathcal{D}\psi_i \int \mathcal{D}f_i \, \exp\left\{ -\frac{\mathcal{H}_{\mathrm{tot}}[f_i, u]}{k_{\mathrm{B}}T} + \mathrm{i} \int_{S_{i,\mathrm{ref}}} d^2x \, \psi_i(\mathbf{x})[u(\mathbf{x}) - f_{i,\mathrm{ext}}(\mathbf{x})] \right\} . \tag{3.67}$$

Similar to the evaluation of the fluctuation part, Sec. 3.2, we introduce multipole moments Ψ_{im} of the auxiliary fields by inserting unity into $\mathcal{Z}$, Eq. (3.67):

$$\mathbb{1} = \int \prod_{i=1}^{2} \prod_{m} d\Psi_{im}^c \, d\Psi_{im}^s \, \delta\left(\Psi_{im}^c - \int_{S_{i,\mathrm{ref}}} d^2x \, (\cosh(m\xi)/\cosh(m\xi_0)) \cos(m\eta) \, \psi_i(\mathbf{x}) \right)$$

$$\times \, \delta\left(\Psi_{im}^s - \int_{S_{i,\mathrm{ref}}} d^2x \, (\sinh(m\xi)/\sinh(m\xi_0)) \sin(m\eta) \, \psi_i(\mathbf{x}) \right) . \tag{3.68}$$

In contrast to the evaluation of the fluctuation term in Sec. 3.2, there will be constraints on the lowest multipoles which contribute to $\mathcal{Z}$. To see this we note that the Hamiltonian $\mathcal{H}_{\mathrm{tot}}$ does not depend on the boundary monopole moments P_{i0} and the dipole moments P_{i1} (through a cancellation between $\mathcal{H}_{i,\mathrm{b}}$ and $\mathcal{H}_{i,\mathrm{corr}}$), and the only dependence of $\mathcal{Z}$ on these moments is through the constraint function $f_{i,\mathrm{ext}}$. Recalling the definition of the integration measure $\mathcal{D}f_i$ for the two boundary conditions (B) and (C) and performing the integration over P_{i0} (B) and P_{i0} and P_{i1} (C), we immediately find

$$\mathcal{Z} \sim \begin{cases} \displaystyle \int \prod_{i=1}^{2} \prod_{m} d\Psi_{im}^s \, d\Psi_{im}^c \ldots \delta(\Psi_{i0}^c) \ldots & \text{case (B)} \\[2ex] \displaystyle \int \prod_{i=1}^{2} \prod_{m} d\Psi_{im}^s \, d\Psi_{im}^c \ldots \delta(\Psi_{i0}^c) \, \delta(\Psi_{i1}^c) \, \delta(\Psi_{i1}^s) \ldots & \text{cases (C)} \end{cases} \tag{3.69}$$

Having noticed these constraints on the auxiliary fields, we proceed by integrating over the field u in Eq. (3.67):

$$\mathcal{Z} \;=\; \int \prod_{i=1}^{2} \mathcal{D}\psi_i \int \mathcal{D}f_i \, \exp\left\{ -\frac{k_{\mathrm{B}}T}{2\gamma} \sum_{i,j=1}^{2} \int_{S_{i,\mathrm{ref}}} d^2x_i \int_{S_{j,\mathrm{ref}}} d^2x_j \, \psi_i(\mathbf{x}_i) \, G(|\mathbf{x}_i - \mathbf{x}_j|) \, \psi_j(\mathbf{x}_j) \right.$$

$$\left. -\frac{1}{k_{\mathrm{B}}T} \left(\mathcal{H}_{i,\mathrm{b}} + \mathcal{H}_{i,\mathrm{corr}} \right) - \mathrm{i} \sum_{i=1}^{2} \int_{S_{i,\mathrm{ref}}} \mathrm{d}^2x \, \psi_i(\mathbf{x}) f_{i,\mathrm{ext}}(\mathbf{x}) \right\} , \tag{3.70}$$

where – as in Eq. (3.46) – G is the Greens function of the capillary wave Hamiltonian. A somewhat longer calculation shows that $\mathcal{Z}$ can be split into into an interaction part (coupling the auxiliary multipole moments $\Psi_{im}^{c[s]}$, P_{im} and Q_{im} for different colloid labels i), a self–energy part (depending on $\Psi_{im}^{c[s]}$, P_{im} and Q_{im} for each value of i separately) and a remainder (the sum of boundary and correction Hamiltonian):

$$\mathcal{Z} = \int \prod_{i=1}^{2} \prod_{m} d\Psi_{im}^{c} d\Psi_{im}^{s} \int \mathcal{D}f_i \, \exp\left\{ -\frac{k_{\rm B}T}{2\gamma} \left(\mathcal{H}_{\rm int}[\Psi_{1m}^{c[s]}, \Psi_{2m}^{c[s]}] + \mathcal{H}_{i,\rm self}[\Psi_{im}^{c[s]}] \right) \right\} \times$$

$$\exp\left(\frac{1}{k_{\rm B}T} (\mathcal{H}_{i,\rm b} + \mathcal{H}_{i,\rm corr}) - {\rm i} \sum_{m} (\Psi_{im}^{c} P_{im} + \Psi_{im}^{s} Q_{im}) \right) \qquad (3.71)$$

The interaction part

$$\mathcal{H}_{\rm int} = 2 \int_{S_{1,\rm ref}} d^2 x_1 \int_{S_{2,\rm ref}} d^2 x_2 \psi_1(\mathbf{x}_1) G_{\rm int}(|\mathbf{x}_1 - \mathbf{x}_2|) \psi_2(\mathbf{x}_2) \qquad (3.72)$$

turns out to be a bilinear form in the auxiliary multipole moments; this is shown using the already used multipole expansion of the Greens function $G(|\mathbf{x}_1 - \mathbf{x}_2|) \simeq -\ln(\gamma_{\rm e}|\mathbf{x}_1 - \mathbf{x}_2|/2\lambda_c)$ (valid for $d \gg a$) which is presented in App. D in more detail. This bilinear form reads

$$2\pi \, \mathcal{H}_{\rm int} = \begin{pmatrix} \widehat{\boldsymbol{\Psi}}_1^c \\ \widehat{\boldsymbol{\Psi}}_1^s \end{pmatrix}^{\rm T} \begin{pmatrix} \widehat{\mathbf{G}}_{\rm int}^{cc} & \widehat{\mathbf{G}}_{\rm int}^{sc} \\ \widehat{\mathbf{G}}_{\rm int}^{sc} & \widehat{\mathbf{G}}_{\rm int}^{ss} \end{pmatrix} \begin{pmatrix} \widehat{\boldsymbol{\Psi}}_2^c \\ \widehat{\boldsymbol{\Psi}}_2^s \end{pmatrix}, \qquad (3.73)$$

where the submatrices $\widehat{\mathbf{G}}_{\rm int}^{cc}$, $\widehat{\mathbf{G}}_{\rm int}^{sc}$ and $\widehat{\mathbf{G}}_{\rm int}^{ss}$ have already been encountered in the calculation of the fluctuation part and are given by Eqs. (3.51)–(3.54). The self–energy part (different from the corresponding one in the calculation of the fluctuation part) is evaluated in App. E, with the result

$$\mathcal{H}_{i,\rm self} = -\frac{\ln\left(\gamma_{\rm e}(a+b)/8\lambda_c\right)}{2\pi} \Psi_{i0}^{c\,2}$$

$$+ \frac{1}{\pi} \sum_{m>0} \frac{1}{m} \left(\frac{\Psi_{im}^{c\,2}}{1 + \tanh(m\xi_0)} + \frac{\Psi_{im}^{s\,2}}{1 + \coth(m\xi_0)} \right) \qquad (3.74)$$

Combining Eqs. (3.71), (3.72), and (3.74), the partition function can be written as

$$\mathcal{Z} = \int \prod_{i=1}^{2} \prod_{m} \mathcal{D}\Psi_{im} \mathcal{D}f_i \, \exp\left\{ -\frac{k_{\rm B}T}{2\gamma} \begin{pmatrix} \widehat{\boldsymbol{\Psi}}_1 \\ \widehat{\boldsymbol{\Psi}}_2 \end{pmatrix}^{\dagger} \begin{pmatrix} \widehat{\mathbf{H}}_{\rm self} & \widehat{\mathbf{H}}_{\rm int} \\ \widehat{\mathbf{H}}_{\rm int} & \widehat{\mathbf{H}}_{\rm self} \end{pmatrix} \begin{pmatrix} \widehat{\boldsymbol{\Psi}}_1 \\ \widehat{\boldsymbol{\Psi}}_2 \end{pmatrix} \right\},$$

$$(3.75)$$

where the vectors $\boldsymbol{\Psi}_i = (\Psi_{i0}^c, P_{i0}, \Psi_{i1}^c, P_{i1}, \Psi_{i1}^s, Q_{i1}, \dots)$ – in contrast to $\widehat{\boldsymbol{\Psi}}_i$ in Sec. 3.2 – contain all involved auxiliary and boundary multipole moments. The elements of the matrix $\mathbf{H}$ describe the coupling of these multipole moments, where the self-energy block couples multipoles defined on the same ellipses $S_{i,\mathrm{ref}}$. Thus the diagonal part of the self energy matrix $\widehat{\mathbf{H}}_{\mathrm{self}}$ can be read off Eq. (3.65) and Eq. (3.74) while the off–diagonal part is determined by the term $-\mathrm{i}\sum_m (\Psi_{im}^c P_{im} + \Psi_{im}^s Q_{im})$ in Eq. (3.71). The elements of the interaction matrix $\widehat{\mathbf{H}}_{\mathrm{int}}$ are determined by the interaction energy $\mathcal{H}_{\mathrm{int}}$ in Eqs. (3.72) and (3.73) and couple the auxiliary multipole moments of different colloids. All matrix elements representing couplings of other multipoles are zero. Similar as in Eq. (3.48), the exponent in Eq. (3.75) is a bilinear form, however, here combined for all types, boundary multipole moments P_{im}, Q_{im} and auxiliary multipoles Ψ_{im}^c, Ψ_{im}^s. The computation of the partition function amounts to the calculation of $\det \widehat{\mathbf{H}}$. Again this is found as a series expansion in a/d, and we may define a similar expansion for the free energy $\mathcal{F}_{\mathrm{in+coll}} = -(k_\mathrm{B}T)\ln\det\widehat{\mathbf{H}}/2$ as before in Eq. (3.56):

$$\mathcal{F}_{\mathrm{in+coll}}(d) = k_\mathrm{B}T \sum_n f_{2n}^{\mathrm{in+coll}} \left(\frac{1}{d}\right)^{2n}. \tag{3.76}$$

The leading coefficients in case (B) (inclusion of fluctuations in the ellipsoids' vertical positions) are given by:

$$f_0^{\mathrm{in+coll}} = f_2^{\mathrm{in+coll}} = 0, \tag{3.77}$$
$$f_4^{\mathrm{in+coll}} = -\frac{1}{2^8}\left[(a^2 - b^2)^2 \cos(2\theta_1 + 2\theta_2) + (a+b)^4\right].$$

In case (C) (inclusion of fluctuations in the ellipsoids' vertical positions and tilt angles with respect to the interface) the leading coefficients are:

$$f_{2n}^{\mathrm{in+coll}} = 0 \quad (n = 0\dots3), \tag{3.78}$$
$$f_8^{\mathrm{in+coll}} = -\frac{9}{2^{16}}\left[(a^2 - b^2)^4 \cos(4\theta_1 + 4\theta_2) + (a+b)^8\right].$$

In contrast to the calculation before, the different leading power laws for the different cases (B) and (C) can be understood easily. We note that the interaction between the

auxiliary multipoles $\Psi_{1m}^{(c,s)}$ and $\Psi_{2n}^{(c,s)}$ in $\mathcal{H}_{\mathrm{int}}$, Eq. (3.72), scales like $(a'/4d)^{m+n}$. After calculating the determinant, the leading order of the total fluctuation induced force between the two colloids is determined by the first non–vanishing auxiliary multipole moment $\Psi_{im'}^{(c,s)}$ and (as follows from $\det \widehat{\mathbf{H}}$) gives rise to a term in the free energy $\propto 1/d^{4m'}$ (for $m' > 0$) or $\propto \ln \ln d$ (for $m' = 0$). As explained in the beginning of this subsection, the different boundary conditions lead to certain constraints on the auxiliary multipoles: According to Eq. (3.69), the leading term in $F(d)$ arises from a monopole-monopole interaction of the auxiliary field in case (A), from a dipole-dipole interaction in case (B), and from a quadrupole-quadrupole interaction in case (C). The constraints of vanishing auxiliary monopole and dipole moments (as in (C)) result from the independence of $\mathcal{H}_{\mathrm{tot}}$ of the boundary monopole and dipole moments and this is only captured correctly by the inclusion of the correction Hamiltonian $\mathcal{H}_{\mathrm{corr}}$. The Casimir attraction is maximal if the major axes of both ellipses are oriented parallel, regardless of the orientation of the distance vector joining their centers. This is a peculiarity in two dimensions, as can be seen also by the general multipole expansion of the interaction between two arbitrary charge distributions in two–dimensional electrostatics.

3.3.1   Limiting cases

In the limit $a = b$ (colloids with circular contact line such as disks and spheres) our results for the cases (A)–(C) reduce to the results reported in Refs. [52, 53]. In the limit $b \to 0$ (colloidal rods or needles with vanishing thickness) we can compare our result for case (C) (fluctuating colloid heights and tilts) to Ref. [54]. There it has been found that the effective free energy asymptotically varies $\propto d^{-4}$ with a coefficient given by Eq. (3.77), i.e. by the result of case (B) (colloid height fluctuations only). The derivation in Ref. [54] suggests that the perturbative treatment employed in our approach should be amended by corrections in the integration measure over the tilts. In our cases, this measure is simply given by $dP_{i1}dQ_{i1}$, the

product of the measures for the cosine and sine dipole moments of the contact line. In order to check the validity of this approximation for the measure, we recalculated the partition function of Ref. [54] by performing the integrations over the auxiliary dipole moments and their conjugate variables, which results in a final integral over the tilts (with the general measure) weighted by an exponential function in the tilts. If $\gamma a^2/(k_{\mathrm{B}}T) \gg 1$, the denominator of the measure in this integral can be expanded in terms of the tilt angles since the exponential function decays much faster than the measure and thus determines the convergence of the integral. In this way, one sees that the higher–order terms in the dipole tilt measure do not provide another leading behaviour in $1/d$ in the partition function compared to the leading quadrupole–quadrupole interaction which arises in our perturbative picture. A breakdown of our perturbative treatment can be expected if the length of the rod a approaches the molecular length scale. This coincides with a simultaneous breakdown of the simple capillary wave picture underlying our analysis.

3.3.2 Comparison between interface mediated interactions: fluctuation–induced versus capillary interactions

As discussed above, for ellipsoidal colloids that are trapped at the interface of two fluid phases, thermally excited height fluctuations of the interface cause a variant of the Casimir interaction which has been derived in this chapter. However, a fluid interface due to its static deformations formed by the presence of anisotropic particles may cause capillary interaction between the particles (see Subsec. 1.2.3). This capillary interaction is dominating for micro–ellipsoidal colloids, only for nano-sized colloids fluctuation–induced forces may become large.

In this subsection we are going to compare the behavior of these two interface mediated interactions.

It is possible to interpret the capillary potential as a two-dimensional electrostatic interaction between two charged colloids. The Young's equation guarantees that the surface charge density of colloids remains constant. The asymptotic form of the capillary interaction between ellipsoidal particles (with major axes a, b, b and $a > b$) that are trapped at a fluid interface is governed by the quadrupole–quadrupole interaction [30]

$$U_{\mathrm{cap}} \sim -\frac{\gamma \Delta u_{\mathrm{max}}^2}{4} \left(\frac{a}{d}\right)^4 \cos(2\phi_1 + 2\phi_2) \,, \tag{3.79}$$

where Δu_{max} is the maximum meniscus height difference along the contact line, and ϕ_i is the polar angle orientation of colloid i in the interface plane.

In general, Δu_{max} depends on the major axes of the ellipsoid and the contact angle. For an order-of-magnitude estimate, one may assume $\Delta u_{\mathrm{max}} \lesssim b$, and thus for micrometer-sized ellipsoids at the air-water interface, the energy scale of the quadrupolar interaction is $10^6 k_{\mathrm{B}} T$. Eq. (3.79) shows that the capillary interaction can be attractive or repulsive with respect to the orientation of ellipsoids within the fluid interface. For instance, the interaction between two ellipsoidal colloids approaching each other side-by-side ($\phi_1 = \phi_2 = \pi/2$) or tip-to-tip ($\phi_1 = \phi_2 = 0$) is attractive and equal. Another feature of the capillary potential is that it does not

diverge when ellipsoidal colloids are in contact.

As it is observed in the results of this chapter, the behavior of the fluctuation–induced interaction between ellipsoidal colloids at a fluid interface is determined by the fluctuations of the particles.

If the ellipsoidal particles fluctuate vertically, the resulting fluctuation–induced interaction can be interpreted as an interaction between fluctuating dipoles of the auxiliary field (see Eq. (3.77)). This interaction has the anisotropy signature of (static) quadrupole–quadrupole interaction (such as in Eq. (3.79)), save for a constant that makes Eq. (3.77) always attractive.

If the ellipsoidal particles are allowed to tilt in addition to their vertical fluctuations, the resulting fluctuation–induced interaction can be understood with regard to an interaction between fluctuating quadrupoles with the anisotropy signature of (static) octupole–octupole interaction (see Eq. (3.78)). Similar to Eq. (3.77), the Casimir energy in Eq. (3.78) is also attractive through an additional constant.

In the limit of short-distance separations (i.e. $h \to 0$, where h is the surface-to-surface distance), the fluctuation–induced forces diverge (see Eq. 3.61). Although at this limit, fluctuations should always "win" compared to the static capillary interactions, this is not observabale for microcolloid ellipsoids (compare $\gamma(\Delta u_{\mathrm{u_{max}}})^2 \approx 10^6 k_{\mathrm{B}} T$ with $k_{\mathrm{B}} T \left(\frac{a}{h}\right)^{1/2}$, implying that $h < 10^{-12} a$ for the fluctuation potential being stronger than the capillary potential). Thus Δu_{max} has to be brought to the nanoscale such that $\gamma(\Delta u_{\mathrm{u_{max}}})^2 \approx 1 k_{\mathrm{B}} T$. Then the Casimir-potential will clearly be dominating for small distances.

Chapter 4

Closing remarks

The aim of this thesis was to investigate interface mediated interactions between uncharged nano–colloidal particles that are trapped at the interface of two fluid phases. The restrictions that these two colloids trapped at a fluid interface impose on the thermally excited interfacial fluctuations (capillary waves) by their sheer presence lead to a thermal Casimir interaction.

In chapter 1, we introduced the definition of colloids, different types and some typical characteristics of these particles. In Sec. 1.1, we had a closer look at the physical properties of fluid interfaces and particles that are trapped at such interfaces. To provide a wider understanding of inter-colloidal interactions, in Sec. 1.2 we reviewed the most common and important interactions which are relevant for particles at interfaces. Having introduced van der Waals and electrostatic interactions that exist both in bulk and at interfaces, we reviewed capillary and fluctuation–induced interactions which are classified as interface mediated interactions. At the end we explained the possibilities of discriminating fluctuation–induced forces from other types of interactions.

As this thesis is mainly focused on the theoretical study of the fluctuation–induced forces, chapter 2 is devoted to a brief review of the most prominant methods of calculating the Casimir interaction. Starting, for historical reasons, from the

mode summation method, we continued by introducing two main approaches: use of Green's function; and also path integral methods, which are then used in chapter 3 to calculate the Casimir interaction between ellipsoidal particles trapped at the interface of two fluid phases.

In chapter 3 we obtained an explicit account for the effect of colloidal anisotropy on the form of the Casimir interaction by studying ellipsoidal (spheroidal) colloids with arbitrary aspect ratio. For the case of fixed colloids and fixed contact lines, the problem is equivalent to the "standard" Casimir problem for a scalar Gaussian field in two dimensions with Dirichlet boundary conditions on the colloid surface. In an expansion in $1/d$ (the inverse center–to–center distance between the colloids) the leading term in the Casimir interaction energy is found to be attractive, isotropic in the interface plane and slowly varying $\propto \ln \ln d$ (see Eq. (3.57)). Anisotropies appear in higher orders of $1/d$ and become important when the closest surface–to–surface distance between the colloids becomes small (see Figs. 3.4-3.7).

If fluctuations in the colloids' vertical positions are permitted, the asymptotic behavior of the Casimir interaction energy changes to a behavior $\propto d^{-4}$ (see Eq. (3.77)). In this case, anisotropies are present in the leading term but the interaction remains attractive for all orientations. If furthermore fluctuations of the colloids' orientation with respect to the interface normal are allowed, the asymptotics changes to a behaviour $\propto d^{-8}$ (see Eq. (3.78)). Interestingly, this change of leading order in the asymptotics of the Casimir energy depending on the type of permitted colloid fluctuations holds for arbitrary aspect ratios. This leads to the speculation that this might be a general feature holding for arbitrary colloid shape.

In our approach the Casimir interaction can be understood as the interaction between fluctuating multipole moments of an auxiliary charge density–like field defined on the area enclosed by the contact lines. These fluctuations are coupled to fluctuations of multipole moments of the contact line position which are a due to the possibly fluctuating colloid height and tilts. Therefore, the system can be viewed as

an example of the Casimir effect with fluctuating boundary conditions. Such fluctuating boundary conditions appear to be difficult to be realizable in three–dimensional systems such as the standard system of charged metallic objects subjected to vacuum fluctuations of the electromagnetic field.

Experimentally, the detection of the Casimir interaction at a fluid interface appears to be possible if competing interactions, especially van–der–Waals and static capillary interactions, are sufficiently weakened. Van–der–Waals interactions are also strongly attractive at small distances, but can be modified by an appropriate core–shell structure of the colloids or by using flat, disk–like particles. Capillary interactions are very strong for ellipsoidal colloids of micrometer size and with contact angle different from $\pi/2$ since the equilibrium contact line in this case is already undulated and gives rise to static deformations of the surrounding interface. These capillary interactions can be minimized by either using truly nanoscopic ellipsoids or synthesizing Janus particles with a contact line which is flat on a nm level. Despite the great advances in particle synthesis over the last years, this appears to be still a big challenge.

Appendix A

Confocal Elliptic Coordinate System

Confocal elliptic coordinates (ξ, η) are planar orthogonal coordinates formed by confocal ellipses or hyperbolae. The foci are located on the x-axis of the Cartesian coordinates, separated by a'. The relation to Cartesian coordinates is defined by

$$
\begin{aligned}
x &= \frac{a'}{2} \cosh(\xi) \cos(\eta) \ , \\
y &= \frac{a'}{2} \sinh(\xi) \sin(\eta) \ ,
\end{aligned}
\tag{A.0.1}
$$

and the scale factors are found as

$$
h_\xi = h_\eta = \sqrt{\frac{a'^2}{8} \left(\cosh(2\xi) - \cos(2\eta)\right)} \ .
$$

ξ and η are called elliptic radius and elliptic angle, respectively. In this coordinate system, $\xi = \xi_0$ represents the equation of an ellipse with axes a, b ($a > b$). The elliptic radius and the distance a' between the foci are given in terms of the ellipse principal axes by

$$
\begin{aligned}
\xi_0 &= \frac{1}{2} \ln \left(\frac{a+b}{a-b}\right) \ , \\
a' &= (a^2 - b^2)^{\frac{1}{2}} \ .
\end{aligned}
\tag{A.0.2}
$$

Therefore, for a circle we have $\xi_0 \to \infty$ and for a line, $\xi_0 \to 0$. Moreover, complex variables in elliptic coordinates are denoted by

$$z = a^{'} \cosh(\xi + i\eta)$$

Appendix B

Fourier expansion in elliptic coordinates

To introduce the Fourier expansion of an arbitrary function, first we look at a general case of expanding a function in terms of a set of orthonormal eigenfunctions of a Hermitian operator.

If $\mathcal{L}$ is a Hermitian operator with a set of eigenfunctions $\{f_i(x)\}$, then

$$\mathcal{L} f_i(x) = \lambda_i \, W(x) \, f_i(x) \, , \tag{B.0.1}$$

where $W(x)$ is a real weight function which is positive in $a \leq x \leq b$ and the same for all eigenvalues λ_i. To show that the eigenfunctions of the Hermitian operator $\mathcal{L}$ are orthogonal, we write

$$\int_a^b dx \, f_j^*(x) \mathcal{L} f_i(x) = \lambda_i \int_a^b dx \, W(x) f_j^*(x) f_i(x) \, , \tag{B.0.2}$$

and

$$\int_a^b dx \, f_i^*(x) \mathcal{L} f_j(x) = \lambda_j \int_a^b dx \, W(x) f_i^*(x) f_j(x) \, . \tag{B.0.3}$$

We write the complex conjugate of equation(B.0.3),

$$\int_a^b dx \, f_j^*(x) \mathcal{L} f_i(x) = \lambda_j \int_a^b dx \, W(x) f_j^*(x) f_i(x) \, . \tag{B.0.4}$$

Substracting Eqs (B.0.2) and (B.0.4), we find

$$(\lambda_i - \lambda_j) \int_a^b dx\, W(x) f_j^*(x) f_i(x) = 0 \,. \tag{B.0.5}$$

Eq. (B.0.5) gives the orthogonality relation between the eigenfunctions of the Hermitian operator $\mathcal{L}$

$$\int_a^b dx\, W(x) f_j^*(x) f_i(x) = 0 \qquad (i \neq j) \tag{B.0.6}$$

Introducing normalized eigenfunctions $\hat{f}_i$, the orthogonality relation is

$$\int_a^b dx\, W(x) \hat{f}_j^*(x) \hat{f}_i(x) = \delta_{ij} \,. \tag{B.0.7}$$

Eq. (B.0.7) indicates that the eigenfunctions $\{f_i(x)\}$ form an orthogonal basis of a space in which an arbitrary function $g(x)$ that is well-defined in $a \leq x \leq b$ can be expanded in terms of $\{f_i(x)\}$

$$g(x) = \sum_i c_i \hat{f}_i(x) \,, \tag{B.0.8}$$

where the coefficients c_i are determined by

$$c_i = \int_a^b dy\, W(y) g(y) \hat{f}_i^*(y) \,. \tag{B.0.9}$$

Inserting Eq. (B.0.9) into Eq. (B.0.8), we have

$$g(x) = \sum_i \hat{f}_i(x) \int_a^b dy\, W(y) \hat{f}_i^*(y)\, g(y) \,, \tag{B.0.10}$$

which gives rise to the closure property of eigenfunctions $\{f_i(x)\}$

$$W(y) \sum_i \hat{f}_i(x) \hat{f}_i^*(y) = \delta(x - y) \,. \tag{B.0.11}$$

For the specific choice of the Hermitian operator $\mathcal{L} = \frac{\partial^2}{\partial \eta^2}$ in which η is the elliptic angle (see appendix A), the eigenfunctions are

$$\hat{f}_m(\eta) = \frac{1}{2\pi} e^{-im\eta} \,. \tag{B.0.12}$$

In this example the weight function is the scale factor in elliptic coordinates $W(\eta) = h_\eta$. The expansion of the function $\psi(\eta)$ in terms of $\{\hat{f}_m\}$ is

$$\psi(\eta) = \frac{1}{2\pi} \sum_m \hat{\psi}_m e^{-im\eta} \ . \tag{B.0.13}$$

Eq. (B.0.13) is the Fourier expansion of $\psi(\eta)$. The coefficient $\hat{\psi}_m$ which is the Fourier transform of the function $\psi(\eta)$ is denoted by

$$\hat{\psi}_m = \frac{1}{2\pi} \int_0^{2\pi} d\eta \, h_\eta e^{im\eta} \psi(\eta) \ . \tag{B.0.14}$$

Appendix C

The Boundary and Correction Hamiltonians

C.1 Boundary Hamiltonian

The boundary Hamiltonain for the case of a pinned contact line (Janus ellipsoids) is governed by the difference in the projected meniscus area, ΔA_{proj} (Eq. (3.39). The meniscus in the reference configuration is an ellipse with elliptic radius ξ_0 and principal axes a, b. If the ellipsoid is tilted in the xz-plane by a small angle α_i, this area is given by

$$\Delta A^{xz}_{\mathrm{proj}} = A(1 - \cos \alpha_i) \approx A \frac{\alpha_i^2}{2} \tag{C.1.1}$$

where $A = \pi ab$ is the ellipse area. The product of the principal axes in elliptic coordinates is given by

$$ab = \frac{a'^2}{2} \sinh(2\xi_0) \,,$$

thus the projected area in elliptic coordinate is denoted by

$$\Delta A^{xz}_{\mathrm{proj}} \approx \frac{\pi}{16} \alpha_i^2 a'^2 \sinh(2\xi_0) \,. \tag{C.1.2}$$

The contact line position $u|_{\partial S_{i,\mathrm{ref}}}$ is determined by using a coordinate system rotation from the xz-plane to the $x'z'$-plane, where the $x'-$ and the z'–axis coincide with the

major and minor axis of the tilted ellipsoid The contact line is located at $z^{'} = 0$ in the new coordinate system

$$
\begin{pmatrix} x^{'} \\ z^{'} \end{pmatrix} = \begin{pmatrix} \cos\alpha_i & -\sin\alpha_i \\ \sin\alpha_i & \cos\alpha_i \end{pmatrix} \begin{pmatrix} x \\ z \end{pmatrix} ,
$$

therefore

$$
\begin{aligned}
z^{'} &= x\sin\alpha_i + z\cos\alpha_i \\
&\approx z - \alpha_i x .
\end{aligned}
\tag{C.1.3}
$$

Eq. (C.1.3) gives the contact line profile u

$$
u|_{\partial S_{i,\mathrm{ref}}} = z|_{z^{'}=0} \approx \alpha_i x .
\tag{C.1.4}
$$

After transforming Eq. (C.1.4) to elliptic coordinates (see appendix (A)) we have

$$
u|_{\partial S_{i,\mathrm{ref}}} \approx \alpha_i (a^{'}/2)\cosh(\xi_0)\cos(\eta_i) .
\tag{C.1.5}
$$

Thus, in the multipole expansion of the tilted contact line (Eq. (3.40)), only a dipole term appears with the dipole moment given by:

$$
P_{i1} = \alpha_i \frac{a^{'}}{2}\cosh(\xi_0) .
\tag{C.1.6}
$$

Inserting Eq. (C.1.6) into Eq. (C.1.2) we obtain

$$
\Delta A_{\mathrm{proj}}^{xz} = \frac{\pi}{2} P_{i1}^2 \tanh(\xi_0) .
\tag{C.1.7}
$$

Applying the same arguments for tilts in the yz-plane, we can express the boundary Hamiltonian in the small–tilt approximation by

$$
\begin{aligned}
\mathcal{H}_{i,\mathrm{b}} &= \gamma\Delta A_{\mathrm{proj}} \\
&= \frac{\gamma\pi}{2}(P_{i1}^2\tanh(\xi_0) + Q_{i1}^2\coth(\xi_0)) .
\end{aligned}
\tag{C.1.8}
$$

C.2 Correction Hamiltonian

The correction Hamiltonian, which is introduced in Eq. (3.64), is determined by minus the surface energy of the meniscus piece $u|_{S_{i,\text{ref}}} \equiv f$ (Eq. (3.63)) extended into the ellipses enclosed by the reference contact lines:

$$
\begin{aligned}
-\mathcal{H}_{i,\text{corr}} &= \frac{\gamma}{2} \int_{S_{i,\text{ref}}} d^2x \left[(\nabla u)^2 + \frac{u^2}{\lambda_c^2} \right] \\
&\stackrel{\lambda_c \to \infty}{=} \frac{\gamma}{2} \int d^2x (\nabla f)^2 \ .
\end{aligned}
\tag{C.2.9}
$$

Thus,

$$
-\mathcal{H}_{i,\text{corr}} = \frac{\gamma}{2} \int_0^{\xi_0} \int_0^{2\pi} d\xi_i d\eta_i \left((\partial_{\xi_i} f)^2 + (\partial_{\eta_i} f)^2 \right) \ .
\tag{C.2.10}
$$

First we perform the integration over the elliptic angle η_i.

The partial derivatives of f with respect to the elliptic coordinates componenets gives

$$
\partial_{\xi_i} f = \sum_m m \left[P_{im} \frac{\sinh(m\xi)}{\cosh(m\xi_0)} \cos(m\eta_i) + Q_{im} \frac{\cosh(m\xi)}{\sinh(m\xi_0)} \sin(m\eta_i) \right] \ ,
\tag{C.2.11}
$$

and

$$
\partial_{\eta_i} f = \sum_m m \left[-P_{im} \frac{\cosh(m\xi)}{\cosh(m\xi_0)} \sin(m\eta_i) + Q_{im} \frac{\sinh(m\xi)}{\sinh(m\xi_0)} \cos(m\eta_i) \right] \ ,
\tag{C.2.12}
$$

the η-integration for the first term in Eq. (C.2.10) is evaluated by using the Eq. (C.2.11)

$$
\begin{aligned}
\int_0^{2\pi} d\eta_i (\partial_{\xi_i} f)^2 = \int_0^{2\pi} d\eta_i \sum_{m,m'} mm' \quad (\quad &A_m A_{m'} \cos(m\eta_i) \cos(m'\eta_i) \\
+ \quad &B_m B_{m'} \sin(m\eta_i) \sin(m'\eta_i) \\
+ \quad &A_m B_{m'} \cos(m\eta_i) \sin(m'\eta_i) \\
+ \quad &A_{m'} B_m \cos(m'\eta_i) \sin(m\eta_i) \quad) \ ,
\end{aligned}
\tag{C.2.13}
$$

where $A_m = P_{im} \frac{\sinh(m\xi_i)}{\cosh(m\xi_0)}$ and $B_m = Q_{im} \frac{\cosh(m\xi_i)}{\sinh(m\xi_0)}$.

Integrals in Eq. (C.2.13) can be easily calculated with the result

$$
\int_0^{2\pi} d\eta_i (\partial_{\xi_i} f)^2 = \pi \sum_m m^2 \left(P_{im}^2 \frac{\sinh(m\xi_i)^2}{\cosh(m\xi_i)^2} + Q_{im}^2 \frac{\cosh(m\xi_i)^2}{\sinh(m\xi_i)^2} \right) \ .
\tag{C.2.14}
$$

Similarly for the second term in Eq. (C.2.10) we have

$$\int_0^{2\pi} d\eta_i \, (\partial_{\eta_i} f)^2 = \pi \sum_m m^2 \left(P_{im}^2 \frac{\cosh(m\xi_i)^2}{\cosh(m\xi_i)^2} + Q_{im}^2 \frac{\sinh(m\xi_i)^2}{\sinh(m\xi_i)^2} \right) \ . \qquad (C.2.15)$$

Adding Eqs. (C.2.14) and (C.2.15) we obtain

$$F(\xi_i) = \int_0^{2\pi} d\eta_i (\nabla f)^2 = \pi \sum_m m^2 \, \cosh(2m\xi_i) \left(\frac{P_{im}^2}{\cosh(m\xi_0)^2} + \frac{Q_{im}^2}{\sinh(m\xi_0)^2} \right) \ . $$
$$(C.2.16)$$

Then the correction Hamiltonian can be obtained after performing the last integration over ξ_i

$$
\begin{aligned}
-\mathcal{H}_{i,\mathrm{corr}} &= \frac{\gamma}{2} \int_0^{\xi_0} d\xi_i \, F(\xi_i) \\
&= \frac{\gamma\pi}{2} \sum_m m \left(P_{im}^2 \tanh(m\xi_0) + Q_{im}^2 \coth(m\xi_0) \right) \ . \qquad (C.2.17)
\end{aligned}
$$

Appendix D

Expansion of Green's function in elliptic coordinates

In this appendix we derive the multipole expansion of the Green's function $G(|\mathbf{x}|) \approx -(1/2\pi)\ln(\gamma_e|\mathbf{x}|/2\lambda_c)$ between two charged elliptic regions (charges are generated by auxilliary fields ψ_i). This Green's function gives the correlation between two points residing either on the same ellipse or different ellipses.

D.1 Self energy part

In the case that $\mathbf{x}_1$ and $\mathbf{x}_2$ are located on the same ellipse of the same size, the Green's function expansion is calculated simillar to Ref. [106]. Since the Green's function is for a two dimensional system, the expansion can be found by using the Green's function definition in the complex space, therefore we should find the real part of the complex Green's function expansion

$$
\begin{aligned}
G(|\mathbf{r}_1 - \mathbf{r}_2|) &= -\frac{1}{2\pi}\ln\left(\frac{\gamma_e|\mathbf{r}_1 - \mathbf{r}_2|}{2\lambda_c}\right) \\
&= -\frac{1}{2\pi}\mathrm{Re}[\ln\left(\frac{\gamma_e(z_1 - z_2)}{2\lambda_c}\right)]\,,
\end{aligned}
\tag{D.1.1}
$$

where $z_i = (a'/2)\cosh(w_i)$ and $w_i = \xi_0 + i\eta_i$.

As it is seen in Eq. (D.1.1) for finding the Green's function expansion, we have to calculte the expansion of $\ln(z_1 - z_2)$

$$\ln(z_1 - z_2) = \ln\left(\frac{a'}{4}\right) + \ln(e^{w_1} + e^{-w_1} - e^{w_2} - e^{-w_2}) , \qquad (D.1.2)$$

the argument of the logarithm in Eq. (D.1.2) may be rewritten as

$$e^{\frac{w_1}{2}-\frac{w_2}{2}}[e^{\frac{w_1}{2}+\frac{w_2}{2}} - e^{-\frac{w_1}{2}-\frac{w_2}{2}}] + e^{-(\frac{w_1}{2}-\frac{w_2}{2})}[e^{-\frac{w_1}{2}-\frac{w_2}{2}} - e^{\frac{w_1}{2}+\frac{w_2}{2}}]$$

$$= [e^{\frac{w_1}{2}+\frac{w_2}{2}} - e^{-(\frac{w_1}{2}+\frac{w_2}{2})}][e^{\frac{w_1}{2}-\frac{w_2}{2}} - e^{-(\frac{w_1}{2}-\frac{w_2}{2})}]$$

$$= 4\sinh(\frac{w_1+w_2}{2})\sinh(\frac{w_1-w_2}{2}) ,$$

then Eq. (D.1.2) reads

$$\ln(z_1 - z_2) = \ln(a') + \ln(\sinh\frac{w_1+w_2}{2}) + \ln(\sinh\frac{w_1-w_2}{2})$$
$$= \ln(a') + \ln\left(\frac{1 - e^{-(w_1+w_2)}}{2e^{-\frac{w_1+w_2}{2}}}\right) + \ln\left(\frac{1 - e^{-(w_1-w_2)}}{2e^{-\frac{w_1-w_2}{2}}}\right) . \ (D.1.3)$$

Therefore

$$\ln(z_1 - z_2) = \ln(\frac{a'}{4}) + w_1 + \ln(1 - e^{-(w_1+w_2)}) + \ln(1 - e^{-(w_1-w_2)}) . \qquad (D.1.4)$$

We note that in Eq. (D.1.4) $\xi_1 > \xi_2$, since the domain of logarithms must be positive. Using the Taylor expansion of logarithm

$$\ln(1 - x) = -\sum_{n=1}^{\infty} \frac{x^n}{n} , \qquad (D.1.5)$$

we obtain

$$\ln(z_1 - z_2) = \ln(\frac{a'}{4}) + w_1 - \sum_{n=1}^{\infty} \frac{2}{n} e^{-nw_1} \cosh(nw_2) . \qquad (D.1.6)$$

One can find the real part of Eq. (D.1.6) by noting

$$e^{-nw} = e^{-n\xi_0}(\cos n\eta - i\sin n\eta) ,$$

$$\cosh(n(\xi_0 + i\eta)) = \cosh n\xi_0 \cos n\eta + i\sin n\xi_0 \sin n\eta . \qquad (D.1.7)$$

In the latter we used $\cosh(u + v) = \cosh u \cosh v + \sinh u \sinh v$. Therefore the real part of expression under the sum in Eq. (D.1.6) reads

$$
\begin{aligned}
\mathrm{Re}[e^{-nw_1} \cosh(n(\xi_0 + i\eta_2))] = \; & e^{-n\xi_0}[\cosh(n\xi_0) \cos(n\eta_1) \cos(n\eta_2) \\
& + \sinh(n\xi_0) \sin(n\eta_1) \sin(n\eta_2)] \; . \quad \text{(D.1.8)}
\end{aligned}
$$

Inserting Eqs. (D.1.6) and (D.1.8) into Eq. (D.1.1) we have

$$
\begin{aligned}
2\pi G(|\mathbf{x}_1 - \mathbf{x}_2|) = \; & -\ln\left(\frac{\gamma_e a' e^{\xi_0}}{8\lambda_c}\right) \\
& + 2\sum_{n=1}^{\infty} \frac{e^{-n\xi_0}}{n} [\cosh(n\xi_0) \cos(n\eta_1) \cos(n\eta_2) \\
& + \sinh(n\xi_0) \sin(n\eta_1) \sin(n\eta_2)] \; . \quad \text{(D.1.9)}
\end{aligned}
$$

D.2 Interaction part

The case that the two points are located on different ellipses, i.e. $\mathbf{x}_1 = \mathbf{r}_1$ and $\mathbf{x}_2 = \mathbf{d} + \mathbf{r}_2$, which furthermore possess an arbitrary orientation in the plane (expressed by the angles θ_1 and θ_2, see Fig. 3.1) is more difficult. We start with a general Taylor expansion of the Green's function:

$$
-\frac{1}{2\pi}\ln\left(\frac{\gamma_e|\mathbf{d} + \mathbf{r}_2 - \mathbf{r}_1|}{2\lambda_c}\right) = -\frac{1}{2\pi}\ln\left(\frac{\gamma_e d}{2\lambda_c}\right) - \frac{1}{2\pi}\sum_{\substack{j_1,j_2=0 \\ j_1+j_2\geq 1}} \frac{(-\mathbf{r}_1.\nabla)^{j_1}}{j_1!} \frac{(\mathbf{r}_2.\nabla)^{j_2}}{j_2!} \ln r \Bigg|_{r=d} \; .
$$

$$\text{(D.2.10)}$$

On the other hand, we can perform this expansion using complex variables $z = x + iy$. In order to calculate the Green's function by using complex space, the Taylor expansion in complex space has to be employed. The Taylor expansion in complex space is associated with the Taylor expansion in two dimensions. The

Taylor expansion in two dimensions in given by

$$
\begin{aligned}
f(\mathbf{r} + \mathbf{a}) &= f(x + a_x, y + a_y) \\
&= \sum_{j=0}^{\infty} \frac{1}{j!} \left(a_x \frac{\partial}{\partial x} + a_y \frac{\partial}{\partial y} \right) f(\mathbf{r}) \\
&= \sum_{j=0}^{\infty} \frac{(\mathbf{a} . \nabla)^j}{j!} f(\mathbf{r}) \,.
\end{aligned}
\tag{D.2.11}
$$

For $\mathbf{r} = \mathrm{Re}[z + z']$ and $\mathbf{a} = \mathrm{Im}[z + z']$, we find the Taylor expansion in complex space

$$
\begin{aligned}
f(z + z') &= f(\mathrm{Re}[z + z'], \mathrm{Im}[z + z']) \\
&= \sum_{j=0}^{\infty} \frac{1}{j!} \left(\mathrm{Re}[z'] \frac{\partial}{\partial \mathrm{Re}[z]} + \mathrm{Im}[z'] \frac{\partial}{\partial \mathrm{Im}[z]} \right)^j f(\mathrm{Re}[z], \mathrm{Im}[z]) \\
&= \sum_{j=0}^{\infty} \frac{1}{j!} (z' \partial_z)^j f(z) \,,
\end{aligned}
\tag{D.2.12}
$$

where

$$
\begin{aligned}
\partial_z &= \frac{\partial}{\partial(x + iy)} \\
&= \frac{\partial}{\partial x} \frac{\partial x}{\partial(x + iy)} + \frac{\partial}{\partial y} \frac{\partial y}{\partial(x + iy)} \\
&= \frac{\partial}{\partial \mathrm{Re}z} - i \frac{\partial}{\partial \mathrm{Im}z} \,.
\end{aligned}
$$

Using Eq. (D.2.12) for a logarithmic function gives

$$
\ln(z - z') = \sum_{j=0}^{\infty} \frac{1}{j!} (-z' \partial_z)^j \ln z \,.
\tag{D.2.13}
$$

The real part of Eq. (D.2.13) is the expansion of the real logarithm, of course

$$
\ln|\mathbf{r} - \mathbf{r}'| = \mathrm{Re} \sum_{j=0}^{\infty} -\frac{1}{j} \frac{(z' z^*)^j}{|z|^{2j}} \,.
\tag{D.2.14}
$$

By comparing Eq. (D.2.14) and the Taylor expansion of $\ln|\mathbf{r} - \mathbf{r}'|$ in real space as in Eq. (D.2.10), we find

$$
\begin{aligned}
\frac{(-\mathbf{r}' . \nabla)^j}{j!} \ln r &= -\frac{1}{j} \mathrm{Re}[\frac{(z' z^*)^j}{|z|^{2j}}] \\
&= -\frac{1}{2j} \frac{(z' z^*)^j + (z'^* z)^j}{|z|^{2j}} \,.
\end{aligned}
\tag{D.2.15}
$$

Introducing complex derivative operators $\zeta_- = \partial_z$, $\zeta_+ = \partial_{z^*}$, we have

$$
\begin{aligned}
\xi_- \ln r &= \partial_z \ln |z| \\
&= \frac{1}{2} \partial_z \ln(zz^*) = \frac{1}{2z} ,
\end{aligned}
\tag{D.2.16}
$$

similarly

$$
\xi_+ \ln r = \frac{1}{2z^*} .
\tag{D.2.17}
$$

Thus

$$
\xi_+ \xi_- \ln r = \xi_- \xi_+ \ln r = 0 ,
\tag{D.2.18}
$$

and

$$
\zeta_\pm^j \ln r = \zeta_\pm^j \ln |z| = \frac{1}{2}(-1)^{j-1}(j-1)!
\begin{cases}
z^j / |z|^{2j} \\[4pt]
z^{*j} / |z|^{2j}
\end{cases} .
\tag{D.2.19}
$$

Identifying Eq. (D.2.15) and (D.2.19) we obtain

$$
\frac{(\mathbf{r}'.\nabla)^j}{j!} \ln r = \frac{1}{j!} \left((z'^*)^j \zeta_+^j + z'^j \zeta_-^j \right) \ln r .
\tag{D.2.20}
$$

By inserting Eq. (D.2.20) into Eq. (D.2.10), we find the Green's function expansion in terms of complex variables z_i

$$
G|\mathbf{x}_2 - \mathbf{x}_1| = -\frac{1}{2\pi} \ln \left(\frac{\gamma_e d}{2\lambda_c} \right) + \frac{1}{2\pi} \sum_{\substack{j_1, j_2 = 0 \\ j_1 + j_2 \geq 1}} \frac{(-1)^{j_2}}{j_1 + j_2} \binom{j_1 + j_2}{j_1} \frac{1}{d^{j_1+j_2}} \mathrm{Re}[z_1^{j_1} z_2^{j_2}] .
\tag{D.2.21}
$$

This general expansion can be used in any coordinate system. In the special case of elliptic coordinates, $z = (a'/2)e^{-i\theta} \cosh(\xi + i\eta)$, where θ is the in-plane rotation angle of the ellipse major axis with respect to a fixed x–axis. (For the configuration of arbitrarily oriented ellipses, the x–axis is given by the line joining their centers, see Fig. 3.1). In order to express Eq. (D.2.21) in elliptic coordinates, one needs z^j

$$
z^j = \left(\frac{a' e^{-i\theta}}{4} \right)^j \left(e^{-(\xi+i\eta)} + e^{(\xi+i\eta)} \right) ,
\tag{D.2.22}
$$

applying the binomial expansion, $(x+x^{-1})^n = \sum\limits_{k=0}^{n} \binom{n}{k} x^{2k-n}$, we rewrite Eq. (D.2.22)

$$z^j = \left(\frac{a' e^{-i\theta}}{4}\right)^j \sum_{k=0}^{j} \binom{j}{k} e^{(2k-j)(\xi+i\eta)} , \qquad (D.2.23)$$

thus

$$z_1^{j_1} z_2^{j_2} = \left(\frac{a'}{4}\right)^{j_1+j_2} e^{-i(j_1\theta_1+j_2\theta_2)} \sum_{k_1=0}^{j_1} \sum_{k_2=0}^{j_2} \binom{j_1}{k_1}\binom{j_2}{k_2} e^{(2k_1-j_1)\xi_1+(2k_2-j_2)\xi_2}$$
$$\times e^{i((2k_1-j_1)\eta_1+(2k_2-j_2)\eta_2)} . \quad (D.2.24)$$

Using the above expansion, Eq. (D.2.21) becomes:

$$
\begin{aligned}
G(|\mathbf{x}_1 - \mathbf{x}_2|) &= -\frac{1}{2\pi} \ln\left(\frac{\gamma_e d}{2\lambda_c}\right) \\
&+ \frac{1}{2\pi} \sum_{\substack{j_1,j_2=0 \\ j_1+j_2\geq 1}} \sum_{k_1=0}^{j_1} \sum_{k_2=0}^{j_2} \frac{(-1)^{j_2}}{j_1+j_2} \binom{j_1+j_2}{j_1}\binom{j_1}{k_1}\binom{j_2}{k_2}\left(\frac{a'}{4d}\right)^{j_1+j_2} \\
&\times \exp(\xi_1(2k_1-j_1) + \xi_2(2k_2-j_2)) \\
&\times \cos(j_1\theta_1 + j_2\theta_2 + \eta_1(j_1-2k_1) + \eta_2(j_2-2k_2)) , \qquad (D.2.25)
\end{aligned}
$$

where the trigonometric function in Eq. (D.2.25) is expanded as

$$
\begin{aligned}
\cos(j_1\theta_1 &+ j_2\theta_2 + \eta_1(j_1-2k_1) + \eta_2(j_2-2k_2)) = \\
&\cos(j_1\theta_1 + j_2\theta_2)\cos(\eta_1(j_1-2k_1) + \eta_2(j_2-2k_2)) \\
- \quad &\sin(j_1\theta_1 + j_2\theta_2)\sin(\eta_1(j_1-2k_1) + \eta_2(j_2-2k_2)) = \\
&\cos(j_1\theta_1 + j_2\theta_2)\left[\cos(\eta_1(j_1-2k_1))\cos(\eta_2(j_2-2k_2))\right. \\
&\qquad\qquad\qquad\left. - \sin(\eta_1(j_1-2k_1))\sin(\eta_2(j_2-2k_2))\right] \\
- \quad &\sin(j_1\theta_1 + j_2\theta_2)\left[\sin(\eta_1(j_1-2k_1))\cos(\eta_2(j_2-2k_2))\right. \\
&\qquad\qquad\qquad\left. + \cos(\eta_1(j_1-2k_1))\sin(\eta_2(j_2-2k_2))\right] . \qquad (D.2.26)
\end{aligned}
$$

The aim is to rewrite the fourfold sum in Eq. (D.2.25) over j_1, j_2, k_1, k_2 as an expansion into multipole coefficients $\cos(m\eta_1)\cos(n\eta_2)$ and $\sin(m\eta_1)\sin(n\eta_2)$ with $m, n \geq 0$. To that end, we define $m = |j_1 - 2k_1|$ and $n = |j_2 - 2k_2|$. The possibility

that $j_i - 2k_i$ may be positive as well as negative makes it necessary to consider the following cases: **(i)** "$m = 0$, $n = 0$", **(ii)** "$m = 0$, $n \neq 0$" or "$m \neq 0$, $n = 0$" and **(iii)** "$m \neq 0$, $n \neq 0$".

Case (i) $m{=}0$, $n{=}0$

Two auxiliary variables l_1, l_2 are introduced through $j_i = 2l_i$, $k_i = l_i$ ($i = 1, 2$). The such constrained sum in Eq. (D.2.25) reduces to

$$\sum_{\substack{l_1,l_2=0 \\ l_1+l_2 \geq 0}} \frac{1}{2(l_1+l_2)} \binom{2(l_1+l_2)}{2l_1} \binom{2l_1}{l_1} \binom{2l_2}{l_2} \left(\frac{a'}{4d}\right)^{2(l_1+l_2)} \cos(2l_1\theta_1 + 2l_2\theta_2) \ .$$

Relabelling $l = l_1 + l_2$ and $l' = l_1$, the above sum is rewritten as

$$\sum_{l=1}^{l} \sum_{l'=0}^{l} \frac{1}{2l} \binom{2l}{2l'} \binom{2l'}{l'} \binom{2(l-l')}{l-l'} \left(\frac{a'}{4d}\right)^{2l} \cos(2l'\theta_1 + 2(l-l')\theta_2) \ . \qquad \text{(D.2.27)}$$

Case (ii) $m{=}0$, $n > 0$

Here, l_1 is introduced as above through $j_1 = 2l_1$ and $k_1 = l_1$. We distinguish the two cases $j_2 - 2k_2 > 0$ and $j_2 - 2k_2 < 0$ via the choice of l_2 through $j_2 = n + 2l_2$ and $k_2 = l_2$ vs. $k_2 = n + l_2$.
For the case $j_2 = n + 2l_2$ and $k_2 = l_2$, the sum (D.2.25) reads

$$\sum_{l_1,l_2=0} \frac{(-1)^n}{n + 2(l_1+l_2)} \binom{n+2(l_1+l_2)}{2l_1} \binom{2l_1}{l_1} \binom{n+2l_2}{l_2} \left(\frac{a'}{4d}\right)^{n+2(l_1+l_2)}$$
$$\times e^{-n\xi_2} \left[\cos\Theta \cos(n\eta_2) - \sin\Theta \sin(n\eta_2)\right] \ , \quad \text{(D.2.28)}$$

here $\Theta = 2l_1\theta_1 + (n + 2l_2)\theta_2$. For $j_2 = n + 2l_2$ and $k_2 = n + l_2$, the sum (D.2.25) may be rewritten as

$$\sum_{l_1,l_2=0} \frac{(-1)^n}{n + 2(l_1+l_2)} \binom{n+2(l_1+l_2)}{2l_1} \binom{2l_1}{l_1} \binom{n+2l_2}{l_2} \left(\frac{a'}{4d}\right)^{n+2(l_1+l_2)}$$
$$\times e^{n\xi_2} \left[\cos\Theta \cos(n\eta_2) + \sin\Theta \sin(n\eta_2)\right] \ . \quad \text{(D.2.29)}$$

Adding up these two cases in the constrained sum (D.2.25) we have

$$\sum_{l_1, l_2 = 0} \frac{(-1)^n}{n + 2(l_1 + l_2)} \binom{n + 2(l_1 + l_2)}{2l_1} \binom{2l_1}{l_1} \binom{n + 2l_2}{l_2} \left(\frac{a'}{4d}\right)^{n + 2(l_1 + l_2)}$$
$$\times 2 \left[\cos \Theta \cosh(n\xi_2) \cos(n\eta_2) + \sin \Theta \sinh(n\xi_2) \sin(n\eta_2)\right] ,$$

(D.2.30)

performing a relabelling analogous to the one leading to expression(D.2.27) ($l = l_1 + l_2$, $l' = l_1$) we obtain

$$2 \sum_{l=0} \sum_{l'=0}^{l} (-1)^n \frac{\Gamma(n + 2l)}{l'^2 (l - l')! (n + l - l')!} \left(\frac{a'}{4d}\right)^{n + 2l}$$
$$\times \left[\cos(2l'\theta_1 + (n + 2(l - l'))\theta_2) \cosh(n\xi_2) \cos(n\eta_2)\right.$$
$$\left. + \sin(2l'\theta_1 + (n + 2(l - l'))\theta_2) \sinh(n\xi_2) \sin(n\eta_2)\right] .$$

(D.2.31)

Similarly we obtain for "$m > 0$, $n = 0$ ":

$$2 \sum_{l=0} \sum_{l'=0}^{l} \frac{\Gamma(m + 2l)}{l'! (l - l')!^2 (m + l')!} \left(\frac{a'}{4d}\right)^{m + 2l}$$
$$\times \left[\cos((m + 2l')\theta_1 + 2(l - l')\theta_2) \cosh(m\xi_1) \cos(m\eta_1)\right.$$
$$\left. + \sin((m + 2l')\theta_1 + 2(l - l')\theta_2) \sinh(m\xi_1) \sin(m\eta_1)\right] .$$

(D.2.32)

Case (iii) *m>0, n>0*

Similarly to the previous cases, j_1 and j_2 are introduced through $j_1 = m + 2l_1$ and $j_2 = n + 2l_2$. The four cases of possible sign combinations of $j_i - 2k_i$ ($i = 1, 2$) are taken into account by the relation sets "$k_1 = l_1$, $k_2 = l_2$", " $k_1 = l_1$, $k_2 = n + l_2$", "$k_1 = m + l_1$, $k_2 = l_2$","$k_1 = m + l_1$, $k_2 = n + l_2$".
For $k_1 = l_1$, $k_2 = l_2$, the sum (D.2.25) can be rewriten as

$$S_{mn}^{l_1 l_2}(d) \, e^{-(m\xi_1 + n\xi_2)} \{\cos \Theta \left[\cos(m\eta_1) \cos(n\eta_2) - \sin(m\eta_1) \sin(n\eta_2)\right]$$
$$- \sin \Theta \left[\sin(m\eta_1) \cos(n\eta_2) + \cos(m\eta_1) \sin(n\eta_2)\right]\} , \quad (\text{D.2.33})$$

where $\Theta = (m + 2l_1)\theta_1 + (n + 2l_2)\theta_2$ and

$$S_{mn}^{l_1 l_2}(d) = \frac{(-1)^n}{m + n + 2(l_1 + l_2)} \binom{m + n + 2(l_1 + l_2)}{m + 2l_1} \binom{m + 2l_1}{l_1} \binom{n + 2l_2}{l_2} \left(\frac{a'}{4d}\right)^{m+n+2(l_1+l_2)} .$$

for $k_1 = l_1$, $k_2 = n + l_2$ we obtain

$$S_{mn}^{l_1 l_2}(d)\, e^{-m\xi_1 + n\xi_2}\{\cos\Theta\,[\cos(m\eta_1)\cos(n\eta_2) + \sin(m\eta_1)\sin(n\eta_2)]$$
$$- \sin\Theta\,[\sin(m\eta_1)\cos(n\eta_2) - \cos(m\eta_1)\sin(n\eta_2)]\} , \qquad \text{(D.2.34)}$$

and for $k_1 = m + l_1$, $k_2 = l_2$ we have

$$S_{mn}^{l_1 l_2}(d)\, e^{m\xi_1 - n\xi_2}\{\cos\Theta\,[\cos(m\eta_1)\cos(n\eta_2) + \sin(m\eta_1)\sin(n\eta_2)]$$
$$- \sin\Theta\,[-\sin(m\eta_1)\cos(n\eta_2) + \cos(m\eta_1)\sin(n\eta_2)]\} , \qquad \text{(D.2.35)}$$

lastly, for the case $k_1 = m + l_1$, $k_2 = n + l_2$ the sum (D.2.25) takes the form

$$S_{mn}^{l_1 l_2}(d)\, e^{m\xi_1 + n\xi_2}\{\cos\Theta\,[\cos(m\eta_1)\cos(n\eta_2) - \sin(m\eta_1)\sin(n\eta_2)]$$
$$+ \sin\Theta\,[\sin(m\eta_1)\cos(n\eta_2) + \cos(m\eta_1)\sin(n\eta_2)]\} . \qquad \text{(D.2.36)}$$

Adding up these four cases in the constrained sum (D.2.25)

$$2S_{mn}^{l_1 l_2}(d)$$
$$\times \cos\Theta\{\cos(m\eta_1)\cos(n\eta_2)\,[\cosh(m\xi_1 + n\xi_2) + \cosh(m\xi_1 - n\xi_2)]$$
$$- \sin(m\eta_1)\sin(n\eta_2)\,[\cosh(m\xi_1 + n\xi_2) - \cosh(m\xi_1 - n\xi_2]\}$$
$$+ \sin\Theta\{\sin(m\eta_1)\cos(n\eta_2)\,[\sinh(m\xi_1 + n\xi_2) + \sinh(m\xi_1 - n\xi_2)]$$
$$+ \cos(m\eta_1)\sin(n\eta_2)\,[\sinh(m\xi_1 + n\xi_2) - \sinh(m\xi_1 - n\xi_2)]\} ,$$

$$\text{(D.2.37)}$$

taking advantage of the addition and subtraction relations between hyperbolic func-

tions in Eq. (D.2.37)

$$\sinh x_1 + \sinh x_2 = 2\sinh(\frac{x_1 + x_2}{2})\cosh(\frac{x_1 - x_2}{2}) \,,$$
$$\sinh x_1 - \sinh x_2 = 2\cosh(\frac{x_1 + x_2}{2})\sinh(\frac{x_1 - x_2}{2}) \,,$$
$$\cosh x_1 + \cosh x_2 = 2\cosh(\frac{x_1 + x_2}{2})\cosh(\frac{x_1 - x_2}{2}) \,,$$
$$\cosh x_1 - \cosh x_2 = 2\sinh(\frac{x_1 + x_2}{2})\sinh(\frac{x_1 - x_2}{2}) \,,$$

$$(\text{D.2.38})$$

and then relabelling as before ($l = l_1 + l_2$, $l' = l_1$) we find:

$$4\sum_{l=0}\sum_{l'=0}^{l}(-1)^n\frac{\Gamma(m + n + 2l)}{(m + l')!l'!(n + l - l')!(l - l')!}\left(\frac{a'}{4d}\right)^{m+n+2l}$$
$$\{\cos\Theta\left[\cosh(m\xi_1)\cos(m\eta_1)\cosh(n\xi_2)\cos(n\eta_2)\right.$$
$$\left. - \sinh(m\xi_1)\sin(m\eta_1)\sinh(n\xi_2)\sin(n\eta_2)\right]$$
$$\sin\Theta\left[\sinh(m\xi_1)\sin(m\eta_1)\cosh(n\xi_2)\cos(n\eta_2)\right.$$
$$\left. + \cosh(m\xi_1)\cos(m\eta_1)\sinh(n\xi_2)\sin(n\eta_2)\right]\} \,, \qquad (\text{D.2.39})$$

where $\Theta = (m + 2l')\theta_1 + (n + 2(l - l'))\theta_2$.

Eqs.(D.2.27), (D.2.31), (D.2.32) and (D.2.39) may be combined into a single expression such that the 2D Green's function in elliptic coordinates reads:

$$G(|\mathbf{x}_1 - \mathbf{x}_2|) = -\frac{1}{2\pi}\ln\left(\frac{\gamma_e d}{2\lambda_c}\right) + \frac{1}{2\pi}\sum_{m,n,l=0}\left(\frac{a'}{4d}\right)^{m+n+2l}$$
$$\times \{A^c_{mnl}\left[\cos(m\eta_1)\cosh(m\xi_1)\cos(n\eta_2)\cosh(n\xi_2)\right.$$
$$\left. - \sin(m\eta_1)\sinh(m\xi_1)\sin(n\eta_2)\sinh(n\xi_2)\right]$$
$$+ A^s_{mnl}\left[\sin(m\eta_1)\sinh(m\xi_1)\cos(n\eta_2)\cosh(n\xi_2)\right.$$
$$\left. + \cos(m\eta_1)\cosh(m\xi_1)\sin(n\eta_2)\sinh(n\xi_2)\right]\} \,. \qquad (\text{D.2.40})$$

In Eq. (D.2.40), the coefficients $A^{(c)}_{mnl}$ are given by

$$A^{(c)}_{mnl} = A^{(c)}_{mnl}(\theta_1, \theta_2) = 2^{H_n + H_m}\sum_{l'=0}^{l}C^{mn}_{ll'}\begin{pmatrix}\cos(\Theta)\\\sin(\Theta)\end{pmatrix} \,, \qquad (\text{D.2.41})$$

where H_j is the discrete step function; $H_j = 1 - \delta_{j0}$, and

$$C_{ll'}^{mn} = (-1)^n \frac{\Gamma(m + n + 2l)}{(m + l')!\, l'!\, (n + l - l')!\, (l - l')!} ,$$

<div align="right">(D.2.42)</div>

with $C_{00}^{00} = 0$.

Appendix E

Self–energy in the case of fluctuating colloids

For fluctuating colloids, the self–energy part of the multipole–multipole interaction of the auxiliary fields Ψ_i was introduced in Eq. (3.71). Here we calculate it explicitly with a method similarly to the one employed in Ref. [54]. As the starting point, we obtain from Eqs. (3.70) and (3.71) the following expession for $\mathcal{Z}_{i,\text{self}} = \exp\left(-\frac{k_{\text{B}}T}{2\gamma}\mathcal{H}_{i,\text{self}}\right)$:

$$
\begin{aligned}
\mathcal{Z}_{i,\text{self}} = \int \prod_{i=1}^{2} \mathcal{D}\psi_i \quad & \delta\left(\Psi_{im}^c - \int_{S_i} d^2x \left(\cos(m\xi)/\cosh(m\xi_0)\right)\cos(m\eta)\psi(\mathbf{x})\right) \\
\times \quad & \delta\left(\Psi_{im}^s - \int_{S_i} d^2x \left(\sinh(m\xi)/\sinh(m\xi_0)\right)\sin(m\eta)\psi(\mathbf{x})\right) \\
\times \quad & \exp\left(\mathrm{i}\sum_m (\Psi_{im}^c P_{im} + \Psi_{im}^s Q_{im})\right) \\
\times \quad & \exp\left(-\frac{k_{\text{B}}T}{2\gamma}\int_{S_i} d^2x \int_{S_i} d^2x'\, \psi_i(\mathbf{x})\, G(|\mathbf{x}-\mathbf{x}'|)\,\psi_i(\mathbf{x})\right. \\
& \left. - \mathrm{i}\int_{S_{i,\text{ref}}} d^2x\, \psi_i(\mathbf{x})\, f_{i,\text{ext}}(\mathbf{x})\right) \ .
\end{aligned}
$$

(E.0.1)

The δ–functions in $\mathcal{Z}_{i,\text{self}}$ may be eliminated by introducing conjugate multipole

138

moments $\widetilde{\Psi}^c_{im}$ and $\widetilde{\Psi}^s_{im}$ to the multipoles $\Psi^{(c)}_{im(s)}$ of the auxiliary fields:

$$\delta\left(\Psi^{(c)}_{im(s)} - \int_{S_{i,\text{ref}}} d^2x \begin{pmatrix} \cosh(m\xi_i)\cos(m\eta_i)/\cosh(m\xi_0) \\ \sinh(m\xi_i)\sin(m\eta_i)/\sinh(m\xi_0) \end{pmatrix} \psi_i(\mathbf{x}_i)\right) =$$
$$\int d\widetilde{\Psi}^{(c)}_{im(s)} \exp\left(\mathrm{i}\widetilde{\Psi}^{(c)}_{im(s)}\left[\Psi^{(c)}_{im(s)} - \int_{S_{i,\text{ref}}} d^2x \begin{pmatrix} \cosh(m\xi_i)\cos(m\eta_i)/\cosh(m\xi_0) \\ \sinh(m\xi_i)\sin(m\eta_i)/\sinh(m\xi_0) \end{pmatrix} \psi_i(\mathbf{x}_i)\right]\right) .$$
$$(\text{E.0.2})$$

Inserting Eq. (E.0.2) into $\mathcal{Z}_{i,\text{self}}$ we obtain:

$$\begin{aligned}
\mathcal{Z}_{i,\text{self}} &= \int \prod_m d\widetilde{\Psi}_{im} \int \mathcal{D}\psi_i \exp\left(-\frac{k_\mathrm{B}T}{2\gamma} \int_{S_{i,\text{ref}}} d^2x \int_{S_{i,\text{ref}}} d^2x' \psi_i(\mathbf{x}_i) G(|\mathbf{x}-\mathbf{x}'|) \psi_i(\mathbf{x}_i) \right. \\
&\quad -\mathrm{i} \int_{S_{i,\text{ref}}} d^2x \, \psi_i(\mathbf{x}_i) \left[\sum_m \frac{\cosh(m\xi_i)}{\cosh(m\xi_0)}(P_{im} + \widetilde{\psi}^c_{im})\cos(m\eta_i) \right. \\
&\quad\quad\quad\quad \left. + \frac{\sinh(m\xi_i)}{\sinh(m\xi_0)}(Q_{im} + \widetilde{\psi}^s_{im})\sin(m\eta_i)\right] \\
&\quad \left. +\mathrm{i}\sum_{m=0}\left[(P_{im} + \widetilde{\Psi}^c_{im})\Psi^c_{im} + (Q_{im} + \widetilde{\Psi}^s_{im})\Psi^s_{im}\right]\right) ,
\end{aligned}$$
$$(\text{E.0.3})$$

where $d\widetilde{\Psi}_{im} = d\widetilde{\Psi}^s_{im} d\widetilde{\Psi}^c_{im}$. The functional integral $\int \mathcal{D}\psi_i$ in Eq. (E.0.3) can be replaced by a functional integral over a constrained height field $h(\mathbf{x})$:

$$\begin{aligned}
\mathcal{Z}_{i,\text{self}} &= \int \prod_m d\widetilde{\Psi}_{im} \exp\left(\mathrm{i}\sum_{m=0}^{\infty}\left[(P_{im} + \widetilde{\Psi}^c_{im})\Psi^c_{im} + (Q_{im} + \widetilde{\Psi}^s_{im})\Psi^s_{im}\right]\right) \\
&\quad \times \int \mathcal{D}h \prod_{\mathbf{x}_i \in S_{i,\text{ref}}} \delta(h(\mathbf{x}_i) - \widetilde{f}_i) \exp\left(-\frac{\gamma}{2k_\mathrm{B}T}\int d^2x \left[(\nabla h)^2 + \frac{h^2}{\lambda_c^2}\right]\right) ,
\end{aligned}$$
$$(\text{E.0.4})$$

where $\widetilde{f}_i = \sum_m \left[\frac{\cosh(m\xi_i)}{\cosh(m\xi_0)}(P_{im} + \widetilde{\Psi}^c_{im})\cos(m\eta_i) + \frac{\sinh(m\xi_i)}{\sinh(m\xi_0)}(Q_{im} + \widetilde{\Psi}^s_{im})\sin(m\eta_i)\right]$.
In the region $S_{i,\text{ref}}$, i.e. the ellipse enclosed by the reference contact line, the height field h is pinned to $\widetilde{f}_i$. Therefore the contribution of the functional integral $\int \mathcal{D}h$ in this region is simply given by the surface energy of $\widetilde{f}_i$ which was determined in

Eq. (C.2.17) and $\mathcal{Z}_{i,\text{self}}$ becomes:

$$
\mathcal{Z}_{i,\text{self}} \overset{\lambda_c \to \infty}{\approx} \int \prod_m d\widetilde{\Psi}_{im} \exp\left(-\frac{\gamma\pi}{2k_{\mathrm{B}}T} \sum_m m \left[(P_{im} + \widetilde{\Psi}^c_{im})^2 \tanh(m\xi_0) \right.\right.
$$
$$
\left. + (Q_{im} + \widetilde{\Psi}^s_{im})^2 \coth(m\xi_0) \right]
$$
$$
\left. + \mathrm{i} \sum_m \left[(P_{im} + \widetilde{\Psi}^c_{im})\Psi^c_{im} + (Q_{im} + \widetilde{\Psi}^s_{im})\Psi^s_{im} \right] \right)
$$
$$
\times \int \mathcal{D}h \prod_{\mathbf{x}_i \in \partial S_{i,\text{ref}}} \delta(h(\mathbf{x}_i) - \widetilde{f}_i) \exp\left(-\frac{\gamma}{2k_{\mathrm{B}}T} \int_{\mathbb{R}^2 \setminus S_{i,\text{ref}}} d^2x \left[(\nabla h)^2 + \frac{h^2}{\lambda_c^2} \right] \right) ,
$$

$$(E.0.5)$$

where the remaining δ-functions describe the pinning of $h(\mathbf{x})$ to the boundaries $\partial S_{i,\text{ref}}$ of the integration domain. The auxiliary field can be separated into two parts, $h = h_0 + h_1$, where $(-\nabla^2 + \lambda_c^{-2})h_0 = 0$ with the boundary conditions $h_0(\mathbf{x}_i)|_{\partial S_{i,\text{ref}}} \equiv \widetilde{f}_i$ and $h_1(\mathbf{x}_i)|_{\partial S_{i,\text{ref}}} = 0$. Applying Gauss' theorem to the integral in the exponent of Eq. (E.0.5) leads to

$$
\mathcal{Z}_{i,\text{self}} = \int \prod_m d\widetilde{\Psi}_{im} \exp\left(-\frac{\gamma\pi}{2k_{\mathrm{B}}T} \sum_m m \left[(P_{im} + \widetilde{\Psi}^c_{im})^2 \tanh(m\xi_0) + \right.\right.
$$
$$
\left. (Q_{im} + \widetilde{\Psi}^s_{im})^2 \coth(m\xi_0) \right]
$$
$$
\left. + \mathrm{i} \sum_m \left[(P_{im} + \widetilde{\Psi}^c_{im})\Psi^c_{im} + (Q_{im} + \widetilde{\Psi}^s_{im})\Psi^s_{im} \right] \right)
$$
$$
\times \exp\left(-\frac{\gamma}{2k_{\mathrm{B}}T} \oint d\mathbf{x}\, h_0(\mathbf{x})\nabla h_0(\mathbf{x}) \right)
$$
$$
\times \int \mathcal{D}h_1 \prod_{\mathbf{x}_i \in S_{i,\text{ref}}} \delta(h_1(\mathbf{x}_i)) \exp\left(-\frac{k_{\mathrm{B}}T}{2\gamma} \int_{\mathbb{R}^2 \setminus S_{i,\text{ref}}} d^2x \left[(\nabla h_1)^2 + \frac{h_1^2}{\lambda_c^2} \right] \right) .
$$

$$(E.0.6)$$

The functional integral over h_1 yield to a constant value independent of any multipole moment, which can be neglected.

The general solution to the Helmholtz differential equation for h_0 in $\mathbb{R}^2 \setminus S_{i,\text{ref}}$ is needed for computing the line integral in Eq. (E.0.6). Rewriting the Helmholz

equation, $(-\Delta + \lambda_c^{-2})h_0 = 0$, in elliptic coordinates would read

$$\frac{\partial^2 h_0}{\partial \xi^2} + \frac{\partial^2 h_0}{\partial \eta^2} - \frac{a'^2}{8\lambda_c^2}(\cosh(2\xi) - \cos(2\eta))h_0 = 0 \ . \tag{E.0.7}$$

Eq. (E.0.7) can be solved by separation of variables method via introducing $h_0 = R(\xi)\Phi(\eta)$

$$\frac{1}{R}\frac{d^2 R}{d\xi^2} + \frac{1}{\Phi}\frac{d^2 \Phi}{d\eta^2} - \frac{a'^2}{8\lambda_c^2}(\cosh(2\xi) - \cos(2\eta)) = 0. \tag{E.0.8}$$

Definig the separation constant a_s, Eq. (E.0.8) separates into angular and radial part

$$\frac{d^2 R}{d\xi^2} - (a_s - 2q\cosh 2\xi)R = 0 \tag{E.0.9}$$

$$\frac{d^2 \Phi}{d\eta^2} + (a_s - 2q\cos 2\eta)\Phi = 0 \ , \tag{E.0.10}$$

where $q = -a'^2/(16\lambda_c^2)$. Eq. (E.0.9) and Eq. (E.0.10) represent the modified Mathieu (radial part) and the Mathieu (angular part) differential equations, respectively. The solution of Eq. (E.0.10), $\Phi_m(\eta)$, is the superposition of cosine–elliptic (ce_m) and sine–elliptic (se_m) functions, and the solution of Eq. (E.0.9), $R_m(\xi)$, is the superposition of odd and even evanescent radial Mathieu functions Ko_m and Ke_m that play a similar role as the modified Bessel functions in polar coordinates [107]

$$\Phi_m(\eta) = A_m \mathrm{ce}_m(\eta; q) + B_m \mathrm{se}_m(\eta; q) \tag{E.0.11}$$

$$R_m(\xi) = A'_m \mathrm{Ke}_m(\xi; q) + B'_m \mathrm{Ko}_m(\xi; q) \tag{E.0.12}$$

However, since in our physical system we should investigate results in $\lambda_c \to \infty$, the solutions to the Mathieu differential equation reduces to standard sine and cosine functions. To determine the solutions of the modified Mathieu differential equation in this limit, one has to find the asymptotic form of the factor $2q\cosh 2\xi$ in Eq. (E.0.9)

$$\begin{aligned}2q\cosh 2\xi \quad &= \quad \frac{a'^2 e^{2\xi}}{16}\left(\frac{1}{\lambda_c^2} + \frac{e^{-4\xi}}{\lambda_c^2}\right) \\ &\overset{\lambda_c \to \infty}{\approx} \quad \left(\frac{a' e^{2\xi}}{4\lambda_c}\right)^2 \ .\end{aligned} \tag{E.0.13}$$

Introducing effective elliptic radius $r_e = \frac{a' e^\xi}{4}$, we rewrite the modified Mathieu differential equation Eq. (E.0.9) in terms of r_e

$$
\begin{aligned}
\frac{d^2 R}{d\xi^2} &= \frac{d}{d\xi}\left(\frac{dR}{d\xi}\right) = \frac{dr_e}{d\xi}\frac{d}{dr_e}\left(\frac{dr_e}{d\xi}\frac{dR}{dr_e}\right) \\
&= r_e^2 \frac{d^2 R}{dr_e^2} + r_e \frac{dR}{dr_e} ,
\end{aligned}
\tag{E.0.14}
$$

where the second line is achieved by using $dr_e = r_e\, d\xi$. Inserting Eq. (E.0.14) into Eq. (E.0.9) we obtain

$$
r_e^2 \frac{d^2 R}{dr_e^2} + r_e \frac{dR}{dr_e} + (\lambda_c^{-2} r_e^2 - a_s) R = 0
\tag{E.0.15}
$$

Eq. (E.0.15) is the modified Bessel differential equation, thus for $a_s = m^2$ the solutions to the radial part would reduce to the modified Bessel functions of the second kind K_m. The final solution is given by

$$
h_0(\mathbf{x}_i) = \sum_m \frac{K_m(a' e^{\xi_i}/4\lambda_c)}{K_m(a' e^{\xi_0}/4\lambda_c)}(A_m \cos(m\eta_i) + B_m \sin(m\eta_i)) .
\tag{E.0.16}
$$

The coefficients in Eq. (E.0.16) are readily determined by comparing to the boundary conditions: $A_m = P_{im} + \widetilde{\Psi}^c_{im}$, $B_m = Q_{im} + \widetilde{\Psi}^s_{im}$ and $B_0 = 0$. Using the asymptotic form of K_m in the limit $\lambda \to \infty$, Eq. (E.0.16) can be rewriten as

$$
h_0(\mathbf{x}_i) = \frac{\ln(\gamma_e a' e^{\xi_i}/8\lambda_c)}{\ln(\gamma_e a' e^{\xi_0}/8\lambda_c)} A_0 + \sum_{m>0} e^{-m(\xi_i - \xi_0)}(A_m \cos(m\eta_i) + B_m \sin(m\eta_i))
\tag{E.0.17}
$$

Reminding the line integral in Eq. (E.0.6)

$$
\begin{aligned}
\oint d\mathbf{x}.h_0(\mathbf{x})\nabla h_0(\mathbf{x}) &= -\int_0^{2\pi} d\eta\, \mathbf{u}_\xi.(\mathbf{u}_\xi\, \partial_\xi h_0.\mathbf{u}_\eta\, \partial_\eta h_0) \\
&= -\int_0^{2\pi} d\eta\, h_0 \partial_\xi h_0
\end{aligned}
\tag{E.0.18}
$$

The above integral can be performed by using Eq. (E.0.17)

$$
\oint d\mathbf{x}.h_0(\mathbf{x})\nabla h_0(\mathbf{x}) = \int_0^{2\pi} d\eta \left[\frac{-1}{\ln(\gamma_e a' e^{\xi_0}/8\lambda_c)} A_0^2 + \sum_{m>0} m(A_m^2 \cos(m\eta)^2 + B_m^2 \sin(m\eta)^2) \right]
\tag{E.0.19}
$$

Then the line integral evaluates to $2\pi g(m)(A_m^2 + B_m^2)$ with $g(m) = m/2$ $(m > 0)$ and $g(0) = -1/\ln(\gamma_{\rm e} a' e^{\xi_0}/8\lambda_c)$. Using this, $\mathcal{Z}_{i,\rm self}$ reads:

$$
\begin{aligned}
\mathcal{Z}_{i,\rm self} \;=\; & \int \prod_m d\widetilde{\Psi}_{im} \exp\Bigg(-\frac{\gamma\pi}{2k_{\rm B}T} \sum_m m \Big[(P_{im} + \widetilde{\Psi}_{im}^c)^2 \tanh(m\xi_0) \\
& \qquad\qquad\qquad\qquad + (Q_{im} + \widetilde{\Psi}_{im}^s)^2 \coth(m\xi_0) \Big] \\
& \qquad + {\rm i} \sum_m \Big[(P_{im} + \widetilde{\Psi}_{im}^c)\Psi_{im}^c + (Q_{im} + \widetilde{\Psi}_{im}^s)\Psi_{im}^s \Big] \Bigg) \\
& \times \exp\Bigg(-\frac{\gamma\pi}{k_{\rm B}T} \sum_{m=0} g(m) \Big[(P_{im} + \widetilde{\Psi}_{im}^c)^2 + (Q_{im} + \widetilde{\Psi}_{im}^s)^2 \Big] \Bigg) \; .
\end{aligned}
$$
$$(\text{E.0.20})$$

The last integration over the conjugate multipole moments can be performed after shifting variables, $\widetilde{\Psi}_{im}^c \to P_{im} + \widetilde{\Psi}_{im}^c$ and $\widetilde{\Psi}_{im}^s \to Q_{im} + \widetilde{\Psi}_{im}^c$. After this integration, the final result for $\mathcal{H}_{i,\rm self} = (-2\gamma)/(k_{\rm B}T)\ln\mathcal{Z}_{i,\rm self}$ is given by:

$$
\begin{aligned}
\mathcal{H}_{i,\rm self} \;=\; & -\frac{\ln(\gamma_{\rm e} a' e^{\xi_0}/8\lambda_c)}{2\pi} \Psi_{i0}^{c\,2} \\
& +\frac{1}{\pi} \sum_{m>0} \frac{1}{m} \left(\frac{\Psi_{im}^{c\,2}}{1 + \tanh(m\xi_0)} + \frac{\Psi_{im}^{s\,2}}{1 + \coth(m\xi_0)} \right) \; .
\end{aligned}
$$
$$(\text{E.0.21})$$

Bibliography

[1] H. Lehle, E. Noruzifar, and M. Oettel, Eur. Phys. J. E **26**, 151 (2008).

[2] E. Noruzifar and M. Oettel, Phys. Rev. E **79**, 051401 (2009).

[3] D. H. Everett, *Basic Principle of Colloid Science* (The Royal Society of Chemistry, 1988).

[4] I.W. Hamley, *Introduction to Soft Matter: Synthetic and Biological Self-Assembling Materials* (Wiley, 2007).

[5] T. Cosgrove, *Colloid Science: Principles, Methods and Applications* (Blackwell Publishing, 2005).

[6] R.A.L. Jones, *Soft Condensed Matter* (Oxford University Press, 2002).

[7] W. Norde, *Colloids and Interfaces in Life Sciences* (Marcel Dekker, 2003).

[8] H.-J. Butt, K. Graf, M. Kappl, *Physics and Chemistry of Interfaces* (Wiley-VCH, 2006).

[9] B.P. Binks and T.S. Horozov,*Colloidal Particles at Liquid Interfaces*, (Cambridge University Press, 2006).

[10] B.P. Binks, Curr. Opin. Colloid Interf. Sci. **7** (2002), 21.

[11] W. Ramsden, Proc. Roy. Soc. **72** (1903), 156.

[12] S.U. Pickering, J. Chem. Soc. **91** (1907), 2001.

[13] B.P. Binks and P.D.I. Fletcher, Langmuir **17** (2001), 4708.

[14] A. Perro, S. Reculusa, S. Ravaine, E. Bourgeat-Lamic and E. Duguet, J. Mater. Chem. **15** (2005), 3745.

[15] T. Young, Phil. Trans., **95** (1805), 84.

[16] J. Israelachvili, *Intermolecular and Surface Forces* (Academic Press, 1998).

[17] F. London, Z. Phys. **63** , 245 (1930).

[18] H. Hettema, *Quantum Chemistry, Classic Scientific Papers* (World Scientific, 2000).

[19] H.B.G. Casimir, D. Polder, Phys. Rev. **73**, 360 (1948).

[20] R.J. Hunter, *Foundation of Colloid Science* (Oxford University Press, 2001).

[21] H.C. Hamaker, Physica **4**, 1058 (1937).

[22] M. Kleman, O.D. Lavrentovich, *Soft Matter Physics, An Introduction* (Springer, 2001).

[23] E. M. Lifshitz, Zh. Eskp. Theor. Fiz. **29**, 94 (1995).

[24] E.M. Lifshitz, Sov. Phys. JETP **2**, 73 (1956).

[25] I.E. Dzyaloshinskii, E.M. Lifshitz, and L.P.Pitaevskii, Zh. Eskp. Teor. Fiz. **37**, 229 (1959).

[26] I.E. Dzyaloshinskii, E.M. Lifshitz, and L.P.Pitaevskii, Adv. Phys. **10**, 165 (1961).

[27] P. G. de Gennes, C. R. Acad. Sci. **271**, 469 (1970).

[28] F. Bresme and M. Oettel, J. Phys.: Condens. Matter (Topical Review) **19**, 413101 (2007).

[29] D. F. Wiliams and J. C. Berg, J. Colloid Interface Sci. **152**, 218 (1992).

[30] M. Oettel and S. Dietrich, Langmuir **24**, 1425 (2008).

[31] O. Stern, Z. Electrochem. **30**, 508 (1924).

[32] P. Debye and E. Hückel, Physikalische Zeitschrift **24**, 185 (1923).

[33] A. J. Hurd, J. Phys. A: Math. Gen. **18**, L1055 (1985).

[34] D. Frydel, A. Dominguez, and M. Oettel, Phys. Rev. E(R) **77**, 020401 (2008).

[35] M. E. Leunissen, A. van Blaaderen, A. D. Hollingsworth, M.T. Sullivan, P.M. Chaikin, Proc. Natl. Acad. Sci. U.S.A. **104**, 2585 (2007).

[36] P. A. Kralchevsky and K. Nagayama, Adv. Coll. Interface Sci. **85**, 145 (2000).

[37] L. Foret and A. Würger, Phys. Rev. Lett. **92**, 058302 (2004).

[38] A. Dominguez, M. Oettel, and S. Dietrich, J. Phys.: Condens. Matter **17**, S3387 (2005).

[39] A. Dominguez, M. Oettel, and S. Dietrich, Europhys. Lett. **77**, 68002 (2007).

[40] M. Oettel, A. Dominguez, and S. Dietrich, J. Phys.: Condens. Matter **17**, L337 (2005).

[41] A. Würger and L. Foret, J. Phys. Chem. B **109**, 16435 (2005).

[42] D. Frydel, S. Dietrich, and M. Oettel, Phys. Rev. Lett. **99**, 118302 (2007).

[43] J.-P. Fournier and P. Galatola, Phys. Rev. E **65**, 031601 (2002).

[44] P. Yang and F. Kim, ChemPhysChem **3**, 503 (2002).

[45] A. B. Brown, C. G. Smith, and A. R. Rennie, Phys. Rev. E **63**, 016305 (2001).

[46] J. C. Loudet, A. M. Alsayed, J. Zhang, and A. G. Yodh, Phys. Rev. Lett. **94**, 018301 (2005).

[47] M. G. Basavaraj, G. G. Fuller, J. Fransaer, and J. Vermant, Langmuir **22**, 6605 (2006).

[48] J. C. Loudet, A. G. Yodh, and B. Pouligny, Phys. Rev. Lett. **97**, 018304 (2006).

[49] H. B. G. Casimir, Proc. K. Ned. Akad. Wet., **51**, 793 (1948).

[50] M. Kardar and R. Golestanian, Rev. Mod. Phys. **71**, 1233 (1999).

[51] R. Golestanian, Phys. Rev. E **62**, 5242 (2000).

[52] H. Lehle, M. Oettel, and S. Dietrich, Europhys. Lett. **75**, 174 (2006).

[53] H. Lehle and M. Oettel, Phys. Rev. E **75**, 011602 (2007).

[54] R. Golestanian, M. Goulian, M. Kardar, Phys. Rev. E **54**, 6725 (1996).

[55] S. K. Lamoreaux, Physics Today **60**, 40 (2007).

[56] J.D. van der Waals, *Over de Continuiteit van den Gas- en Vloeistoftoestand*, doctoral thesis, Leiden, (1873).

[57] H. B. G. Casimir, Comments Mod. Phys. **5-6**, 175 (2000).

[58] B. M. Axilrod, E. Teller, J. Chem. Phys. **11**, 299 (1943).

[59] M. E. Fisher and P. G. de Gennes, C. R. Acad. Sci. Paris B **287**, 207 (1978).

[60] C. Hertlein, L. Helden, A. Gambassi, S. Dietrich and C. Bechinger, Nature **451**, 172 (2008).

[61] M. Goulian, R. Bruinsma, and P. Pincus, Europhys. Lett. **22**, 145 (1993); **23**, 155(E) (1993).

[62] M. J. Sparnaay, Physica **24**, 751 (1958).

[63] S. K. Lamoreaux, Phys. Rev. Lett. **78**, 5 (1997).

[64] U. Mohideen and A. Roy, Phys. Rev. Lett. **81**, 4549 (1998).

[65] G. L. Klimchitskaya, A. Roy, U. Mohideen and V. M. Mostepaneko, Phys. Rev. A. **60**, 3487 (1999).

[66] A. Roy, C. Y. Lin, and U. Mohideen, Phys. Rev. D. **60**, 111101(R) (1999).

[67] B. W. Harris, F. Chen, and U. Mohideen, Phys. Rev. A. **62**, 052109 (2000).

[68] F. Chen, U. Mohideen, G. L. Klimchitskaya, and V. M. Mostepanenko, Phys. Rev. Lett. **88**, 101801 (2002).

[69] F. Chen, U. Mohideen, G. L. Klimchitskaya and V. M. Mostepaneko, Phys. Rev. A. **66**, 032113 (2002).

[70] A. Ganshin, S. Scheidemantel, R. Garcia and M. H. W. Chan, Phys. Rev. Lett. **97**, 075301 (2006).

[71] R. Garcia and M. H. W. Chan, Phys. Rev. Lett. **88**, 086101 (2002).

[72] M. Fukuto, Y. F. Yano, and P. S. Pershan, Phys. Rev. Lett. **94**, 135702 (2005).

[73] F. Soyka, O. Zvyagolskaya, C. Hertlein, L. Helden, and C. Bechinger, Phys. Rev. Lett. **101**, 208301 (2008).

[74] D. Beysens, and D. Esteve, Phys. Rev. Lett. **54**, 2123 (1985).

[75] F. Schlesener, A. Hanke and S. Dietrich, J. Stat. Phys. **110**, 981 (2003).

[76] D. Beysens, T. Narayanan, J. Stat. Phys. **95**, 997 (1999).

[77] G. Plunien, Berndt Müller and W. Greiner, Phys. Rep. **134**, 87 (1986).

[78] M. Abramowitz and I. A. Stegun, *Handbook of Mathematical Functions with Formulas, Graphs, and Mathematical Tables* (Dover, 1964).

[79] T. H. Boyer, Phys. Rev. **174**, 1764 (1968).

[80] B. Davis, J. Math. Phys. **13**, 1324 (1972).

[81] K. A. Milton, *The Casimir effect: physical manifestations of zero-point energy* (World Scientific, 2001).

[82] K. A. Milton, J. Phys. A: Math. Gen. **37**, R209 (2004).

[83] M. Bordag, D. Hennig and D. Robaschik, J. Phys. A: Math. Gen. **25**, 4483 (1992).

[84] M. Bordag, K. Kirsten and D. Vassilevich, Phys. Rev. D **59**, 085011 (1999).

[85] K. A. Milton, J. Phys. A: Math. Gen. **37**, 6391 (2004).

[86] R. Kantowski and K. A. Milton, Phys. Rev. D **35**, 549 (1987).

[87] I. Brevik, B. Jensen and K. A. Milton, Phys. Rev. D **64**, 088701 (2001).

[88] M. Lüscher, K. Symanzik and P. Weisz, Nucl. Phys. B **173**, 365 (1980).

[89] M. Lüscher, Nucl. Phys. B **180**, 317 (1981).

[90] T. Emig, N. Graham, R. L. Jaffe, and M. Kardar, Phys. Rev. D **77**, 025005 (2008).

[91] T. Emig, N. Graham, R. L. Jaffe, and M. Kardar, Phys. Rev. Lett. **99**, 170403 (2007).

[92] J. Schwinger, Lett. Math. Phys. **1**, 43 (1975).

[93] H. Li and M. Kardar, Phys. Rev. Lett. **67**, 3275 (1991).

[94] K. Binder, *In Phase Transitions and Critical Phenomena*, C. Domb and J. L. Lebowitz, eds. (Academic, London, 1986), Vol. 10, p. 75.

[95] S. Gnutzmann and U. Ritschel, Z. Phys.B **49**, 391 (1995).

[96] O. Vasilyev, A. Gambassi, A. Maciołek and S. Dietrich, Phys. Rev. E **79**, 041142 (2009).

[97] O. Vasilyev, A. Gambassi, A. Maciołek and S. Dietrich, Phys. Rev. E **80**, 039902 (E) (2009).

[98] F. P. Buff, R. A. Lovett and F. H. Stillinger, Phys. Rev. Lett. **15**, 612 (1965).

[99] D. Jasnow, in *Phase Transitions and Critical Phenomena* **10**, ed. by C. Domb and J. L. Lebowitz (Academic, 1986).

[100] M. Oettel, A. Dominguez and S. Dietrich, Phys. Rev. E **71**, 051401 (2005).

[101] M. S. Wertheim, J. Chem. Phys. **65**, 2377 (1976).

[102] J. Stecki, J. Chem. Phys. **107**, 7967 (1997).

[103] B. Derjaguin, Kolloid-Zeitschrift **69**, 155 (1934).

[104] R. Büscher and T. Emig, Phys. Rev. A **69**, 062101 (2004).

[105] W. H. Press, W. T. Vetterling, S. A. Teukolsky and B. P. Flannery, *Numerical Recipes in C++* (2nd edn.), (Cambridge University Press, 2002).

[106] P. M. Morse and H. Feshbach, *Methods of Theoretical Physics*, (McGraw-Hill, 1953) p. 1202.

[107] J.C. Gutiérrez-Vega, R.M. Rodríguez-Dagnino, M.A. Meneses-Nava, and S. Chávez-Cerda, Am. J. Phys. **71**, 233 (2003).

Acknowledgements

Curriculum Vitae

Name:	Ehsan Noruzifar
Date of birth:	3. September 1981
Place of birth:	Tehran, Iran

1999 – 2003:	BSc Solid State Physics, K. N. Toosi University of Technology, Tehran, Iran.
2003 – 2006:	MSc Condensed Matter Physics, Shahid Beheshti University, Tehran, Iran.
2006 – 2009:	PhD student in Condensed Matter Theory Group of Prof. Dr. Kurt Binder under the supervision of Dr. Martin Oettel.